UNIVERSITY OF TROMSØ UIT

FACULTY OF SCIENCE AND TECHNOLOGY
DEPARTMENT OF GEOLOGY

Slope displacement patterns observed using satellite InSAR data in the Storfjord-Kåfjord-Lyngen region, Troms

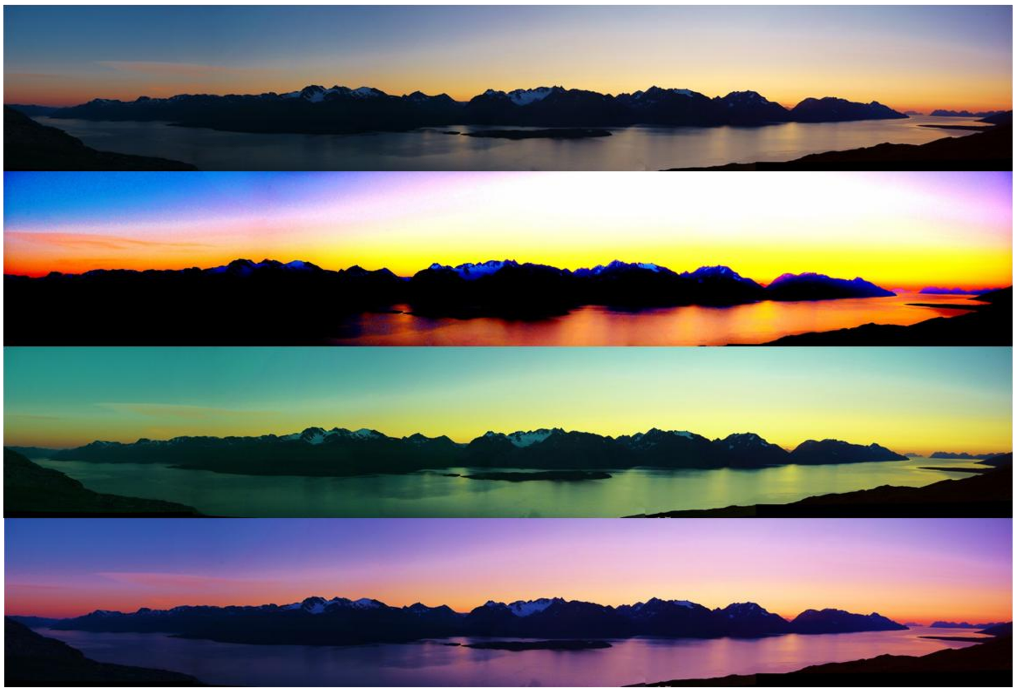

Author

Harald Øverli Eriksen

GEO-3900 Master's Thesis in Geology
May 2013

Abstract

Norway is particularly susceptible to large rockslides due to its many fjords and steep mountains. One of the most dangerous hazards related to rock slope failures are tsunamis that can lead to large loss of life. Many rockslides are clustered east of the Storfjord and Lyngen fjord in Troms county, northern Norway, where several mapped unstable rock slopes occur within the zone of sporadic permafrost. Among these, the Nordnes rockslide has been classified as high-risk due to the severe consequences should catastrophic failure occur.

In order to fully understand the kinematics and geometric configurations susceptible for sliding, it is imperative to obtain precise measurements of the stability of potential unstable rock slopes.

Multi-temporal satellite interferometric synthetic aperture radar (InSAR) techniques involve comparing the phase information from multiple spaceborne SAR images, produced at different times, to detect millimeter to centimeter scale ground deformation patterns. However, the satellite radar is only capable of measuring displacement that has a component in the radar line-of-sight (LOS). By combining InSAR data acquired in both ascending and descending orbits, it is possible to extract more information about the true displacement vector, increasing the interpretability of the displacement patterns.

In this thesis, multi-temporal InSAR methods are applied to an extensive time series of TerraSAR-X data collected in both ascending and descending geometries during the summer seasons in the period 2009-2012. The estimated deformation rates from the ascending and descending geometries are decomposed into 2D InSAR data consisting of deformation in the vertical and east/west directions, dip angle and total displacement. The computed 2D InSAR displacement data are validated with GPS data from the Nordnes rockslide.

For the study area, the 2D InSAR are related to geomorphological- and structural elements in different slope processes; a rock glacier, solifluction tongues, a fast moving rockslide (Gamanjunni3) and the Nordnes rockslide.

Findings suggest that 2D InSAR data give a more adequate and comprehensible presentation of displacement in slope processes, with increased sensitivity to displacement. Produced 2D InSAR data show numerous examples of correlation between geomorphological- and structural elements and pattern observed in the 2D InSAR data. This includes identifying elements like solifluction tongues, outer extents of and ridge formations on rock glaciers, back fractures, fractures separating blocks and lateral borders of rockslides. 2D InSAR data have the possibility to enlighten the inner dynamics of slope processes. E.g. make prediction about displacement patterns for blocks, to what extent they are fragmenting or moving as one body and to what extent the displacement pattern in a slope process are controlled by the slope gradient. Displacement patterns originating from rotation of fault blocks, caused by a listric detachment fault or toe-zone compression uplifting the front of the fault block (thrust duplex) have been observed. There are good indications that 2D InSAR data can contribute to classification of slides, revealing listric of planar fault geometry and to state the controlling factors of rockslides.

Acknowledgements

I am grateful to a lot of people who made it possible for me to write this thesis. My supervisors at University of Tromsø, Geoffrey D. Corner and Steffen Berg for giving me this thesis, for their patience, guidance and good conversations in the field. My external supervisor, Tom Rune Lauknes from Norut for his continuous encouragement and guidance in the, for me, new field of remote sensing. Further he put me in contact with key persons at Geological Survey of Norway, Nordnorsk fjellovervåkning and Åknes/Tafjord Beredskap. And last but not least for introducing me to the coffee machine at Norut. Yngvar Larsen from Norut for giving me expert advice during InSAR processing and for giving me access to his decomposing scripts that made it possible for me to produce 2D InSAR data. I would like to thank the handymen at Nordnorsk fjellovervåkning for their good humor and hospitality, which resulted in both accommodation and transportation during my field work. Further, I would thank John Dehls at Geological Survey of Norway and Jan P. Holm for University of Tromsø for teaching me tricks in ArcMap. Halvor Sverre Sæter Bunkholt and the rest of the gang from Geological Survey of Norway, for letting me participate on educational and fun days in the mountains during their field campaign in August 2012. Lars Harald Blikra for giving me detailed description, good advice, and insights into the sleeping dragon of the Nordnes rockslide while inspecting drill cores. I would like to thank my Mum, Dad and my Sister for encouraging me and correcting numerous spelling errors. Thanks to the gang at “The Red Barracks" at The Department of Geology. I appreciate the many good conversations we have had during lunches and field excursions over the years.

Norut together with The Department of Geology in The Faculty of Science and Technology at the University of Tromsø, supported me with funding that made it possible to conduct my field work and attend the AGU conference in San Francisco.

This thesis would not be possible without the good will of certain people sharing their datasets. Åknes/Tafjord Beredskap IKS shared their mapped structures from Nordnes rockslide. The TerraSAR-X data used, have been provided through the German Aerospace Centre (DLR) TerraSAR-X AO projects #GEO0565 and GEO0764. GPS data originate from Nordnorsk fjellovervåkning. The digital elevation model was provided by Norwegian Mapping Authority (NMA) and orthophotos used were provided by

NorgeDigitalt/NorgeiBilder. In addition my supervisor, Geoffrey D. Corner, let me use his quaternary geological map over Storfjord that is still under preparation.

I consider myself lucky to have been part of at rewarding and challenging journey, and have saved the greatest thanks of all to my sweet and caring wife Anita and our wonderful children Sigrid, Gabriel and Sondre. Thanks for your patient and support.

Table of contents

1 Introduction ... 1

  1.1 Motivation ... 5

  1.2 Overview of study area ... 5

  1.3 Slope processes included in the thesis ... 7

  1.4 Regional geology ... 9

2 Methods ... 17

  2.1 Reference systems and conventions ... 18

  2.2 Introduction to SAR and interferometry, limitations and sources of error ... 21

    2.2.1 Interferometry ... 23

    2.2.2 Limitations caused by high gradient topography ... 27

    2.2.3 Decorrelation and incoherence ... 27

    2.2.4 Reference point selection ... 28

    2.2.5 Other limitations ... 28

  2.3 Processing of InSAR dataset ... 30

  2.4 Calculation of 2D InSAR displacement dataset ... 31

  2.5 Other datasets and tools ... 36

  2.6 Verification of 2D InSAR data ... 37

  2.7 Study area ... 38

3 Results, interpretation and discussion ... 41

  3.1 Verification of InSAR technique and 2D InSAR data ... 41

  3.2 Overview of InSAR data from the whole Storfjord-Kåfjord-Lyngen area ... 48

  3.3 Displacement patterns at selected localities ... 52

    3.3.1 Nordnes Rockslide ... 52

    3.3.2 Gamanjunni3 rockslide in Manndalen ... 67

3.3.3 Rock glacier in Helvetesdalen on Nordmannviktinden....................................79
3.3.4 Joppolbakkan area with tongue shaped features on east side of Nordnes peninsula..88
4 Summary and conclusions 99
4.1 Suggestions to further work...105
5 Acronyms...107
6 Appendix 1 – Corner (in prep) – Storfjord – Quaternary geological map 109
7 Appendix 2 – Tolgensbakk og Sollid (1988) – Kåfjord – Quaternary geological map ..111
8 Appendix 3 – Calculation of horizontal and vertical displacement vectors from ascending and descending InSAR-data...113
9 Appendix 4 – InSAR processing..119
9.1 InSAR data used for verification against GPS at the Nordnes rockslide 119
9.2 InSAR data related to geomorphological- and structural elements 120
10 References 125

1 Introduction

The importance of mapping, monitoring and mitigating geohazards is increasing due to an increasing awareness of geohazards and a need to adopt new land for homes, roads and other human activity. Mapping of landslides have traditionally been conducted based on mapping of historical slides, interviews with locals, field investigations, calculation of runout-distances and estimation of risk. Remote sensing techniques like Interferometric Synthetic Aperture Radar (InSAR) have made it possible to map and monitor much larger areas than can be monitored using traditional GPS (Global Positioning Systems).

Historically the mountains and fjords in the Northern Troms have experienced large rockslides in the past. Church books tell about a rockslide event in 1810 in Pollfjellet that reached the Lyngen fjord, created a devastating tsunami with meter scale run-up at 20 km distance that killed 14 people and wrecked 3 farms (Dahl and Sveian, 2004). At present, the most imminent danger in the Troms is considered to be the possible collapse of the rockslide at Nordnes (Jettan) (Blikra, 2009). The worst-case scenario predicts a 11 Mm3 slide, creating a tsunami with maximum 25-45 m run-up height. It will shatter local communities in the Storfjord, Kåfjord and Lyngen, threatening the lives of thousands of people.

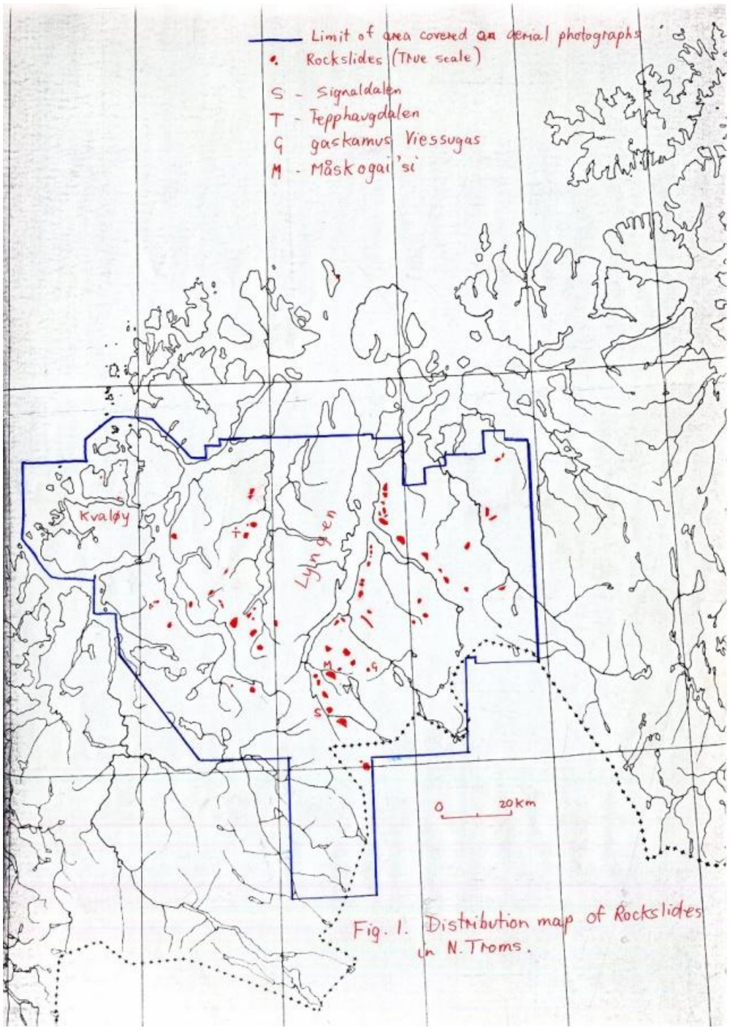

Fig. 1 - Distribution of rockslides in North Troms, Norway (Corner, 1972).

The first work describing rockslides in the region was performed by (Corner, 1972). His work with aerial photographic interpretation resulted in a rockslide distribution map for North

Troms (Fig. 1). Recently a lot of work concerning rockslide activity in the region has been conducted by several authors e.g. (Blikra, 2009; Blikra et al., 2006; Braathen et al., 2004; Bunkholt et al., 2011; Henderson et al., 2008, 2009, 2010; Henderson et al., 2007).

This thesis is a continuation of the project "ROS Fjellskred i Troms". This is a joint project between the Geological Survey of Norway (NGU), University of Tromsø (UIT) and Norut (Northern Research Institute) and the municipalities of Tromsø, Lyngen, Kåfjord, Storfjord, Kvænangen, Kvæfjord and Nordreisa. The projects main goal was to map high risk objects and document the risk associated with them. The “ROS Fjellskred i Troms” project combed data from three remote sensing techniques; Light Detection and Ranging (LIDAR), satellite based interferometric synthetic aperture radar (InSAR) and ground based InSAR with GPS data and data collected during mapping of geological structures in the field. This has proven an effective tool for pinpointing high-risk objects.

There have been three former theses carried out during the "ROS Fjellskred i Troms" project emphasizing on rockslides (Hannus, 2012; Husby, 2011; Rasmussen, 2011). The main focus of each of these theses, has been to investigate a single rockslide with regard to regional fault-, lineament- and foliation- directions, deformation structures, permafrost appearance, drainage patterns and finally suggest the factors controlling the deformation.

Norway with its steep and mountainous topography rising from deep fjords is exposed to rockslides with potential to generate tsunamis capable of devastating communities in whole fjord systems. In this context InSAR, as opposed to light detection and ranging (LIDAR)-, GPS and field based surveys, has a great advantage to regular cover larger areas. Depending on repeat pass time and frequency of the InSAR satellite, it can monitor ground displacement in the scale of centimeters to millimeters.

This thesis is a result of interdisciplinary work combining both geology and remote sensing. The main goal of this thesis is to combine InSAR data from two different satellite geometries (ascending and descending (Fig. 2)) to decomposed InSAR (2D InSAR) data. Then discuss if 2D InSAR data can give a more adequate and comprehensible presentation of displacement than studying the ascending- and descending InSAR data separately.

InSAR are decomposed InSAR data in East-West plane. This includes total displacement, horizontal-, vertical displacement components (all measured in mm/y) and dip of the total displacement vector (degrees).

(Fig. 2). The name 2D InSAR, refer to the fact that all data are vectors in the East-West plane. See Section 2.4 for a more thorough explanation of decomposition of ascending- and descending InSAR displacement data to 2D InSAR displacement data.

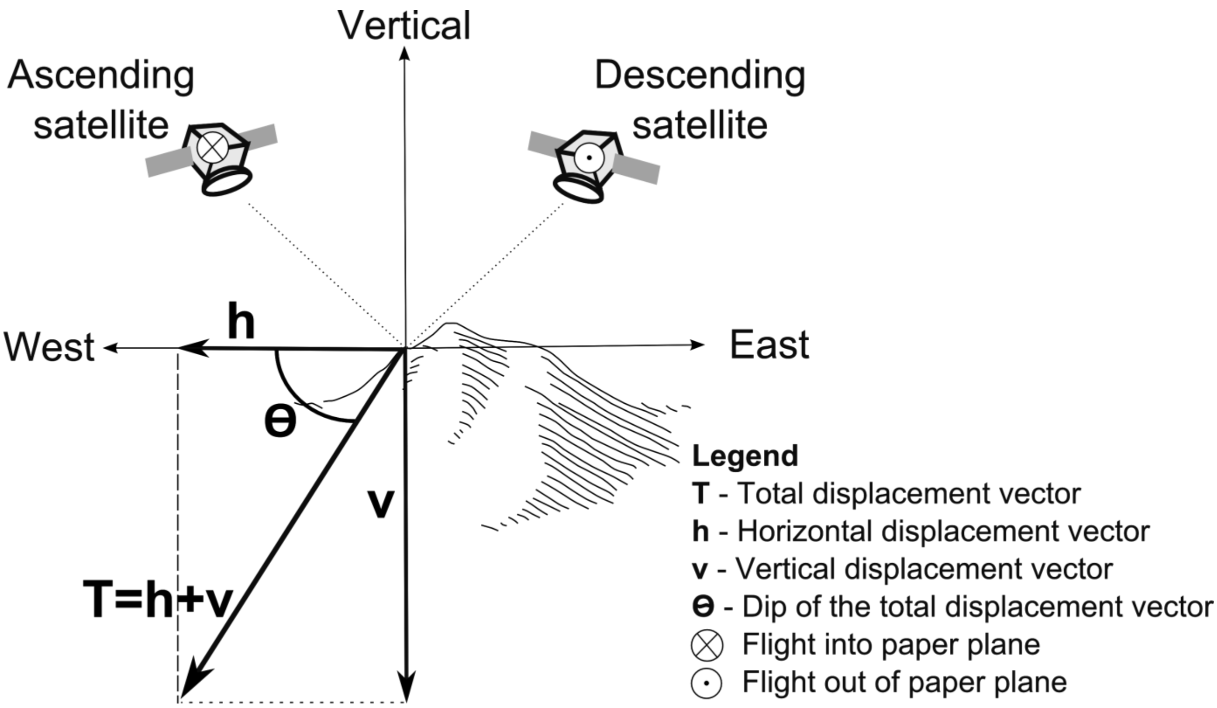

Fig. 2 - Profile view of 2D InSAR data

The objectives can be summarized as follows:

A) Processing of InSAR data and calculation of 2D InSAR data
B) Verifying results against displacement data from GPS
C) Relating InSAR and 2D InSAR data to different forms of slope processes in the study area

Datasets used are TerraSAR-X radar satellite data (2009 to 2011) from the German Aerospace Centre (DLR), GPS data (2011) from Nordnorsk Fjellovervåkning (NNFO), geological structures from Åknes/Tafjord Beredskap IKS (ÅTB), digital elevation model (DEM) and orthophotos from The Norwegian Mapping Authority (NMA).

First the SAR data (TerraSAR-X) have been processed to produce displacement maps using the GSAR application from Norut. These results have been decomposed to 2D InSAR data based on code from Norut. InSAR data and 2D InSAR data were then verified against GPS data from the Nordnes rockslide. Lastly the InSAR- and 2D InSAR datasets were compared to geological- and morphological structures, observations in the field, on orthophotos and mapped by ÅTB, using the ESRI ArcMap application.

1.1 Motivation

The use of Interferometric Synthetic Aperture Radar (InSAR) to map displacement in the earth's surface and landslide areas has been documented by many studies e.g. (Berardino et al., 2002; Hilley et al., 2004; Lauknes, 2010; Massonnet and Feigl, 1998; Strozzi et al., 2005) . Studies decomposing InSAR data to 2D InSAR data have focused on earthquakes (Wright et al., 2004) and ice flows (Joughin et al., 1998). This study will add to previous work by visualizing displacement patterns and kinematics of slope processes including rock glaciers, rockslides and solifluction.

Interpreting InSAR displacement maps correctly can be challenging. Knowledge of the line of sight (LOS) direction for the space born satellite when capturing data, is a necessity for understanding how much of the ground displacement that can be measured. To complicate the picture even more, this sensitivity to displacement can vary due to different satellite tracks. InSAR data captured in different satellite tracks is sensitive to displacement in different directions. In this thesis, an attempt to make the remote sensing technique more sensitive to displacement by combining InSAR data from two satellite tracks to 2D InSAR data. Resulting horizontal- and vertical displacement are then verified against displacement data from GPS. 2D InSAR data are then used to produce displacement maps that hopefully are easier to interpret correctly.

1.2 Overview of study area

The study area is situated in the northern part of Troms County in Northern Norway. This is an area with mountainous topography formed by multiple glaciations. Steep mountains are surrounding fjords and valleys. The study area is defined by the area covered by both the ascending- and descending data from the TerraSAR-X satellite(Fig. 3).

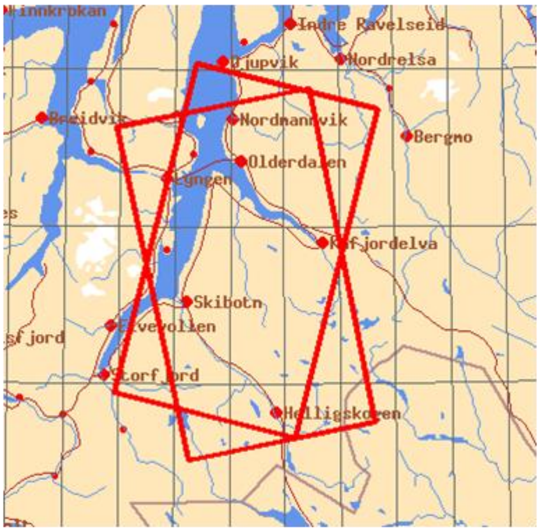

Fig. 3 – Study area defined by ascending- and descending TerraSAR-X data.

The field localities are located in Storfjord, Kåfjord and the Lyngen fjord (Fig. 4). Kåfjord is a North-West to South-East striking fjord with a large number of rockslides (Bunkholt et al., 2011). Storfjord is NS striking fjord also susceptible to large number of rockslides on the East side. Localities are selected to test the application of 2D InSAR data on different kind of slope processes in the study area. The chosen localities are a rock glacier on Nordmannviktinden, tongues shaped formation at Joppolbakkan on East side of Nordnes, Gamanjunni3, a fast moving rockslide in Manndalen and the Nordnes rockslide (Fig. 4).

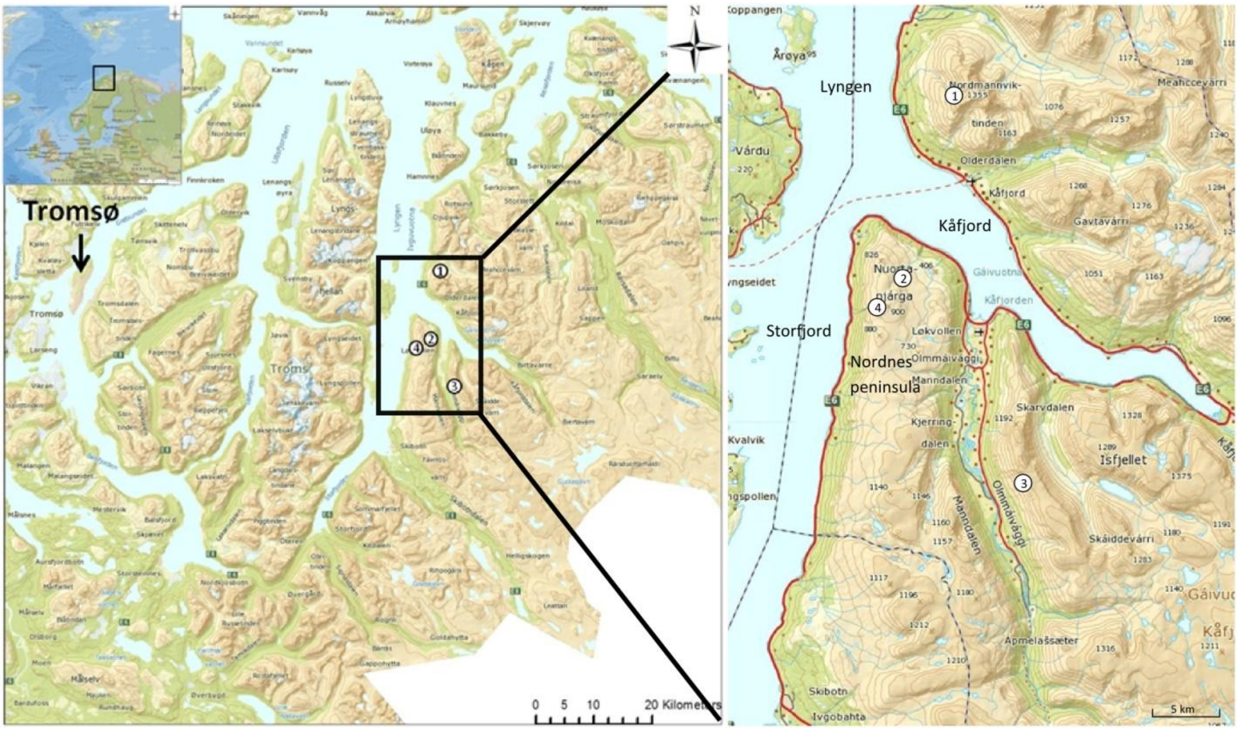

Fig. 4 – Localities marked with numbered circles: Rock glacier on Nordmannviktinden (1), solifluction tongues at Joppolbakkan (2), Gamanjunni3 fast moving rockslide (3), Nordnes rockslide (4). (Kartverket)

1.3 Slope processes included in the thesis

Rock-slope failures will be described using terminology from (Braathen et al., 2004). They can be sub-divided into rockfall areas, rockslide areas and complex fields (Fig. 5). Rockfall or toppling involve one or more unstable block in steep (sub-vertical) terrain. Rockslide areas are slope parallel, have sliding planes along weak zones in the bedrock (foliation, exfoliation) and are found in moderate dipping terrain. Complex fields have complicated internal deformation. They may have listric or planar fault geometry (domino style) controlled by deep-seated, low-angle detachments. The structures and morphology include elements as rotated fault blocks, trenches and sink-holes, fault scarps, crevasses, a back-bounding graben, terraces, benches, ridges, talus areas and tongue shaped.

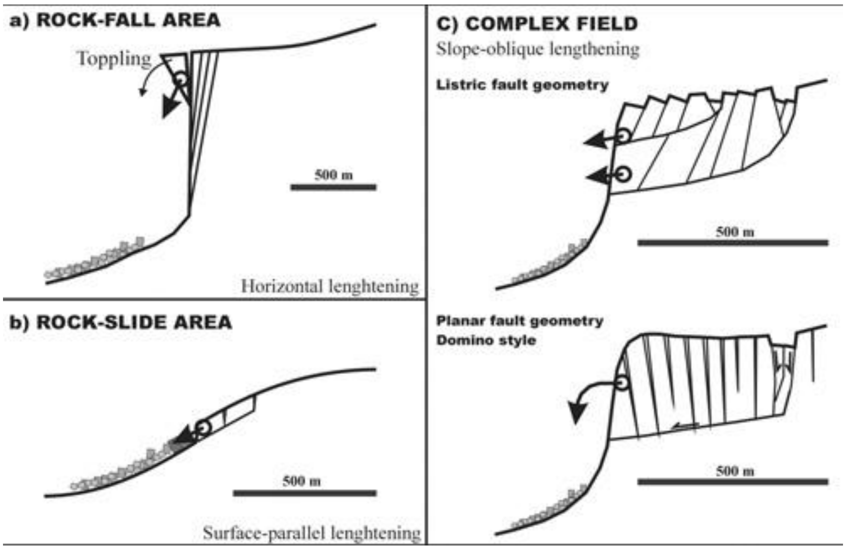

Fig. 5 - Geometric model for rock-slope failures, distinguishing between joints, extension fractures, shear fractures and faults (Braathen et al., 2004).

Rock glaciers have are defined by (Singh et al., 2011) as follows: “A rock glacier is a lobate or tongue-shaped landform consisting of rock debris and either an ice core or an ice-cemented matrix. This landform is distinguished by its distinctive series of ridges and furrows on the surface, which give the form its characteristic “wrinkled” pattern. Rock glaciers serve as distinctive reservoir for debris and water in alpine drainage basins”. It flows downslope resembling the form a glacier. It has a steep front and side slopes. The surface has ridges and furrows sub-perpendicular to the direction of flow. More than 100 rock glaciers were found in the Kåfjord area after detailed geomorphological mapping (Tolgensbakk, 1988) (see Appendix 2 – Tolgensbakk og Sollid (1988) – Kåfjord – Quaternary geological map). They are thought to origin from rockslide activity during the early Holocene due to neotectonic activity (Frauenfelder et al., 2008). Some are relic and some are active as documented by (Frauenfelder et al., 2008).

Solifluction is defined as a “slow gravitational down slope movement of water saturated, seasonally thawed materials” (Thomas and Goudie, 2000). Solifluction can develop at low gradients. For solifluction to develop, the slopes has to be sufficiently gradual to retain water and yet sufficiently steep to allow downslope gravitational movement of materials. Freezing and thaw processes move the sediments up orthogonal to the slope gradient when freezing and down with an angle close to the slope gradient when melting. The result is tongue shaped lobes and terraces. The influence of permafrost can give the melted sediment a frozen detachment to slide on (Singh et al., 2011).

1.4 Regional geology

In this Section the geological context of the study area will be described.

Topography, relief and geomorphology

Scandes, name proposed by Ljungner (1944, 1948), is the mountain range covering one third of Norway, one-tenth of Sweden and a small part of Finland. Scandes has a long geologic and geomorphic incremental evolution. It can be divided into six stages describing the rise and fall of the Caledonian mountain range, periods of erosion, stages of uplift and last glacial erosion forming the Scandes mountain range we see today (Fig. 7, left and middle) (Corner, 2005b).

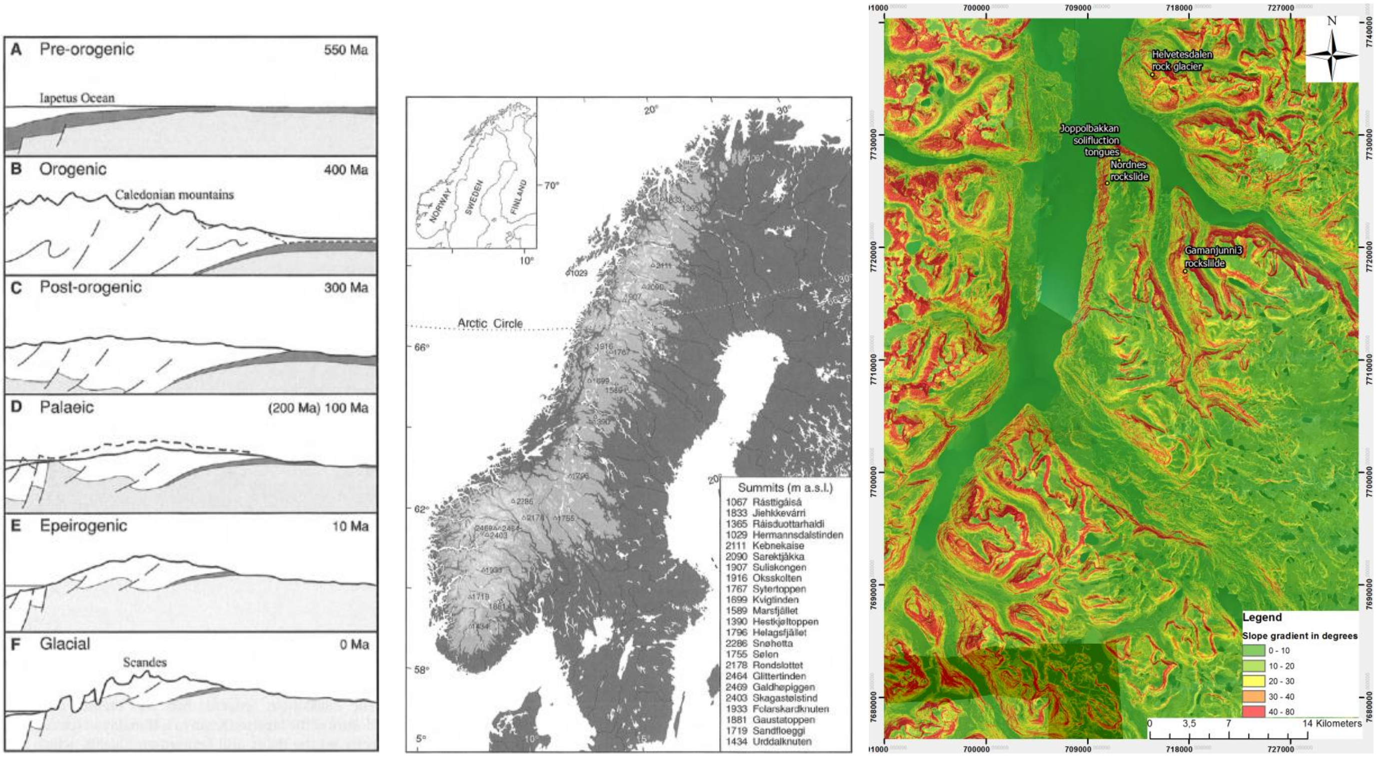

Fig. 6 Left: Geology- and geomorphic evolution stages of Scandes (Corner, 2005b). Middle: Scandes mountain today (Corner, 2005b) Right: Slope gradient map for the study area

Storfjord, Kåfjord the Lyngen fjord are part of the fjord coast with well developed fjords and alpine mountains (Corner, 2005a). Multiple glaciations have shaped the fjord morphology creating fjord basins, sills and shaped the mountains in a characteristics alpine style with horns, hanging valleys, arêtes and cirques (Fig. 8). The result is an alpine high–relief topography, with mountain peaks well above 1000 m (Fig. 6, right).

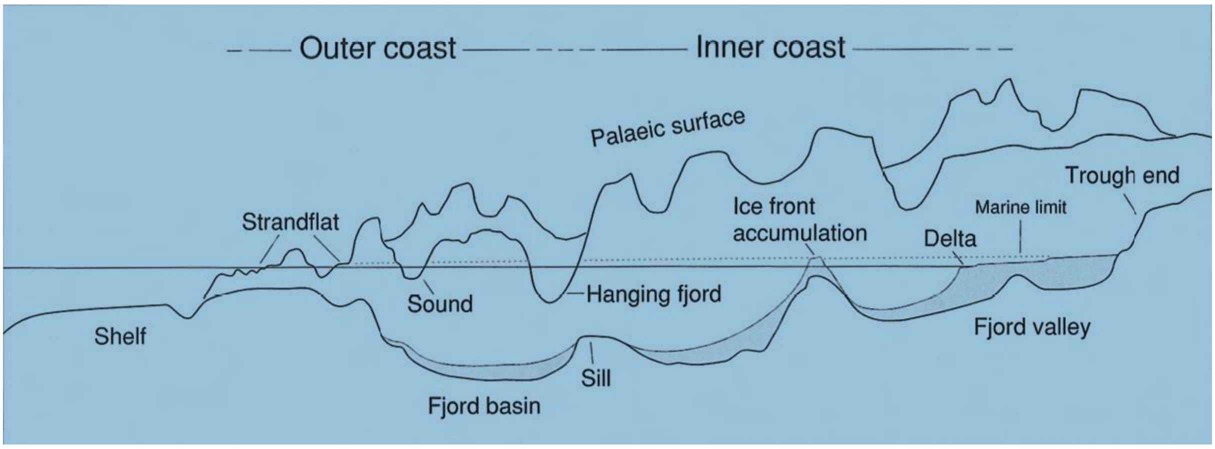

Fig. 8 - Transect of high-relief part of the Norwegian coast from outer coast to inner coast (Corner, 2005a)

Bedrock geology

Rocks in the region are part of the Caledonian nape sequence (Fig. 9). They origin from different geological environments and were stacked into present position during the closure of Iapetus ocean and the following Caledonian orogeny in Silur (Vorren and Mangerud, 2007). The napes where trusted over Precambrian basement rocks and there is an increase in metamorphoses grade from the lower to the upper napes.

All the field localities in this thesis are part of the upper nape unit. This nape contains rocks with a large variation in deformation style and composition.

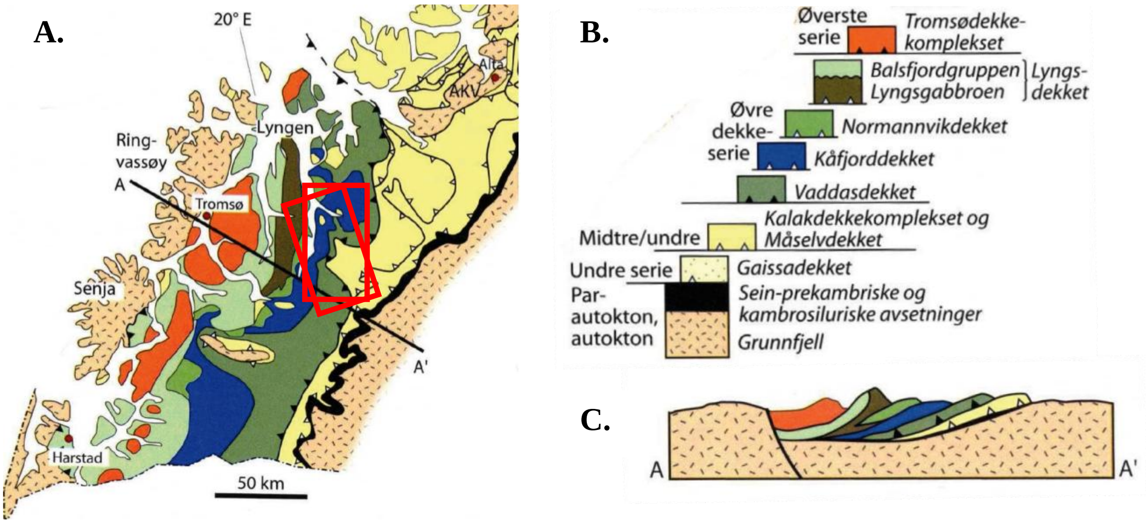

Fig. 9 –A: Map view of the Caledonian nape sequence with red rectangles showing study area defined by satellite data (Modified after Bryhni et al., 2007) B. Legend (Bryhni et al., 2007) C. Profile view AA' of Caledonian nape sequence (Bryhni et al., 2007). See for map view of profile line A-A'.

In the study area napes from the upper and middle/lower allochtone, lower allochtone together with para-autochtone Late-Precambrian and Cambro-Silurian rocks and autochtone Precambrian basement is outcropping. From the upper allochtone the Reisa nape complex with Nordmannvik nape, Kåfjord nape and Vaddas nape is represented in the study area (Zwaan, 1988).

Previous work show that both onshore and offshore fault systems on Lofoten and Vesterålen Margin (LVM) are dominated by NNE-SSW striking, right stepping en echelon faults. They developed as a consequence of Triassic through early Cretaceous WNW-ESE extension direction(Hansen, 2009) (Fig. 10).

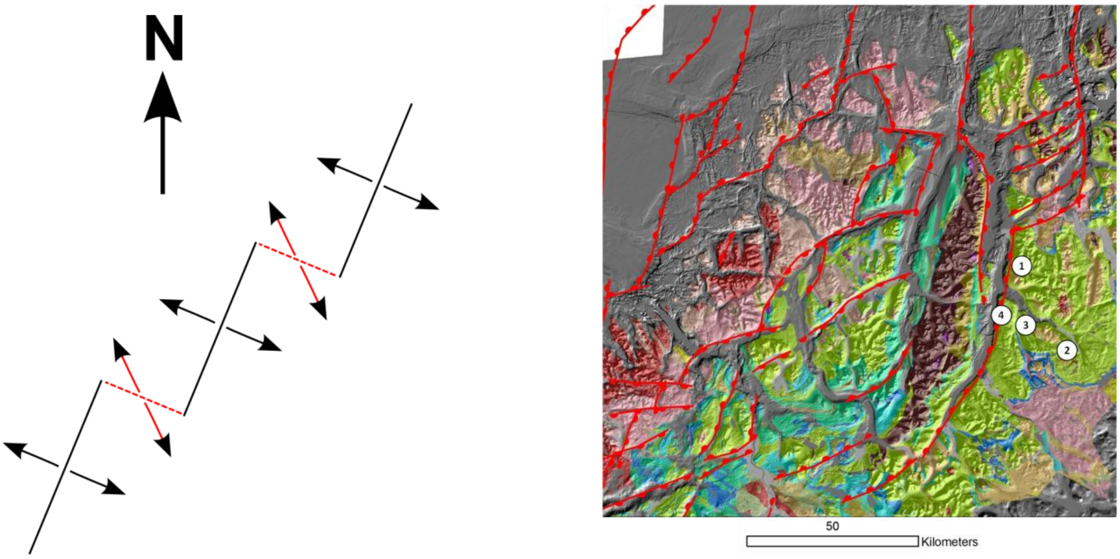

Fig. 10 – Left: Solid black lines indicates NNE-SSW striking, right stepping en echelon faults as a consequence of Triassic through early Cretaceous WNW-ESE extension direction (black arrows). Dashed red lines indicate NE-SW to E-W striking transfer zones from late Cretaceous to Paleogene NNW-SSE extension (red arrows)

Right: Fault zones of North Norway with field localities (Hansen et al., 2011)

The NNE-SSW striking faults are linked by NE-SW to E-W striking transfer zones. These NE-SW to E-W transfer zones correspond to late Cretaceous to Paleogene NNW-SSE extension direction (Hansen, 2009). These NE-SW trending lineaments are noticeable in the Caledonian nape terrains for example the Vestfjorden-Vanna Fault and the Kvaløysletta-Straumhella Fault (Gabrielsen et al., 2002).

Glaciation- and deglaciation history

During the Neogene period (23 – 2.5 Ma) the global temperature dropped considerably resulting in a series of glaciations in the Quaternary period (2.5 Ma – present). Deep ocean logs document about 50 cycles of climatic variation from 2,7 Ma to 0.9 Ma which indicates the same number of small glaciations on the northern hemisphere. They lasted between 41 000 and 23 000 years. The last 600 000 years, glaciations have been larger with a frequency of around 100 000 years (Vorren and Mangerud, 2007). The present morphology, topographic gradient and landscape together with the ongoing isostatic uplift are results of these glaciations. Warmer climate made the ice shield retreated from Eggakanten after last glacial maximum (LGM), about 18 000 – 20 000 C14 years ago. The ice shield re-advanced several times and halted before retreated. Today we find moraines documenting these re-advances. The oldest one is from the “Coast stage” followed by the “Fjord stage” (Landmark and Møller, 1979). Then the Skarpnes event followed with a longer colder period called the Younger Dryas (Tromsø-Lyngen event). This lasted from 11 000 – 10 000 years from now and resulted in the most notable glacial formations in the region (Vorren and Mangerud, 2007). Work by (Corner, 1980) conclude that there have been local re-advances (Ørnes event c. 9800-9900 ±150 B.P., the Skibotn event 9500-9600 ±250 B.P., and a younger event c. 9400

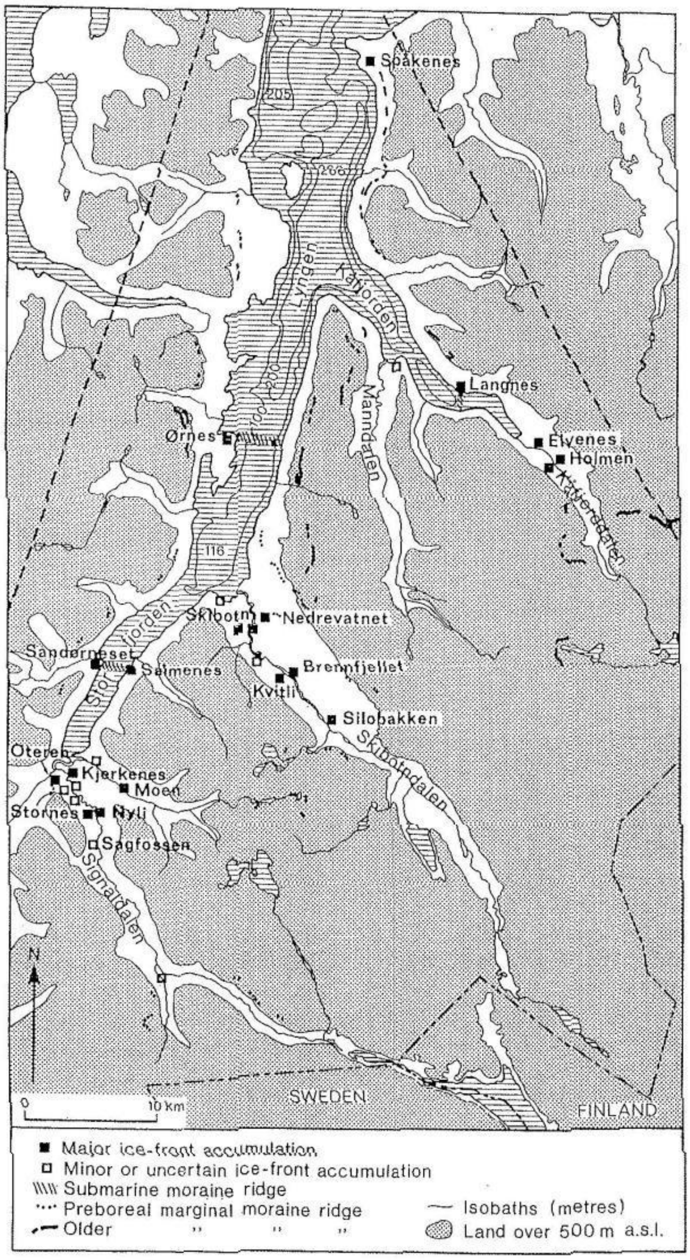

Fig. 11 - Major ice-front accumulations, submarine moraine ridges and Preboreal marginal moraine ridges in Lyngen-Kåfjord-Storfjord (Corner, 1980)

±250 B.P.) during the Preboreal period in the area as a result of climatic variations. By plotting marine limit (ML) on shore line diagrams he correlated and dated major ice-front accumulations, submarine moraine ridges and Preboreal marginal moraine ridges in Storfjord-Kåfjord-Lyngen (Fig. 11) (Corner, 1980). This detailed dating can tell how long slop processes have been active in the area (Corner, D. G., 2013, personal communication)

Present climate

Present climate is in the region is subarctic, characterized by long cold winters and short cool summers. The state of the present distribution of permafrost is not well mapped and ongoing research projects. The present permafrost state in the Northern Norway has been documented from borehole data (Christiansen et al., 2010). The findings indicate a rise in ground temperature and an increase in thickness of the active layer. Permafrost is found in discontinuous patches as low as 550 m.a.s.l. in the inner part of the northern Scandinavian mountains, and above 990 m.a.s.l. at the coast (Christiansen et al., 2010).

Preliminary results in ongoing studies with temperature loggers at Nordnes (Blikra, L. H., 2013, personal communication) indicates presence of patches of permafrost down to 200 m.a.s.l.

Glacio-isostatic uplift

The Earth’s crust is elastic. Extra weight added by ice during glaciations led to depressions in the crust. When the ice sheet melts and weight is released, the crust will uplift to its original position before the glaciation. This isostatic rebound started after the LGM and is still an ongoing process in Fennoscandia with seismic events. An example is the recent earthquake activity in the Stuorragurra Fault in the Mierujavre-Sværholt Fault Zone in Finnmark is an example of this (Dehls, 2000; Gabrielsen et al., 2002). The coastline of Troms has a yearly uplift of 1-1,5 mm (Dehls, 2000). The isostatic rebound is correlated with the thickness of the ice and the time from glaciations. During LGM the peak of the ice mass was located in the area of Botniske Viken in Sweden. Ice below a certain depth conducts plastic deformation and flow as a liquid from high areas to lower laying areas. This flow of ice united into ice streams that drained the Fennoscandian ice sheet from Botniske Viken towards the margins. The crust in the inner part of the Storfjord-Kåfjord-Lyngen area therefore experienced more subsidence than the outer part during the glaciations, thus more isostatic rebound today (Fig. 12).

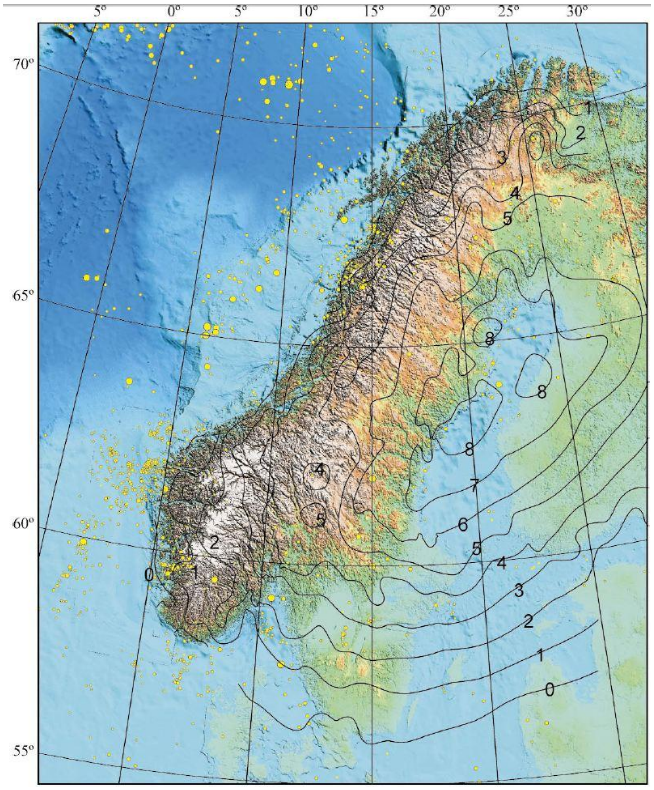

Fig. 12 - Current apparent uplift rates (in mm/yr) and locations of earthquakes with magnitudes greater than 3.0 since 1965 (Dehls, 2000).

Sea level, shore lines and marine limit

Marin limit (ML) is the highest elevation above today’s sea-level that have been affected by sea after LGM. ML is the uppermost shoreline. The level of shorelines is affected by two components, the level of local isostatic rebound changes in the global sea level, the global eustasy. When the ice sheets gradually melted after LGM the global sea level increased by 120 m, but because of an even larger simultaneous local isostatic rebound the oldest shore lines (ML) are located above the today’s sea level (Dahl and Sveian, 2004). The height of ML varies from about 100 m.a.s.l. in the inner parts of Storfjord to about 50 m.a.s.l. in the outer parts of Lyngen ((Corner, 1980) and Fig. 13 right). The Main line, shoreline produces during the cool Younger Dryas period (11 000 – 10 000 years from now) and the Tapes line, produced in a period when the sea level increased as fast as or faster than the isostatic rebound depending on location, are the most prominent shorelines preserved (Fig. 13 left). They were produced when the sea level were constant over a longer period of time (Dahl and Sveian, 2004).

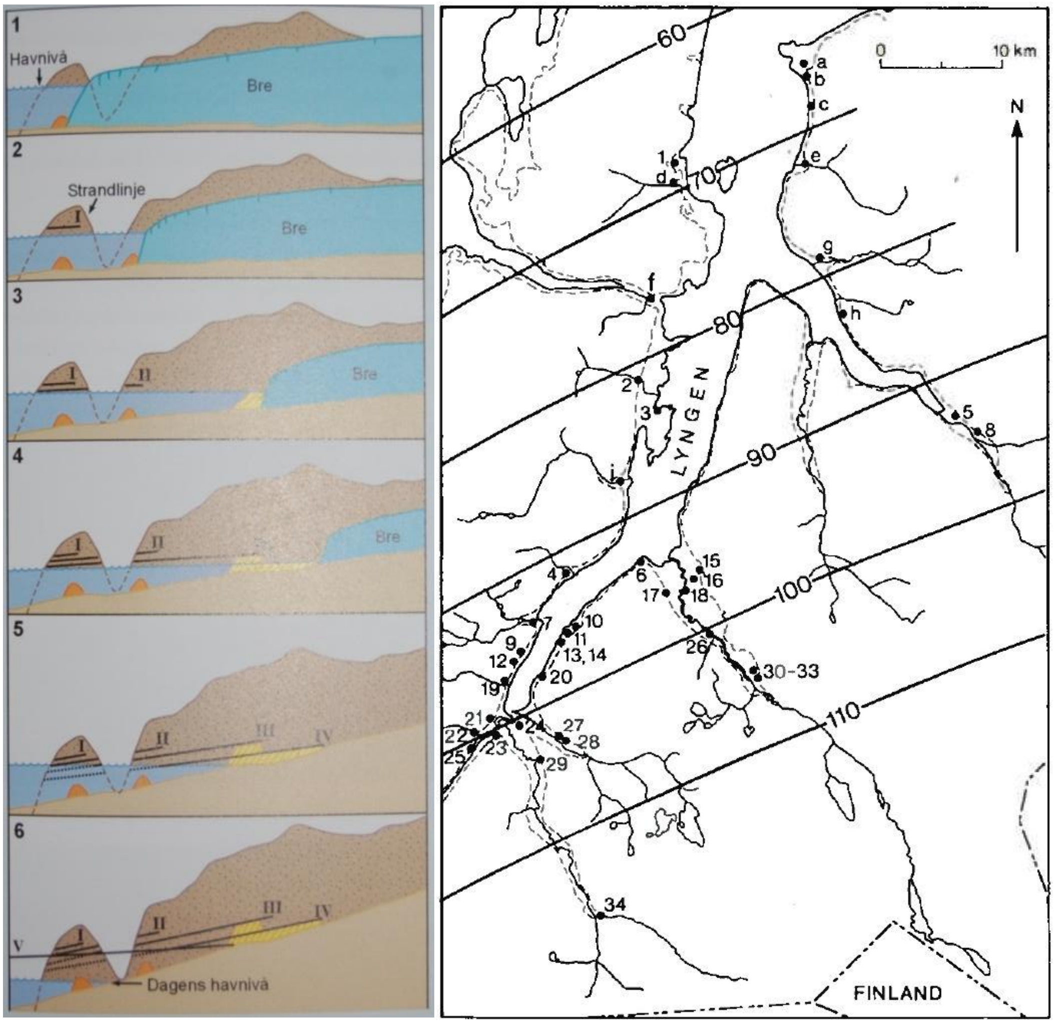

Fig. 13 Left: Examples showing profile of inclined isostatic rebound from coast to fjord after LGM with retrograding ice sheet and development of tilted shore lines, ice contact deltas, (Vorren et al., 2007). The Main line is produced in situation 3. Tapes line was formed during transgression in situation 5).

Right: Isobases for the sea level during the Tromsø-Lyngen event (Corner, 1980)

Surficial geology

Surficial deposits, exposed bedrock, sediment grain sizes, thickness and stratigraphy, direction of ice movement and surface morphology have been mapped in high detail in two Quaternary geological maps covering parts of the study area. One covering Storfjord and Skiboten area (see Appendix 1) (Corner, (in prep.)), and one covering outer part of Kåfjord area, (see Appendix 2 – Tolgensbakk og Sollid (1988) – Kåfjord – Quaternary geological map) (Tolgensbakk, 1988).

Superficial deposits in the study area include glacial-, marine- , fluvial- , mass-movement and colluvium deposits, weathered material, peat/bog- and anthropogenic material. The glacial deposits include till, marginal moraines, glaciofluvial deposits and are found in the valleys. Marine deposits and marine shore deposits are found from marine limit and down. Peat and bog material, most likely overlaying marine clays, are found in the valley plains below marine limit. Fluvial deposits are found in the lower parts of the valleys. Mass-movement deposits are found in the valley sides and other areas with high gradient. Areas with exposed bedrock lay as a band between the mass-movement deposits and the weathered material found on the upper part of the mountains. Surface morphological elements like avalanche paths, rock-avalanche fronts, rockslides, ridges, rock glaciers, talus cones, debris flow levees, pro talus ramparts and faults document a high degree of mass-movement in the study area(Corner, (in prep.); Tolgensbakk, 1988).

2 Methods

In this Section methods and data used in this thesis will be described. An introduction to the InSAR technique with its possibilities, limitations, and error sources are given. The decomposition of InSAR data to 2D InSAR data will be explained in Section 2.4. and

Appendix 3 – Calculation of horizontal and vertical displacement vectors from ascending and descending InSAR-data, contains the geometrical calculations regarding the decomposition of InSAR- to 2D InSAR data.

2.1 Reference systems and conventions

All lineations and geological structures are given by the right hand rule as described in (Pollard and Fletcher, 2005).

In this thesis displacement rates in mm per year (mm/y) from ascending- and descending InSAR data are represented as colors draped on orthophotos. Displacement **towards** the radar are blue, zero displacement is green and **away** from the radar are red (Fig. 14). Ascending and descending displacement rates from -5 to 5 mm/y are made transparent. Values in this order of magnitude are expected to be smaller than the uncertainty of the InSAR data.

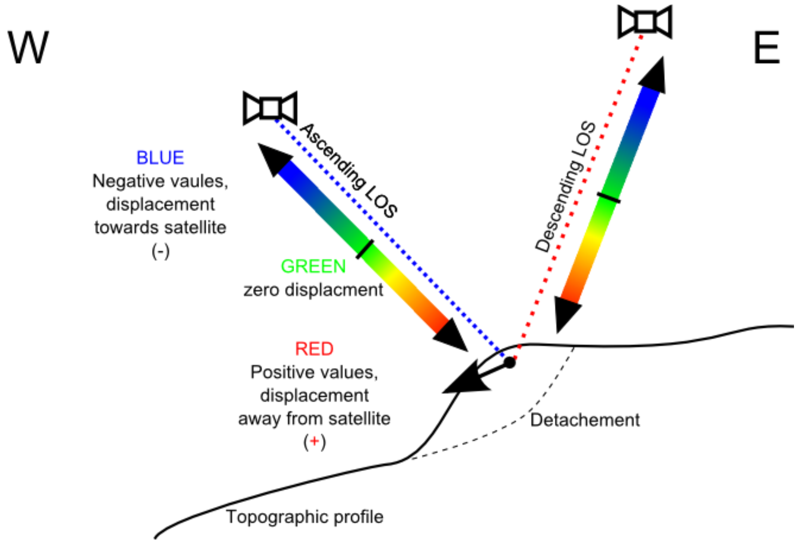

Fig. 14 – Colors or used to represent displacement direction in ascending- and descending geometry

2D InSAR data are also represented with color bar from red through green to blue. Negative horizontal displacement towards West is red. Positive horizontal displacement towards East is blue. Vertical downward displacement is negative and red. Vertical upward displacement is positive and blue (Fig. 15).

Length of total displacement vector (**T**) data is represented with a red-green-blue color bar. Red is maximum displacement observed and blue is zero displacement.

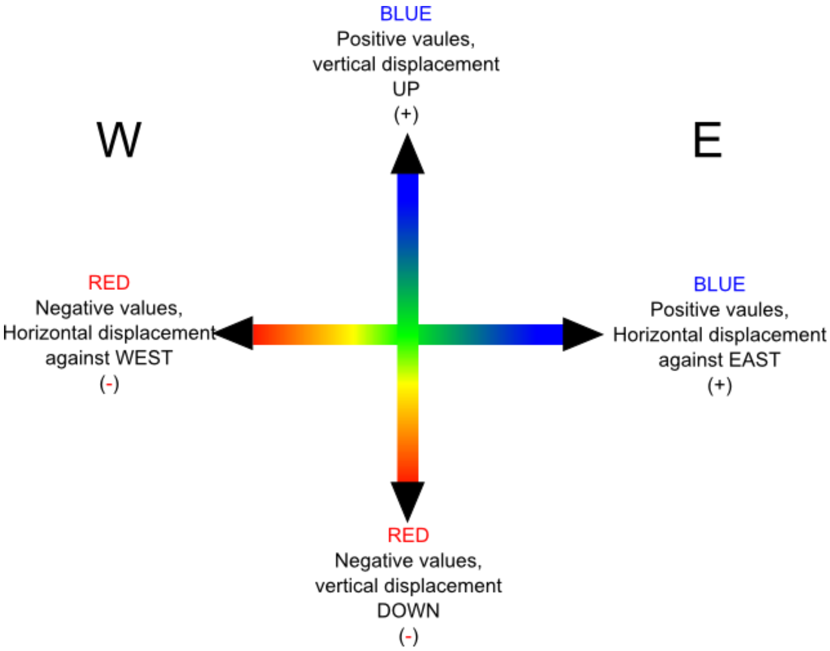

Fig. 15 - Reference system for horizontal and vertical 2D InSAR data

Data for the dip of total displacement vector is represented with a color palette divided into sectors of 45° (Fig. 16).

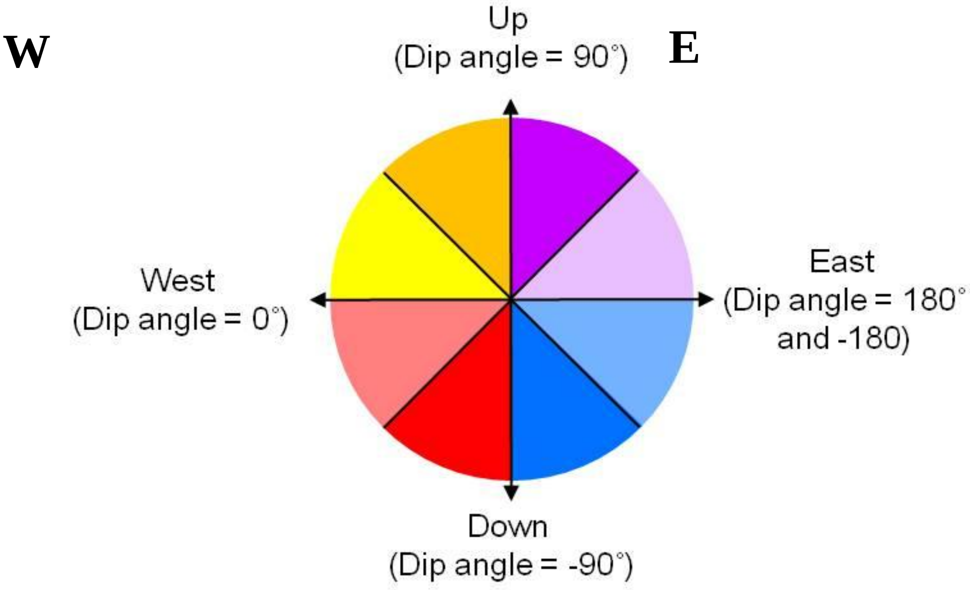

Fig. 16 – East-West profile with color palette for dip of total displacement vector.

GPS data in this thesis is given in three components in space (Fig. 17). dN is displacement in North-South direction, where North is positive. dE is displacement in East-West direction, where East is positive. dH is displacement in up-down direction, where up is positive.

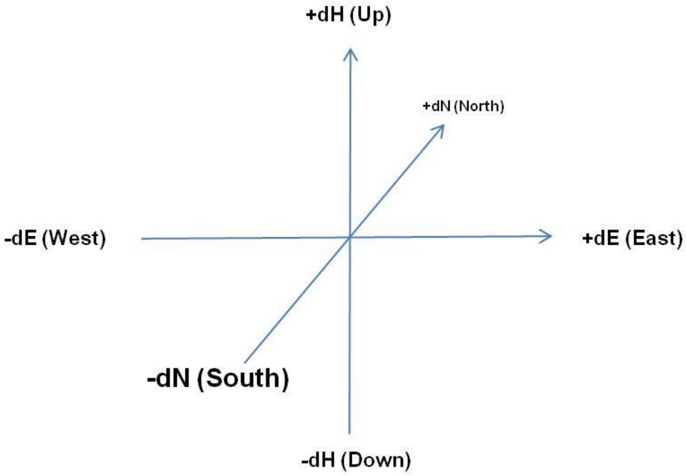

Fig. 17 - GPS reference system

2.2 Introduction to SAR and interferometry, limitations and sources of error

Synthetic Aperture Radar (SAR) is a space borne instrument, imaging the earth. The SAR instrument uses an active form of remote sensing. It transmitting radiated microwave pulses and receives reflected echoes (backscatter) from an illuminated area on the ground (ground swath) (Fig. 18) (Hanssen, 2001).

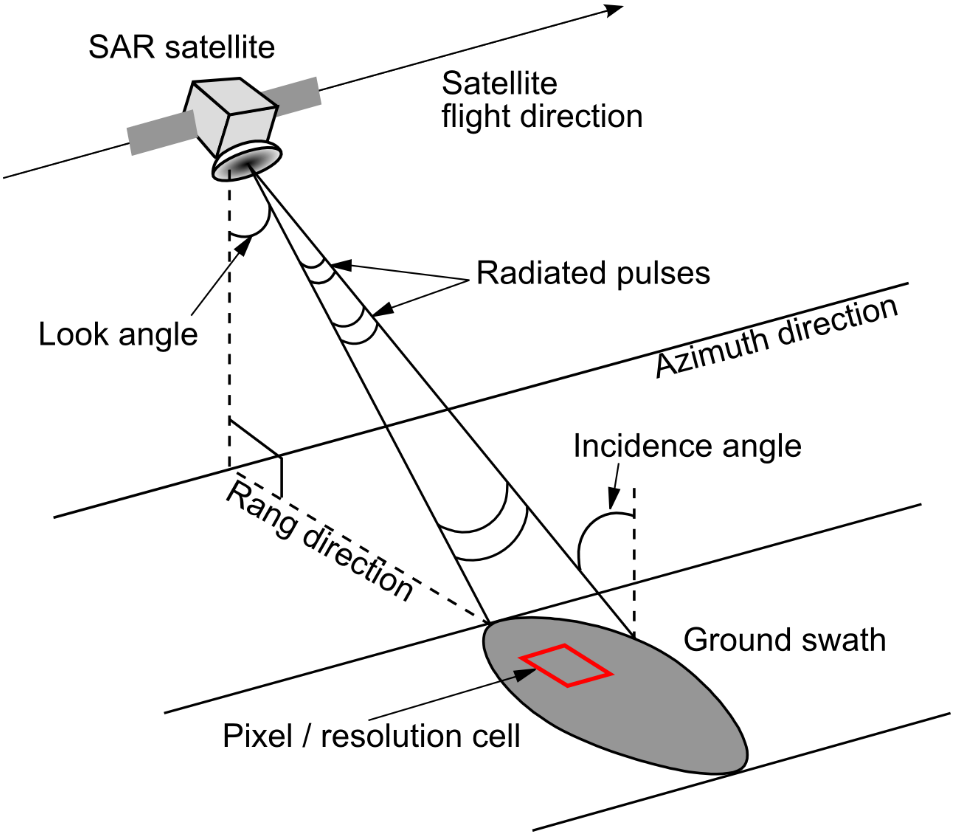

Fig. 18 - Geometry of a synthetic aperture radar (SAR) system. Modified after (Lauknes, 2010)

SAR data is organized in radar coordinates; range and azimuth (Fig. 18). Range is the distance from the radar to the ground. Azimuth is the distance along the flight-path. Range of an object is found by timing the return of the reflected echo. The object in azimuth direction is resolved by taking advantage of a phenomenon called the Doppler spread. This means that the echoes reflected from objects in front of the satellite is shifted relative to echoes reflected from behind (Rosen et al., 2000). The radar coordinates are converted to map coordinates in a process called geo-coding.

Ascending and descending satellite orbits

A polar orbiting satellite, orbits the earth from pole to pole. In ascending pass, it orbits from the South Pole to the North Pole, looking down and to the east-northeast. In descending pass, it orbits from the North Pole to the South Pole, looking down and to the west-northwest (Fig. 19). As the satellite passes over the same area in descending and ascending passes, it illuminates it from different directions.

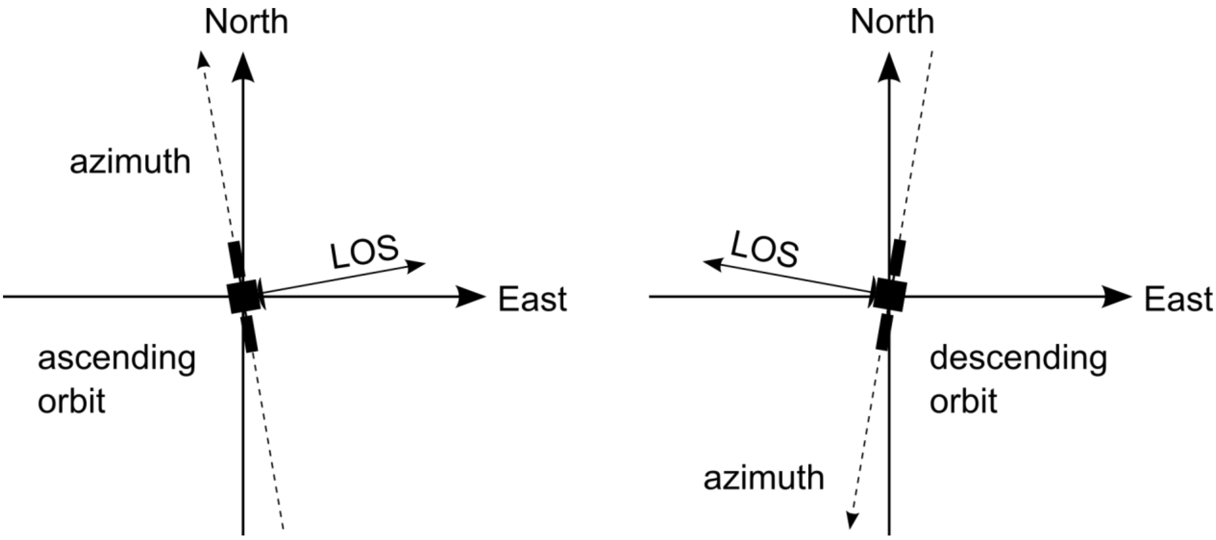

Fig. 19 – Map view of ascending and descending satellite orbits. Modified after (Lauknes, 2010).

Focusing, using a synthetic aperture

By using a process called focusing it is possible to improve the azimuth resolution by three orders of magnitude (Fig. 20 A and B). This is done by combining information from many pulses as the radar moves over and illuminates the terrain (Hanssen, 2001) (Fig. 20 C). Focusing radar images in this way improves the resolution equivalent of having a 20 km antenna instead of the normal ~10 m antenna.

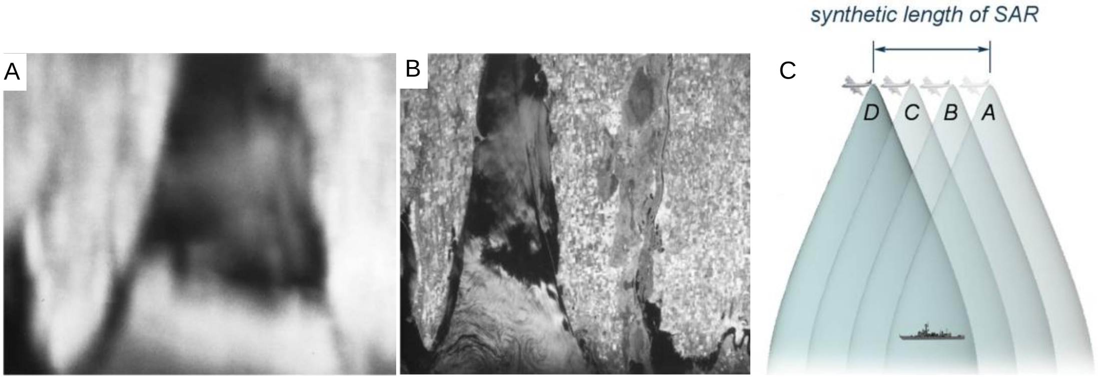

Fig. 20 –A. 100 x 100 km image acquired by ERS-1 over Crimea with 5 km azimuth and 14 km range resolution before focusing. B. Full resolution image as it looks after focusing (Massonnet and Feigl, 1998). C. Synthetic length of SAR antenna (Modified after Christian Wolff 2008 http://www.radartutorial.eu).

Amplitude and phase

The basic principle behind the radar technique (Radio Detection And Ranging), is sending out a pulse of electromagnetic waves and measuring the time it takes for the echo to return. Electromagnetic waves are quantified by their amplitude and phase. They are represented as complex numbers in a radar image. The amplitude of a radar image gives the terrains ability to reflect the microwave radiation. Dark areas indicate low signal and bright areas strong signal. Water can appear dark in a radar image if it is calm, reflecting the radar signal away. Angular structure forms, such as, fault-scarps, roofs and windows have a good reflectivity and appear very bright (Massonnet and Feigl, 1998). Phase is the instantaneous position of a waveform of a returning radar echo recorded by radar, measured in radians. For a radar image, the phase value is the sum of many different parameters of the ground. It is therefore random, thus uniformly distributed between $-\pi$ and π. The phase is the quantity used when calculating the displacement rates in InSAR data.

2.2.1 Interferometry

There are several interferometry configurations possible based on the application and the scale of displacement that will be monitored. Because of the contribution from multiple objects on the ground, the phase recorded for a pixel is random (Fig. A).

By combining two SAR-images from repeated acquisitions, it is possible to produce an interferogram showing the difference in phase. This is called interferometric phase (Fig. 23 B). This technique is called interferometry. The interferogram shows an interference pattern of fringes. This is lines with equal phase. A phase cycle of 2π is often referred to as a fringe (Hanssen, 2001). The fringes contain contribution from ground displacement, difference in perspective, topography, difference in atmospheric path delay, ground displacement and noise (Fig. 25) (Massonnet and Feigl, 1998).

This technique with a repeat-pass from days to years, was first used by (Goldstein et al., 1993) to study the dynamics of glaciers, (Massonnet et al., 1995) to document volcano deformation, (Massonnet and Feigl, 1998) studied earthquakes and (Berardino et al., 2003) used the technique to study land- and rockslides.

The phase contribution from ground displacement

If surface displacement has occurred between the acquisitions of the two SAR-images, this will introduce a phase contribution ($\Delta\phi_{displ}$ in Eq. (1)).

Phase contribution from the difference in perspective

Spatial baseline decorrelation is phase changes introduced in the interferogram because the radar where in slightly different positions when acquiring the two SAR-images. The difference in look gives a different backscatter signal in the two SAR-images. With precise knowledge about the satellite orbits used to acquire the two SAR-images it is possible to simulate and subtract this contribution from the phase. The distance between the satellites is called baseline (Fig. 21).

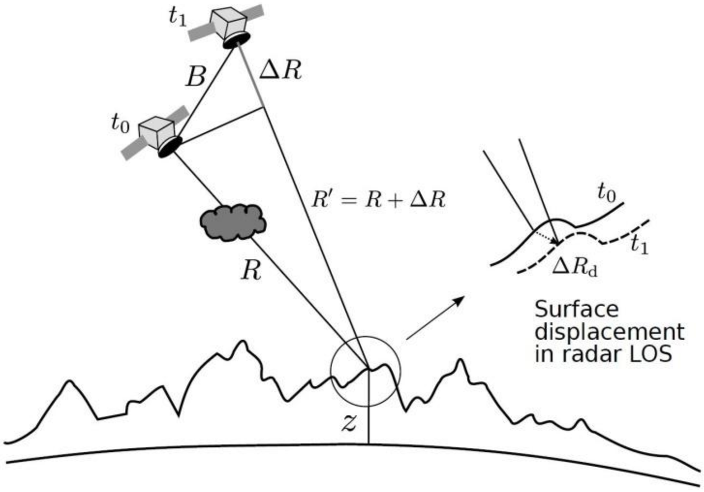

Fig. 21 – Surface displacement by between time t_0 and t_1 leading to a phase difference ΔRd detected. Cloud introduces phase contribution due to atmospheric path delay, $\Delta\phi_{APS}$. Altitude Z represent the phase contribution from the topography, $\Delta\phi_{topo}$. B is the baseline or distance between the orbits for the two acquisition times (Lauknes, 2010).

Phase contribution from the topography

This difference in position when acquiring the two SAR-images creates a phase difference introduced by the topography ($\Delta\phi_{topo}$ in Eq. (1)). By using a DEM, it is possible to calculate and remove this contribution.

The phase contribution from difference in atmospheric path delay

Phase contribution from atmospheric path delay (ϕ_{APS} in Eq. (1)) rise because of stratified or turbulent atmosphere during acquisition of SAR-images. Examples of atmospheric disturbance to phase signal produced by weather fonts and high winds giving contribution of 4 mm differences over the distance of 15 km, has been documented by (Massonnet and Feigl, 1998). They also give examples of cases where ionospheric perturbation caused by neutralization of the ionosphere after earthquakes and during volcanic eruptions. Steep mountains and deep fjords can produce a topography-like atmospheric signal where the phase differences are following topographic contour lines (Massonnet and Feigl, 1998) (Fig. 22).

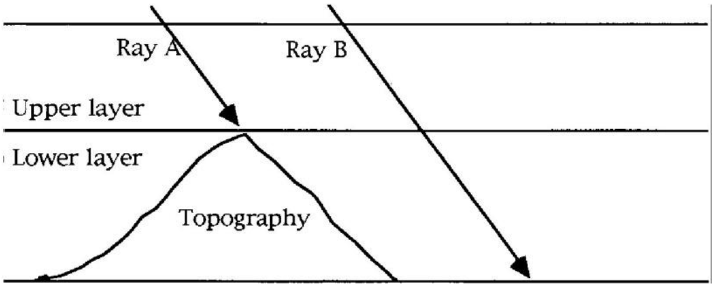

Fig. 22 - Hydrostatic troposphere effect (Massonnet and Feigl, 1998)

Calculating ground displacement

Interferometric phase $\Delta\phi$ in Eq. (1), can be used to calculate the ground displacement, $\Delta\phi_{displ}$, of the target that have occurred during the time between the two SAR-images were acquired. To achieve this, the phase contribution from the topography, $\Delta\phi_{topo}$, has to be subtracted together with the contribution from difference in atmospheric path delay $\Delta\phi_{APS}$ and other noise contributions like drift in frequency of the radar ($\Delta\phi_{decorr}$).

$\Delta\phi = \Delta\phi_{topo} + \Delta\phi_{displ} + \Delta\phi_{APS} + \Delta\phi_{decorr}$ (1)

Rearranging Eq. (1) gives phase contribution from surface displacement in Eq (2):

$\Delta\phi_{displ} = \Delta\phi - \Delta\phi_{topo} - \phi_{APS} - \Delta\phi_{decorr}$ (2)

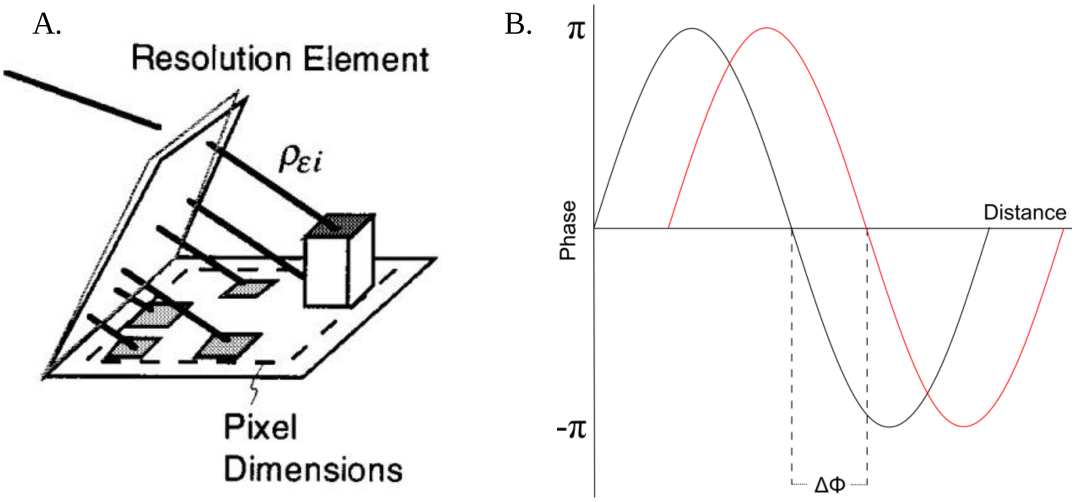

Fig. 23 – A. Signal in one resolution element in a SAR image is the sum of backscatter from multiple objects in the terrain (Rosen et al., 2000). B. Interferometric phase $\Delta\phi$ between two SAR-images.

Coherence

Coherence (γ) is a quality measure of the interferometric phase. The coherence value is between 0 and 1. If a pixel in an interferogram has a coherence value of 1, it means that the phase correlate perfectly between the two SAR-images used to form the interferogram. Phase noise and different forms of interferometric decorrelation will reduce the coherence. Temporal decorrelation arises from changes in geometrical or electrical properties of the terrain. Change in the position of leaves and grass are examples of short temporal geometrical changes leading to temporal decorrelation of the phase. Surfaces having high water content, such as wetlands and bogs result in reduced temporal decorrelation because of different scattering properties (Lauknes, 2010).

InSAR time series, stacking and the Small baseline method

During the 1990's while demonstrating the usefulness of InSAR to study surface displacement, it was discovered how large other contributions, like difference in atmospheric path delay and drift in frequency of the radar, could have on the final result. Using single interferograms for studying terrain displacement is vulnerable to errors in the DEM used to correct for the topographic contribution to the phase, orbital errors or contribution from difference in atmospheric path delay between the two SAR-images (Lauknes, 2010). To mitigate this, a technique averaging many interferograms was introduced. This stacking technique produce a mean displacement velocity map with reduced atmospheric noise (Zebker and Villasenor, 1992). Further the small baseline (SB) method was introduced by (Berardino et al., 2002). It made it possible to combine SAR images separated by large baselines into interferograms enhancing the chance to identify and filter out atmospheric phase artifacts. Using stacking technique it is possible to follow the temporal evolution of displacement phenomenons.

2.2.2 Limitations caused by high gradient topography

Foreshortening

When mapping mountainous regions using SAR some geometrical effects can limit the area that is possible to cover. One effect is stacking of radar pulses on slopes facing the satellite and a stretching of radar pulses on slopes facing away from the satellite. This is called foreshortening. A consequence of stacking is smaller pixels and higher resolution on slopes facing the satellite. Stretching gives larger pixels and lower resolution on slopes facing away from the satellite.

Layover and shadow

In steep terrain, when the top of the mountain is closer to the radar than the bottom, the echo from the top will return to the receiver antenna at the same time as the echo from the bottom. This is called layover. It occurs when signals are added together in a resolution cell. The result is a SAR image containing areas with very high intensity. In (Fig. 24), high intensity areas with layover are almost white. Shadow is another effect that is visible as black areas (Fig. 24). These are areas invisible to the satellite because they are in the radar shadow of steep mountains. In mountainous areas, layover- and shadow effects can mask out considerable amounts of the interferogram. These effects are dependent on the incidence angle of the satellite and the topography of the area.

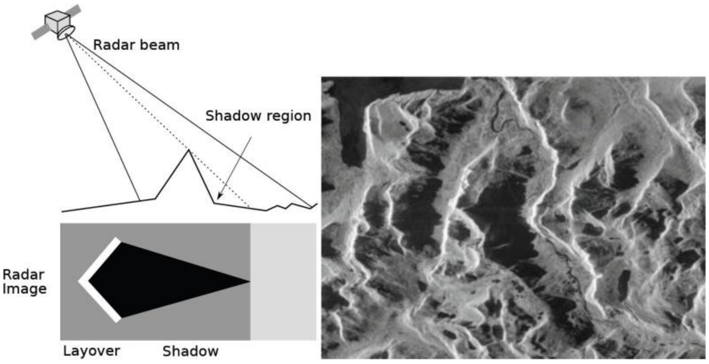

Fig. 24 – Layover and shadow are geometrical effects that occur in mountainous areas. (Lauknes, 2010).

2.2.3 Decorrelation and incoherence

To produce a coherent interferogram, there must be constant phase contribution between the two images. Imaging snow and water are extreme examples of the opposite; this is called decorrelation or incoherence. Each pixel will show a random phase change in the interferogram. Se ocean in the lower left corner of (Fig. 25) (Massonnet and Feigl, 1998).

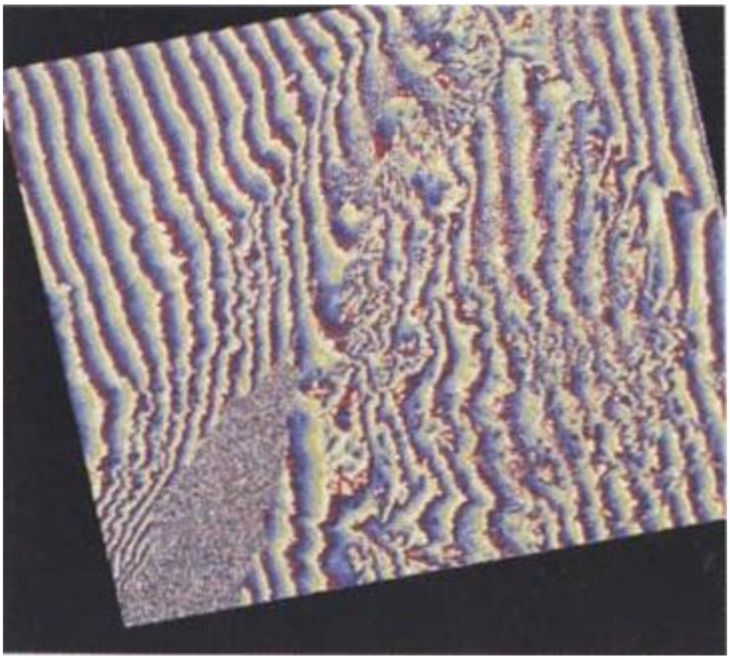

Fig. 25 - Interferogram fringe patterns over land and decorrelated water in the bottom left corner (Massonnet and Feigl, 1998)

2.2.4 Reference point selection

InSAR is a relative technique, depending on a reference point (zero displacement). It is important to select a stable reference point. Any displacement in the reference point will cause a shift in the resulting displacement. Reference points in this thesis are based on GPS data, orthophoto- and field investigation.

2.2.5 Other limitations

Displacement gradient is the maximum detectable displacement or difference in phase per pixel. This is one fringe (2π) per pixel. The TerraSAR-X satellite has a wavelength of 31 mm. One fringe (2π) is equal to half a wavelength (1,55 mm). With a pixel size of 10m x 10m the displacement gradient will be 1,55 mm displacement/m. For the ERS satellite the gradient is 2,83 mm/m.

Phase wrap around

If the displacement rate of an object is big or the time between acquisition for the SAR-images used to create the interferogram is too long, the phase difference in the interferogram will be larger than 2π. The phase value will then start over (wrap around) creating ambiguity about displacement.

Unwrapping errors often occur due to temporal decorrelation. In mountainous terrain and when displacement (fringes) cross fjords this can occur. Too large displacement can also give unwrapping errors. Unwrapping errors lead to errors in the final InSAR displacement map.

Limited temporal details

A limitation in the areas of high latitude, like the Northern Norway, is the irregularity in sampling frequency caused by short snow-free summers and long winters. This can result in underestimation of displacement rates due to problems linking interferograms from autumn in one season to spring in the next season (Dehls et al., 2012).

2.3 Processing of InSAR dataset

All processing was done using a generic differential interferometric SAR processing system called GSAR. GSAR is an interactive data language (IDL) application developed at Norut in Tromsø (Larsen et al.). This is a flexible and fully automatic D-InSAR processing facility; though some of the processing steps require input of parameters selected by an experienced person. The inputs to the GSAR application are SAR images, orbit data and a DEM. The output is geocoded InSAR displacement data. The processing starts with a setup of general information concerning the processing and selection of input data. Images are then resampled, to get the same pixel size and coregistered, or align, in space. A selection of interferograms is performed based on baseline and time of acquisition, followed by generation of interferograms. Goldstein filtering reduces the noise-level in the interferograms. Then a visual quality of interferograms is performed to rule out noisy interferograms. Other important steps are removal of atmospheric phase contribution, unwrapping of phase, the middling process and selection of reference point. The last step of the processing is geocoding of displacement data from radar geometry to a geographic coordinate system. InSAR data for the different localities was produced with assistance from Tom Rune Lauknes at Norut.

TerraSAR-X InSAR data used in this thesis is provided through the German Aerospace Centre (DLR). The swath width is 5-30 km resulting in a ground range resolution of 1.1-3.3 m for the unprocessed SAR-images. The revisit time for TerraSAR-X is 11 days (Lauknes, 2010). The TerraSAR-X satellite has a frequency of 9,65 GHz and a wavelength of 3,10 cm. It orbits the earth at a distance of 514 km and has an adjustable incidence angle from 20-55°.

To illustrate the dynamic of slope processes and relate them to geomorphological- and structural geological elements, interferograms from the snow free season of 2009 to 2012 were used. A short temporal baseline (maximum time between acquisition) of 33 days was chosen to be able to detect fast moving objects. This resulted in a lower number of interferograms, but still high enough to get a good signal to noise ratio. The advantage of using a large number of interferograms is reduced noise and atmospheric contribution. The disadvantage is an underestimation of displacement. The short temporal baseline gave interferograms not connected from season to season (Fig. 26) reducing the middling, giving a more reliable displacement rate as a consequence (Dehls et al., 2012). When investigating the correlation between geological elements and InSAR data, exact measurements of displacement rates are not crucial. Spatial variations and displacement patterns in InSAR data are more interesting in this context. The mean velocity stacking algorithm was used to reduce the atmospheric contribution. This algorithm creates a mean yearly displacement rate for each pixel based on all the interferograms. This is a quite simple middling technique that has proven good results when including a large number of interferograms.

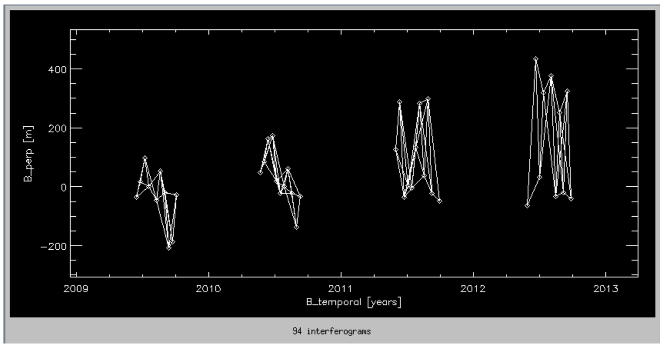

Fig. 26 – Plot from the GSAR application of interferograms used for the rock glacier on Nordmannviktinden. Dots represent SAR-images and lines interferograms.

2.4 Calculation of 2D InSAR displacement dataset

Using satellite data from ascending- and descending geometries to study slope processes can be demanding. The InSAR technique can only measure displacement in the line of sight (LOS) direction. To make out true displacement from ascending- and descending InSAR data, the directions of the LOS vectors for the two geometries have to be considered. In addition the satellites sensitivity to displacement has be taken into account. Each geometry has a blind plane orthogonal to the LOS with low sensitivity to displacement. By combining InSAR data from ascending- and descending geometry into 2D InSAR, we have improved sensitivity to displacement.

To exemplify this, the ascending- and descending LOS vectors are plotted in a West-East profile in (Fig. 27). Different displacement scenarios (D1-D8) for an unstable block B is plotted together with the displacement component possible to measure in ascending and descending geometry. Scenario D4 is in blind plane of the ascending geometry, thus not possible to detect for the satellite in ascending orbit. D1 and D8 are in the blind plane of the descending geometry, not possible to detect for the satellite in descending orbit.

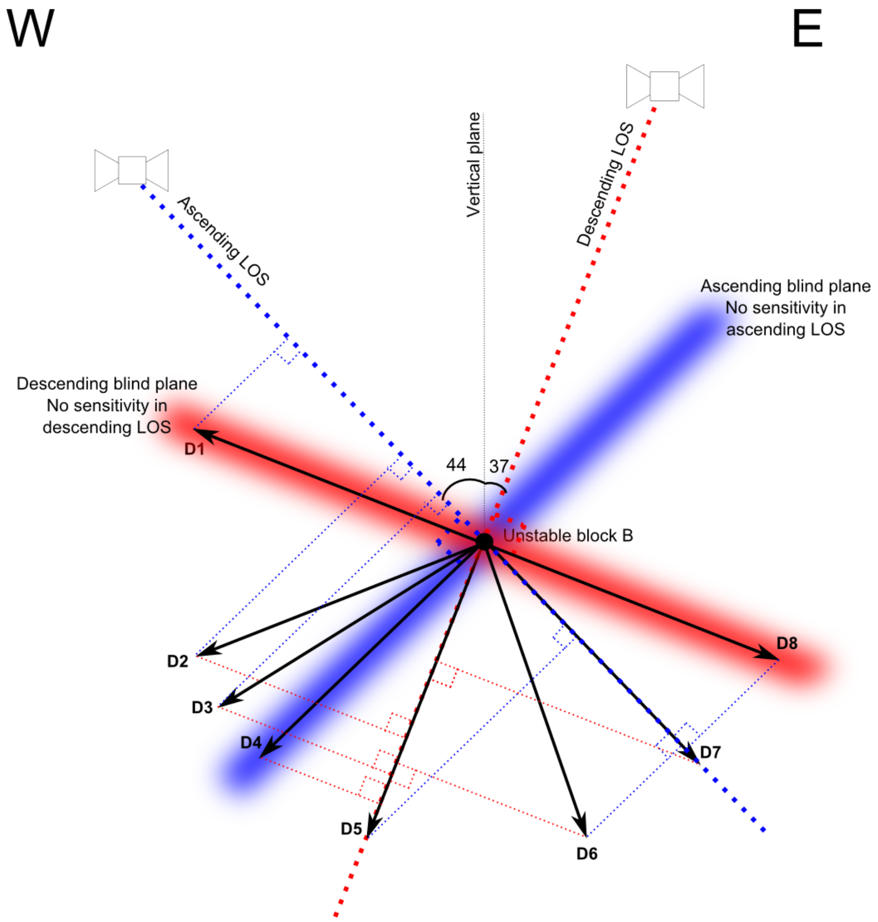

Fig. 27 – Profile showing sensitivity in ascending and descending geometry

Looking isolated on data from one geometry, it is impossible to verify if the variation in displacement is a result of change in the direction of displacement or change in the magnitude of displacement. A constant displacement rate with a change in displacement direction will result in a variation in the measured displacement as illustrated by displacement scenario D2 and D3 in (Fig. 28) and (Fig. 29).

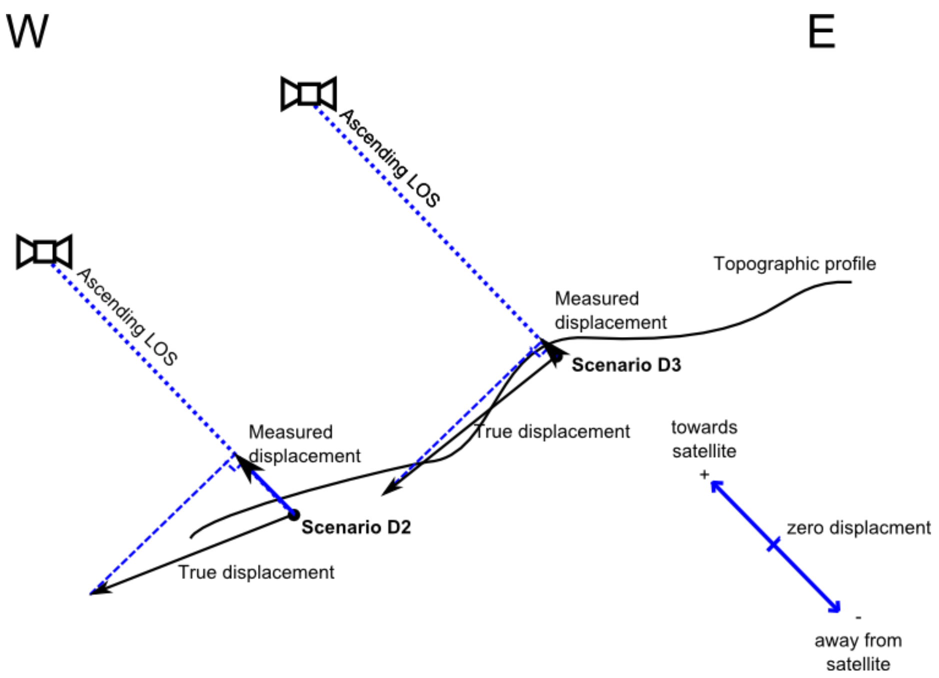

Fig. 28 - Sensitivity to different displacement directions in ascending geometry

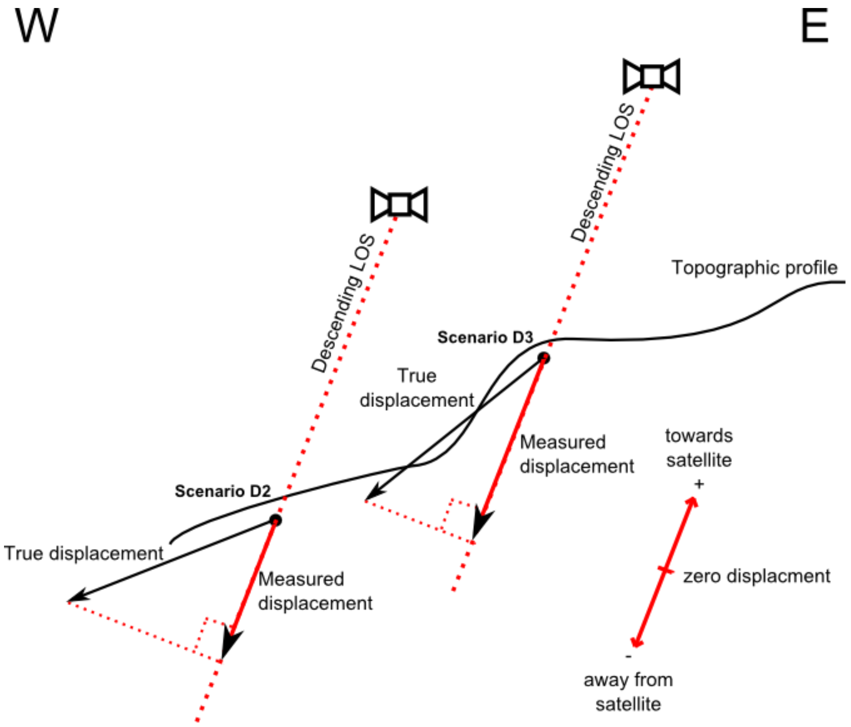

Fig. 29 - Sensitivity to different displacement directions in descending geometry

In this thesis we have combined InSAR data from two SAR geometries in an attempt to mitigate the challenge with the blind zone by calculating 2D InSAR data. The idea is that the displacement not visible in ascending LOS but visible in descending LOS, and vice versa, can be detected. The LOS vectors for the ascending- and the descending satellite defines a plane (LOS-plane) (Fig. 30 left). From displacement in ascending- and the descending LOS, a total displacement vector (**T**) in the LOS-plane was calculated. From **T**, horizontal (**h**)- and vertical (**v**) components were decomposed and projected into the East-West plane (Fig. 30 right). The angle (ϴ) between the horizontal plan and the total displacement vector **T** were also found. Calculation have been done based on code from, and with the help of Yngvar Larsen at Norut. For details see

Appendix 3 – Calculation of horizontal and vertical displacement vectors from ascending and descending InSAR-data.

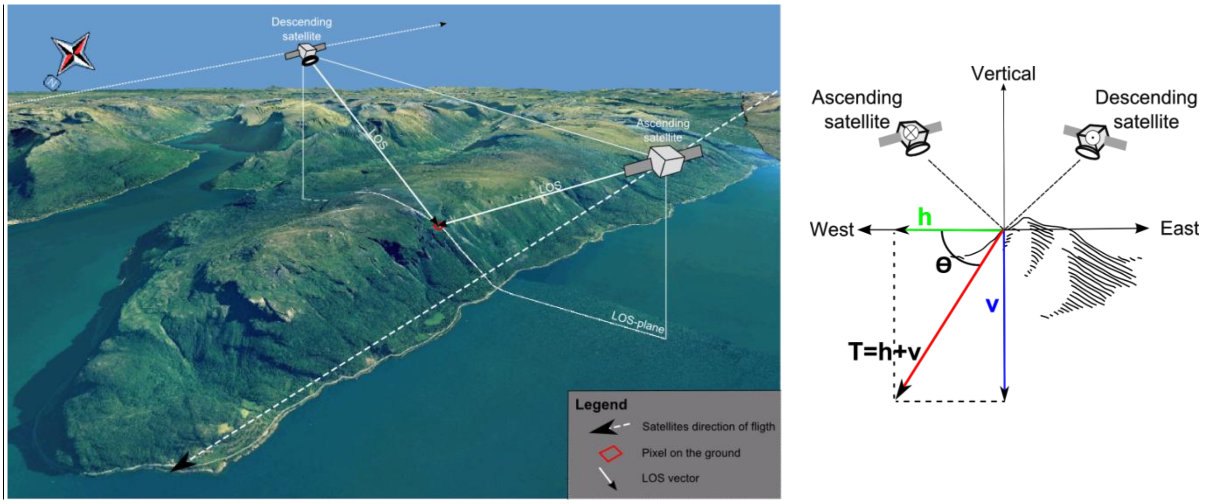

Fig. 30 - Left: Orthophoto draped on DEM showing the Nordnes peninsula with the Nordnes rock slide pinpointed by the two satellites LOS vectors. Kåfjord is to the East of peninsula and Storfjorden to the West. Right: East-West profile showing relationship between total displacement vector T, horizontal displacement vector h, vertical displacement vector v together with angle ϴ between the horizontal plan and the total displacement vector T.

Because **T** lay in the LOS-plane, we can only measure displacement that has a component in this plane. The small North component of the ascending- and descending LOS vectors (Tab. 1), give an almost vertical and west striking (right hand rule) orientation of the LOS-plane. The consequence is low sensitivity to displacement in North-South direction and is a limitation of the 2D InSAR technique.

Tab. 1 - Unit vector for ascending and descending LOS.

Directions	Unit vector ascending LOS	Unit vector descending LOS
un	-0,14224032	-0,14755357
ue	-0,68470808	0,59815772
uh	0,71480245	0,78767714

2.5 Other datasets and tools

After the ascending- and descending InSAR data had been produced together with the 2D InSAR data, a map study was conducted to identify suitable field location demonstrating different slope processes. The main tool for this task was the ArcMap- and ArcGlobe applications from ESRI. They are capable of making and manipulating maps and 3D models. The ArcMap application has been used to create all maps produced in this thesis. The ArcScene application, also from ESRI, was used to make the 3D-representation of displacement data.

GPS data from Nordnes rockslide was provided by Nordnorsk Fjellovervåking. There are 10 GSP stations distributed inside the rockslide area and one reference GPS is situated on stable ground outside the rockslide area.

Orthophotos and observations from field were used for relating geomorphological- and geological structures to InSAR and 2D InSAR data. Orthophotos origin from www.norgeibilder.no. They have a resolution of 0,4x0,4 m.

The digital elevation model (DEM) used when processing InSAR data and in the ArcMap- ArgGlobe- and ArcScene applications origin from the Norwegian Mapping Authority (NMA). The DEM has a resolution of 10x10 meters.

Quaternary maps with scale 1:50 000 by (Corner, (in prep.)) covering Storfjord and Skiboten area and by (Tolgensbakk, 1988) covering outer part of the Kåfjord area have been digitalized, geo-referenced and draped over the DEM using ArcMap. This made it possible to compare displacement patterns with features from quaternary maps.

Geological maps over Storfjord with scale 1:50 000 (Boyd, 1985), Manndalen with scale 1:50 000 (Quenardel and Zwaan, 2008) and Nordreisa in scale 1:250 000 (Zwaan, 1988) were used to get an overview of the geological units in the area. Digital geological maps used, origin from www.ngu.no.

During 6 days, 4 different localities where visited. Field data gathered include descriptions, digital pictures, sketches and profiles of landforms, terrain and lithologies. GPS-positions and measurements of strike/dip, gradients and orientations for geological elements considered important were collected. Data collected in the field was summarized in short field rapports. GPS-positions and strike/dip measurements where collected in ArcMap for later analyzes. GPS waypoints and route information were collected using a Garmin eTrex Legend HCx GPS. The GPS data were stored using the MapSource (6.16.3) application by Garmin Ltd and imported to ArcMap using the GPSBabel (1.4.4) application by Robert Lipe and S. Khai Mong.

In addition to own measurements, digitalized data describing structures like foliation, open fractures, slide fronts, slide scarps and back scarps from Åknes/Tafjord Beredskap have been used to relate geomorphological- and geological structures to InSAR and 2D InSAR data. Contour lines have been produced based on data from Felles kartdatabase (FKB) data from http://norgedigitalt.no.

2.6 Verification of 2D InSAR data

To verify the reliability of the 2D InSAR technique, both the input and output has been verified against data from a stationary GPS at the Nordnes rockslide. Ascending and descending InSAR data are the inputs to the 2D InSAR calculation. Horizontal- and vertical displacement data, together with the length of and the dip of the total displacement vectors, are the outputs of the 2D InSAR calculation. All displacements measured in mm/y, dip in degree. This will be discussed in more details in Section 3.1.

For the verification of GPS data against InSAR data, interferograms from May to October 2011 and GPS data from 2011 were used. InSAR data from only one season was chosen to get even more reliable displacement rates. As a consequence of a low number of interferograms, the data contains more noise. The small baseline subset algorithm (SBAS) was used to remove the atmospheric contribution (Berardino et al., 2002) (Lauknes, 2011). We used spatial multilooking with 5 looks in range and 4 looks in azimuth. This produced pixels ~9,7x7,5 m. This is a more advanced algorithm that generates displacement data in millimeters between each acquisition. This makes it possible to study the seasonable variations and the nature of displacement in an area through time.

2.7 Study area

In this Section, the field localities and the datasets used are presented. In order to compare displacement patterns in InSAR data with geological processes four field localities have been selected. A rock glacier on Nordmannviktinden, solifluction tongues at Joppolbakkan, a fast moving rockslide called Gamanjunni3 and a well instrumented rockslide at Jettan Nordnes (Fig. 4).

Rock glacier in Helvetesdalen on Nordmannviktinden

Helvetesdalen valley contains blocky material, colluviums and weathered material together with a tongue shaped formation interpreted by (Tolgensbakk, 1988) as a rock glacier with a non-glacier origin.

The rock glacier is located between 800 to 1000 m.a.s.l., it has a clear outline against the valley floor, and a steep slope in the front area. It has ridges and depressions on the top. The shape and morphology indicates a flowing motion down the valley.

The direction of displacement for the rock glacier and the strike and dips of Helvetesdalen, are assumed to be equal because the rock glacier is confined by the valley.

This rock glacier was included in the project because it shows interesting displacement patterns on InSAR data.

Gamanjunni3 rockslide

Gamanjunni3 is situated on the East side of Manndalen. This locality is under surveillance by NGU, and run out distance calculations suggest that a maximum collapse (8 Mm^3) of Gamanjunni3 could dam Manndalen River and cause a catastrophic collapse of the dam that could threaten settlement in the valley. Gamanjunni3 consist of a block, ~300m in North direction, ~200m in East direction and ~200m in vertical direction that has moved down an approximately 40 degree sliding plane. Horizontal displacement is 120 m and vertical displacement is 100 m (Bunkholt et al., 2011). Gamanjunni3 has the morphology of a complex slide. The slide has large moving intact blocks, fast moving talus lobes, ridges, anti-ridges, benches and more intact bedrock with congruent cracks opening.

The lithology in the slide area is divided. From the top to around 200 m.a.s.l consist of rock metamorphosed at high grade from the Kåfjord Nappe. At around 200 m.a.s.l, the thrust fault of the Kåfjord Nappe divides the Kåfjord Nappe from the Váddás Nappe. Starting from the top there is pale to medium gray mica schist (U1), with more muscovite than biotite, containing amphibolite lenses and layers on the uppermost part of the slide. From around 600 to 800 m.a.s.l., a dark grey mica schist layer (U2), with more biotite then muscovite, also containing amphibolite lenses and layers. From 600 to 200 m.a.s.l, the U1 unit outcrops. Below the thrust fault of the Kåfjord Nappe at 200 m.a.s.l, rocks classified as banded, hornblende bearing calcareous mica schist is found (Quenardel and Zwaan, 2008). TLS LiDAR investigations have reviled 8 different discontinuities sets in addition to the foliation. The most prominent structures are the back-scarp, and the SE-bounding lateral release surface. Rotational movement is documented by a difference in the dip of the S1 foliation from 025/10 on the back-scarp to 025/28 on the unstable block (Bunkholt et al., 2011).

Because of the short acquisition time of the TerraSAR-X satellite, fast moving object can be monitored. (Bunkholt et al., 2011) show that the direction of the displacement has a large component in West-East direction. This, together with large displacement rates, makes Gamanjunni3 suitable as a case in this thesis.

Nordnes rockslide

The Nordnes rockslide (Jettan) at the outer part of the Nordnes peninsula has been, and still is the target of many ongoing research projects. These activities include among others displacement monitoring (NNFO, Norut and ÅTB), permafrost mapping (Blikra and Christiansen, 2012; Christiansen et al., 2010), connection between geological structures and driving forces (UIT ongoing).

Jettan has been classified as a complex field by (Braathen et al., 2004). It covers an area from around 30 to 800 m.a.s.l. with a gradient of ~30°. The slide has a defined back-scarp to the East and a lateral boundary to the North visible as a cliff. The slide area include rotated fault blocks, synthetic (towards the cliff) and antithetic normal faults (Braathen et al., 2004). Preliminary results from multi-beam surveys have discovered rock avalanche debris in the fjord most likely originating from the Nordnes rockslide (personal communication, Matthias Forwick). The worst case scenario with a total collapse, has been estimated to involve 10-12 Mm^3 (Blikra, 2012).

Previous studies in the area have mapped well-foliated amphibolite, dolomite- and calcite marble and garnet-quartz-mica schist from the Kåfjord Nappe (Andersen, 1988; Zwaan, 1988). The Northern lateral border shows layering of light-colored chalk-silicates and mafic garnet-bearing gneisses. Marbles had lenses of garnet-bearing gneiss and gneissic sigma clasts deformed top to SE. Assumed Caledonian deformation.

Structures in the slide has been documented by (Braathen et al., 2004) , (Henderson, 2010) and Åknes/Tafjord Beredskap IKS (ÅTB) (Fig. 38). Foliation is dipping gently to the West. (Henderson, 2010) identify four crack patterns from LIDAR, controlling the slide. For a more detailed description of geological structures, geomorphology and deformation structures see (Braathen et al., 2004; Henderson et al., 2010).

Displacement rates and direction at the Nordnes rockslide has been monitored with GPS stations from 2010 and is well documented (Blikra, 2012, 2009; Braathen et al., 2004; Henderson et al., 2008). This makes Nordnes a good location for comparing InSAR- and 2D InSAR data against GPS data and a good case for relating InSAR and 2D InSAR to the kinematic and morphology of a rockslide.

Solifluction tongues at Joppolbakkan

Joppolbakkan is an East facing hill covered with hummus and sparse vegetation. This location was selected because tongue shaped features was identified from orthophotos. In addition the area show interesting displacement patterns from InSAR and are facing East, thus InSAR data from ascending geometry has good sensitivity to displacement in this direction.

3 Results, interpretation and discussion

This section starts with a verification of the InSAR technique and 2D InSAR data produced. Then results, interpretations and discussion for each locality are presented. The results consist of InSAR- and 2D InSAR displacement data produced together with a description of the general trends. The interpretation and discussion will focus on displacement patterns found in the InSAR- and 2D InSAR data. Patterns will be compared with geological- and geomorphological structures from other sources and observation from the field. A discussion of the limitations and possibilities of the InSAR technique has been emphasized.

3.1 Verification of InSAR technique and 2D InSAR data

The validation was done in two steps; first the input to the decomposition, ascending and descending InSAR TSX data from 2011 was compared to and verified against GPS displacement. Then the 2D InSAR calculation was verified.

Verification of InSAR technique

To verify the InSAR technique, GPS data provided by Nordnorsk Fjellovervåking (NNFO) from the Nordnes rockslide are compared to the produced ascending- and descending InSAR data.

The trend of the GPS data is assumed to be the true displacement. In the verification, 2011 data from GPS station YN3 was compared to temporal ascending- and descending SBAS processed TSX InSAR data from end of May to beginning of October 2011. 11 SAR-images from ascending- and 14 SAR- images from descending geometry was used as input. A temporal baseline of 33 days resulted in 26 interferograms in ascending- and 14 in descending geometry. 3 InSAR verification pixels from the ascending dataset and 14 from the descending dataset were selected. They were all situated on the same block as GPS station YN3 (Fig. 31). A mean displacement between each interferogram was calculated. This was done for each verification point in both geometries. These mean InSAR displacement was then compared to data from GPS station YN3.

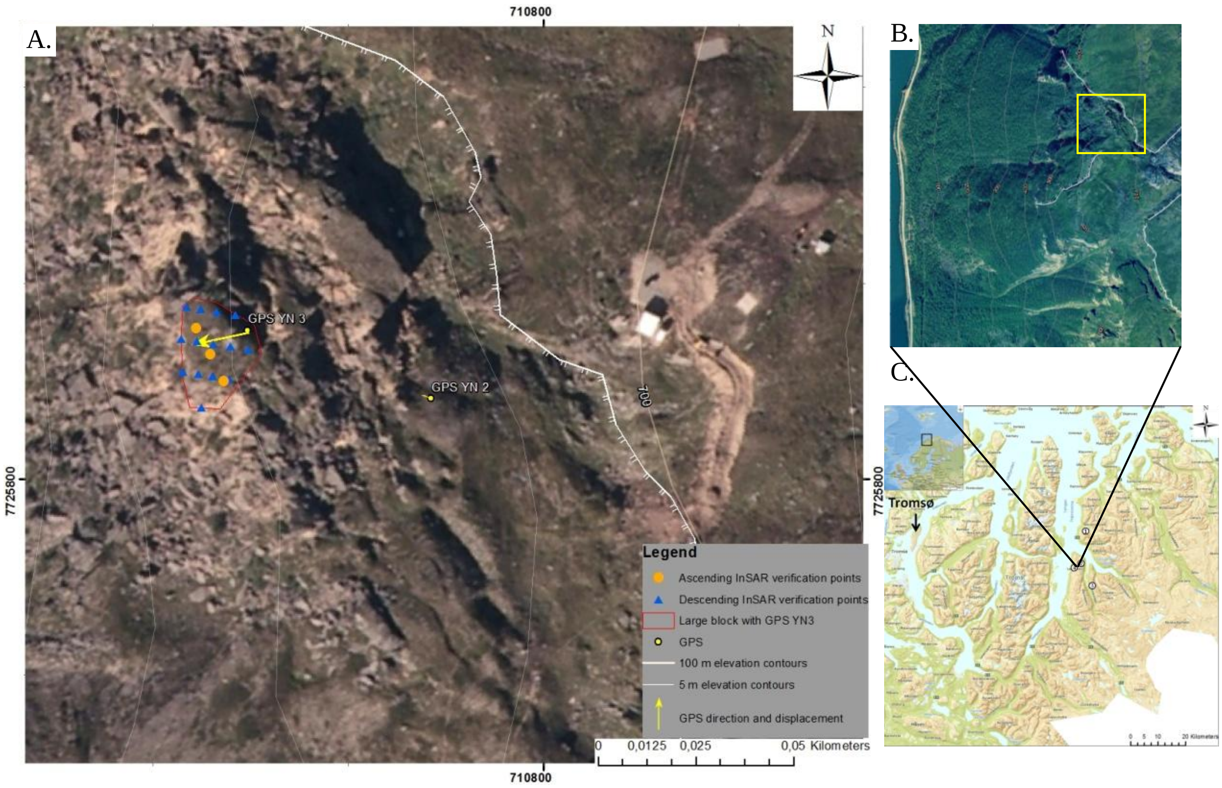

Fig. 31 – A. GPS and InSAR verification points on the Nordnes rockslide. Location of block with verification points and GPS station YN3 is marked with yellow square in Fig. 31 B. B and C. Local and regional location of Nordnes rockslide.

(Fig. 32) shows GPS data from GPS station YN3 from 2011. All data series have negative trends. GPS station YN3 is moving down and to the West-Southwest. The dE component is the largest. dN is displacement in North–South direction, dE is displacement in East-West direction and dN is displacement in North–South direction.

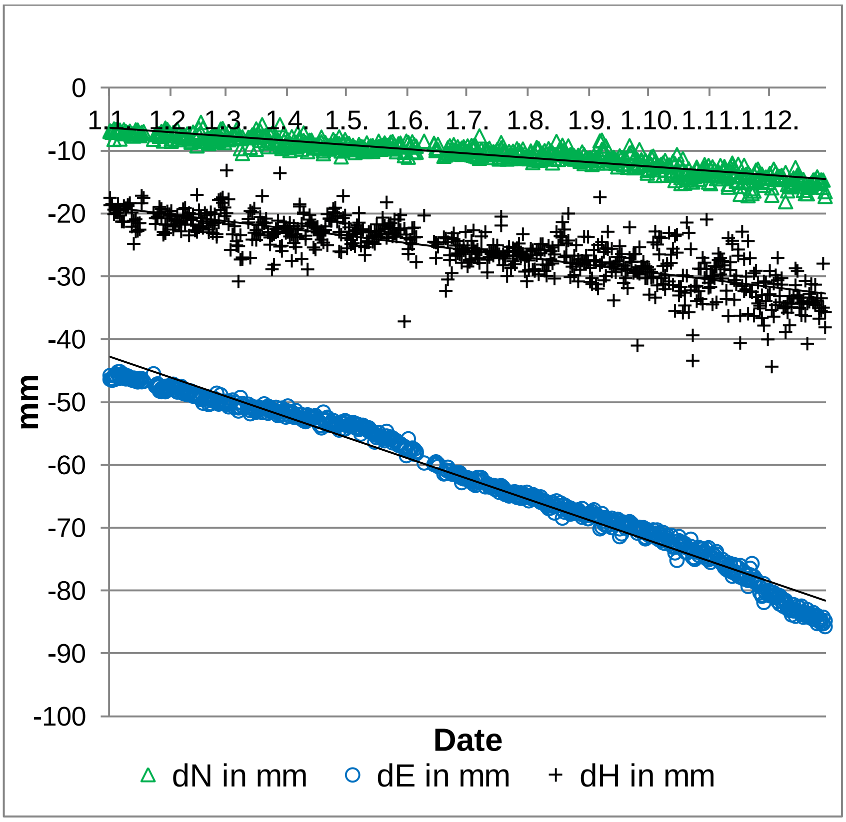

Fig. 32 - Displacement data for GPS station YN3 at Nordnes for 2011 (NNFO, 2012)

The GPS measurements from GPS station YN3 were projected into the LOS direction for the satellites in ascending- and descending orbits. This projection gives the part of the displacement measured by GPS, possible for the InSAR satellite to measure. The projected GPS data was plotted in the same graph as the actual InSAR data from the ascending- and descending geometry (Fig. 33). For GPS station YN3 there is a good fit between displacement measured by GPS and by descending InSAR data. The trend of ascending InSAR data has some deviation from the trend in the GPS data. The deviation might be due to low sensitivity to displacement in this direction for the ascending data. A mean direction of displacement for GPS station YN3 has been calculated from the 2011 GPS data to be (258/19) (Tab. 3). This is close to the blind plane of ascending geometry as in the D3 displacement scenario pictured in (Fig. 27), and explained in Section 2.4. The ascending InSAR displacement data might also be influenced by atmospheric phase contribution not removed by the SBAS algorithm. GPS station YN3 is located in an area that most likely has a complex displacement pattern. The GPS station measure displacement at one exact point, while the InSAR technique is a mean displacement calculated from many reflectors in a rectangle (9,7 x 7,5 m) on the ground. The deviation in the ascending data and the GPS data could be a consequence of differences in the measuring technique.

The deviation between the trend of the GPS data projected into ascending LOS, and the trend of the InSAR data measured in the ascending LOS, is around 4 mm/y from 1. June to 30. September. This is equal to 2,7 mm/y in the East-West direction and 2,8 mm/y in vertical direction. The deviation between the trend of the GPS data projected into descending LOS and the trend of the InSAR data measured in the descending LOS, is around 1 mm/y from 26. May to 5. October. This gives a vertical- and horizontal deviation of less than a millimeter. The errors discussed here are smaller than and therefore not masking the displacement patterns of interest, which have variations above 10 mm/y.

The GPS data and the input to the decomposition procedure, ascending- and descending InSAR TSX data, have a good correlation. The errors are smaller than the displacement patterns of interest in this thesis. In other words, the ascending- and descending InSAR datasets are reliable in the area around GPS YN3.

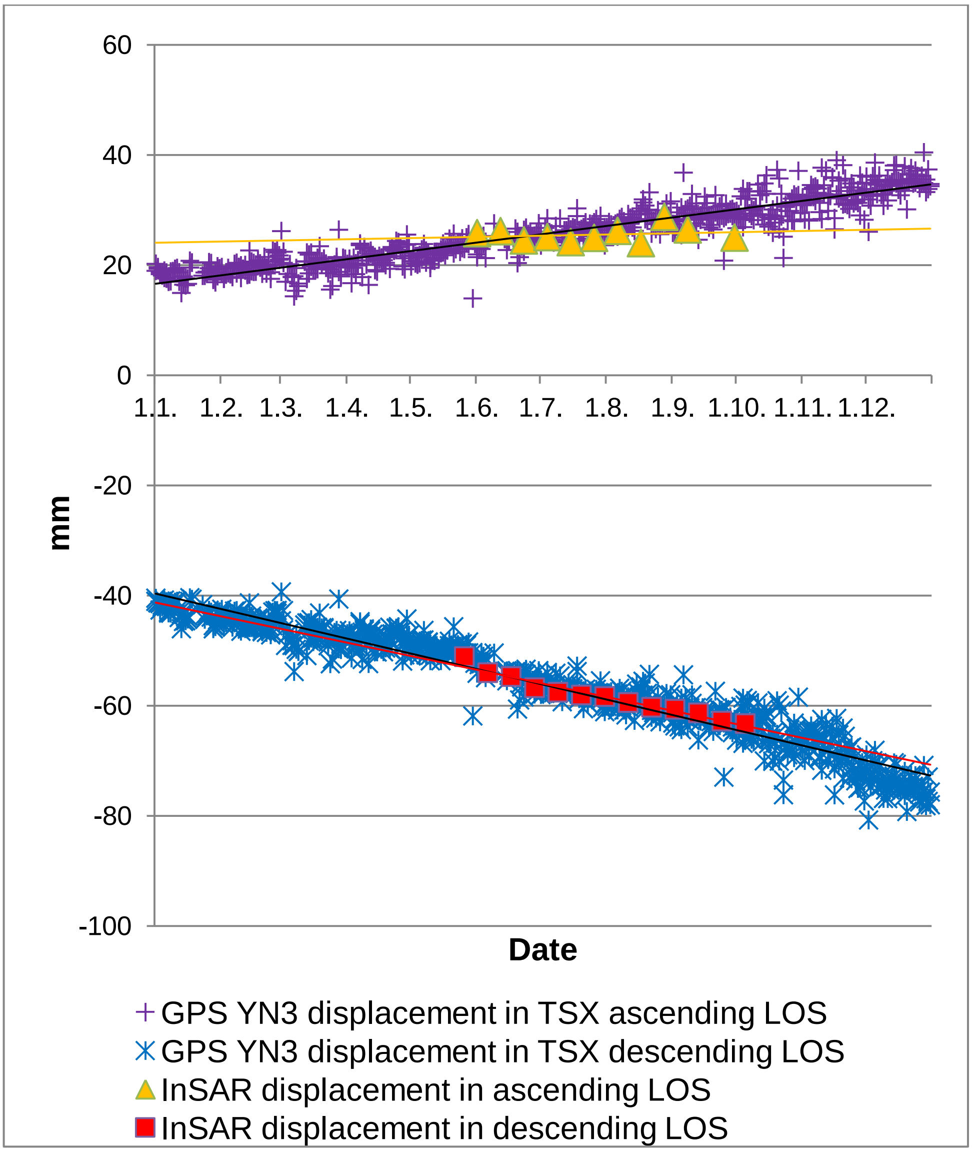

Fig. 33 - GPS station YN3 data projected into TSX ascending and descending LOS and compared to InSAR displacement

Verification of 2D InSAR data calculation

For this verification, East-West displacement components (dE) and vertical displacement components (dH) from GPS station YN3 data projected into ascending- and descending LOS, were used as test data and input to the 2D InSAR decomposition procedure. The results were horizontal- and vertical components. If the 2D InSAR calculation is correct, the output horizontal- and vertical components should correlate with the original input East-West displacement component (dE) and the vertical displacement (dH) component.

First the data from the GPS station YN3 (dE- and dH displacement components) were projected into ascending and descending LOS. These projections were used as input into the

2D InSAR decomposition procedure. The result is presented in scatter plots (Fig. 34) and (Fig. 35). In (Fig. 34) the output (decomposed horizontal displacement component) match the input (original dE displacement component) perfect with a calculated Pearson correlation of 1. This verifies that the 2D InSAR decomposition is producing horizontal displacement components in the East-West plane as expected.

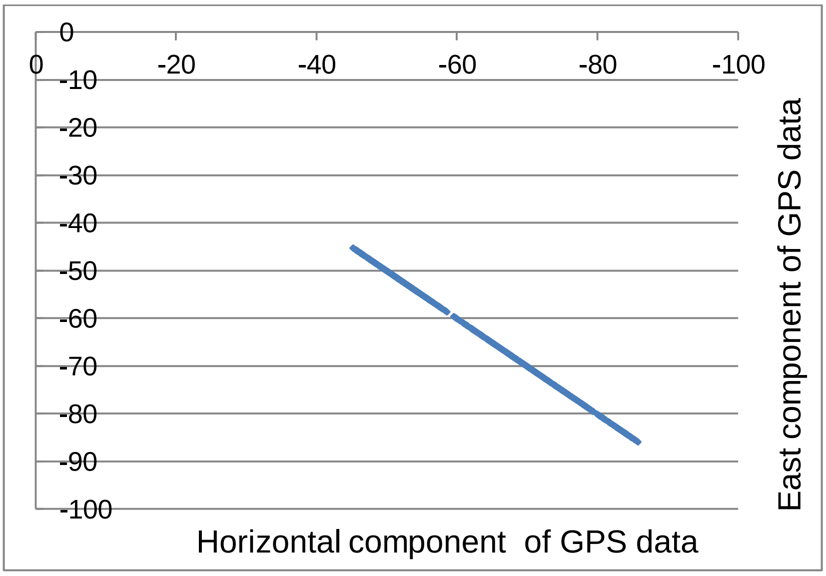

Fig. 34 - Comparison of GPS station YN3 data decomposed into horizontal component and East component (dE) of GPS station YN3 data for 2011.

There is a larger variability when comparing output from decomposition of GPS station YN3 data into vertical displacement component, and original vertical displacement component (dH) of GPS station YN3 (Fig. 35). A Pearson correlation of 0,99830439 shows that the 2D InSAR decomposition has a lower, but still sufficient sensitivity to vertical displacement and produce vertical displacement components as expected.

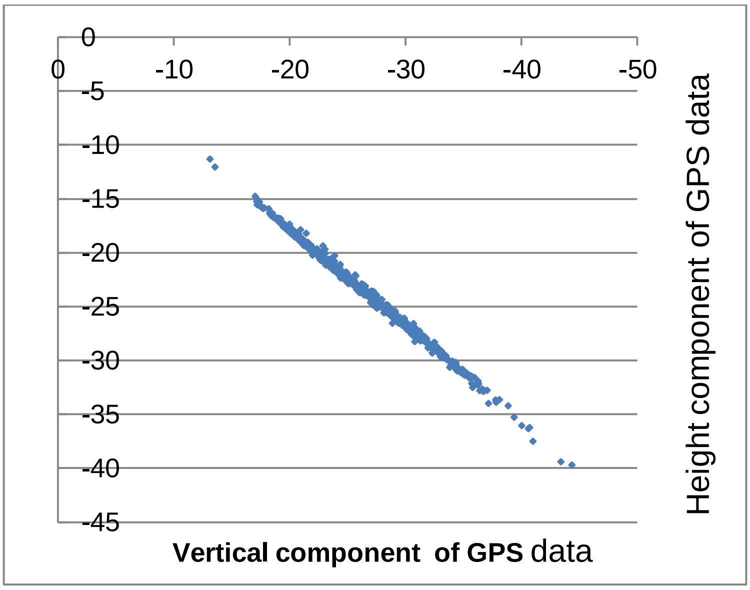

Fig. 35 - Comparison of GPS station YN3 data decomposed into vertical component and East component (dE) of GPS station YN3 data for 2011.

The sensitivity to displacement for the SAR system is given by the LOS unit vector or sensitivity vector. The sensitivity vector has the length of 1, and describes how the LOS is oriented. For the ascending- and descending dataset, the sensitivity vector has high absolute values in East-West and vertical displacement components. This indicates good sensitivity for displacement in these directions (Tab. 2). In contrast, there is low sensitivity to the North-South displacement component in both geometries (-0,14224032 and -0,14755357). The North-South displacement (dN) in (Fig. 32) is therefore almost not possible to detect in InSAR- and 2D InSAR data.

Tab. 2 - Sensitivity vectors for the ascending and descending LOS. Reference system in Section 2.1.

Direction	Ascending LOS unity vector	Descending LOS unity vector
North-South	-0,14224032	-0,14755357
East-West	-0,68470808	0,59815772
Up-Down	0,71480245	0,78767714

With the use of GPS data from GPS station YN3 projected into LOS for ascending- and descending geometry as test data, the 2D InSAR calculation has produced output (horizontal- and vertical displacement components) that correlates with the original horizontal and vertical displacement components from GPS station YN3. In other words, the 2D InSAR calculations works as expected.

3.2 Overview of InSAR data from the whole Storfjord-Kåfjord-Lyngen area

The wavelength of the TerraSAR-X SAR (TSX) makes it sensitive to atmospheric variations and variations in the dielectric properties of the ground, for example humidity variations. Because of this, the ascending- and descending dataset show varying results when focusing on processes with slow displacement rates, like isostatic rebound, regional- and local tectonic displacements that stretch over large distances. The slow displacement rates are overprinted by the much larger contribution from the atmosphere. Phase change due to atmospheric or tropospheric contribution is a phenomenon spanning several kilometer. (Massonnet and Feigl, 1998) found 9 cm displacement over 5-10 km (See “The phase contribution from difference in atmospheric path delay“ in Section 2.2).

To produce overview map in (Fig. 36 and Fig. 37), data from the TSX satellite from 2009-2012 have been used. A long temporal baseline was chosen, resulting in a large number of interferograms. This gave a high degree of middling capable of removing the atmospheric contribution to the phase signal in the vicinity of the selected InSAR reference point. Even though, large parts of the study area shows displacement rates from + 20 to -20 mm/y in LOS direction. These displacements most likely origin from atmospheric contribution due to their extent of spatial distribution. The reference point is in the vicinity of the Nordnes rockslide. Note the lack of contribution from the atmosphere (displacement rates from + 20 to -20 mm/y) in the area around the Nordnes rockslide (marked as Nordnesfjellet).

Because of frequent acquisitions, TerraSAR-X data are much more useful detecting high-displacement objects. By tuning the color table, used to present the InSAR data, to a vide value-range, it is possible to make these objects stand out clearly. In (Fig. 36 and Fig. 37) displacement data from + 10 to – 10 mm/y have been masked out, revealing high-displacement object in the study area. Many of these are objects mapped and/or monitored by NGU.

The InSAR dataset used in this study covers a large area and include multiple displacement phenomena and changing landforms, like rock glaciers, alluvial fans, rockslides, solifluction lobes and ice-cored moraines. Identifying, mapping and classifying all elements in motion are a huge task that should be left to other studies that focus mainly on this.

This thesis will elaborate into certain displacement phenomenons at selected localities: An active rock glacier in Helvetesdalen on Nordmannviktinden, tongues shaped features at

Joppolbakkan on East side of Nordnes peninsula, Gamanjunni3, a fast moving rockslide in Manndalen and the Nordnes rockslide.

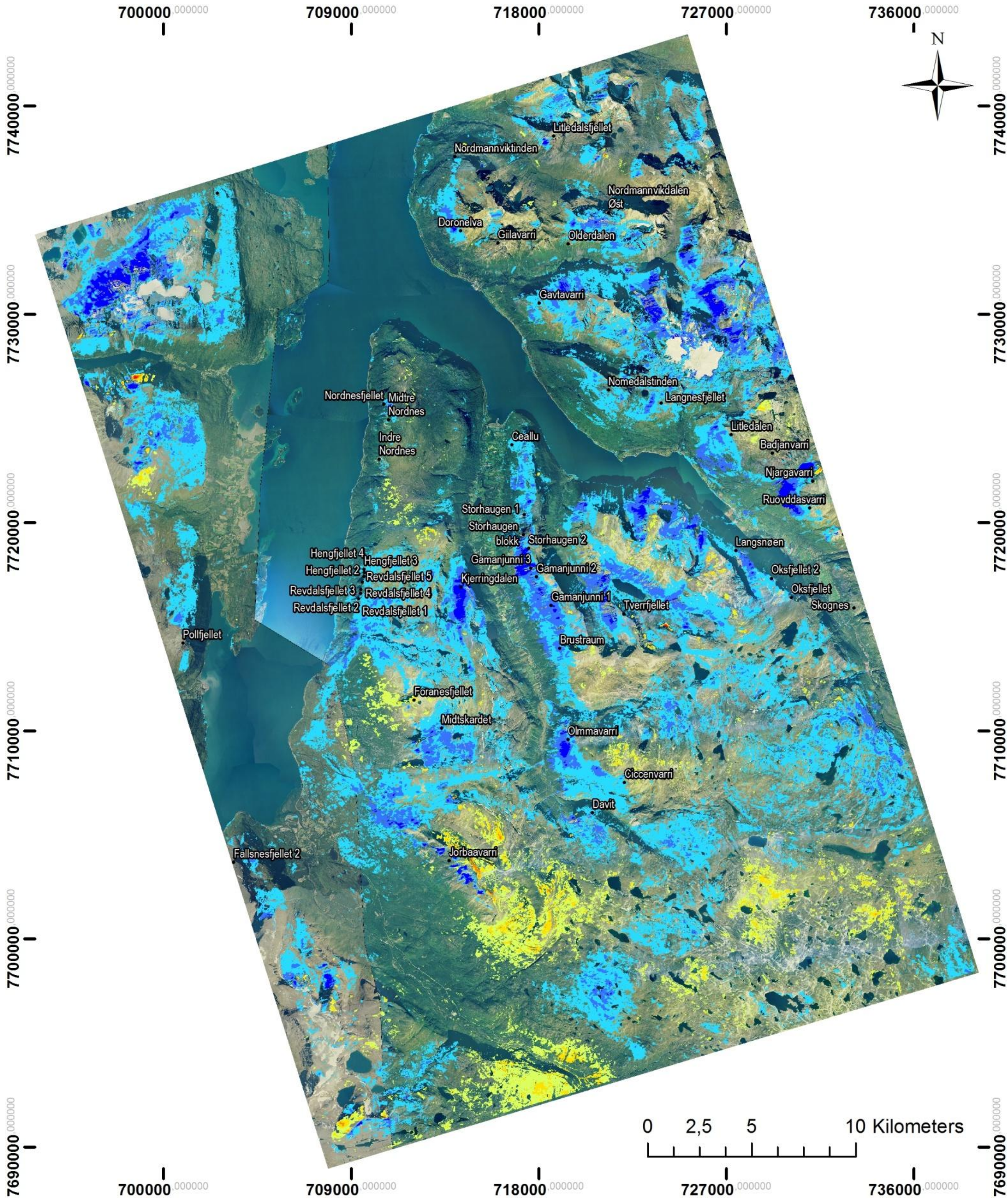

Fig. 36 - Ascending InSAR data in mm/y for 2009-2012 for the study area. Name and location of objects mapped and/or monitored supplied by NGU.

Legend

Displacement in ascending LOS

- 🟥 -113 - -60
- 🟧 -59 - -40
- 🟨 -39 - -20
- 🟩 -19 - -10
- ⬜ -9 - +10
- 🟦 +11 - +20
- 🟦 +21 - +30
- 🟦 +31 - +60

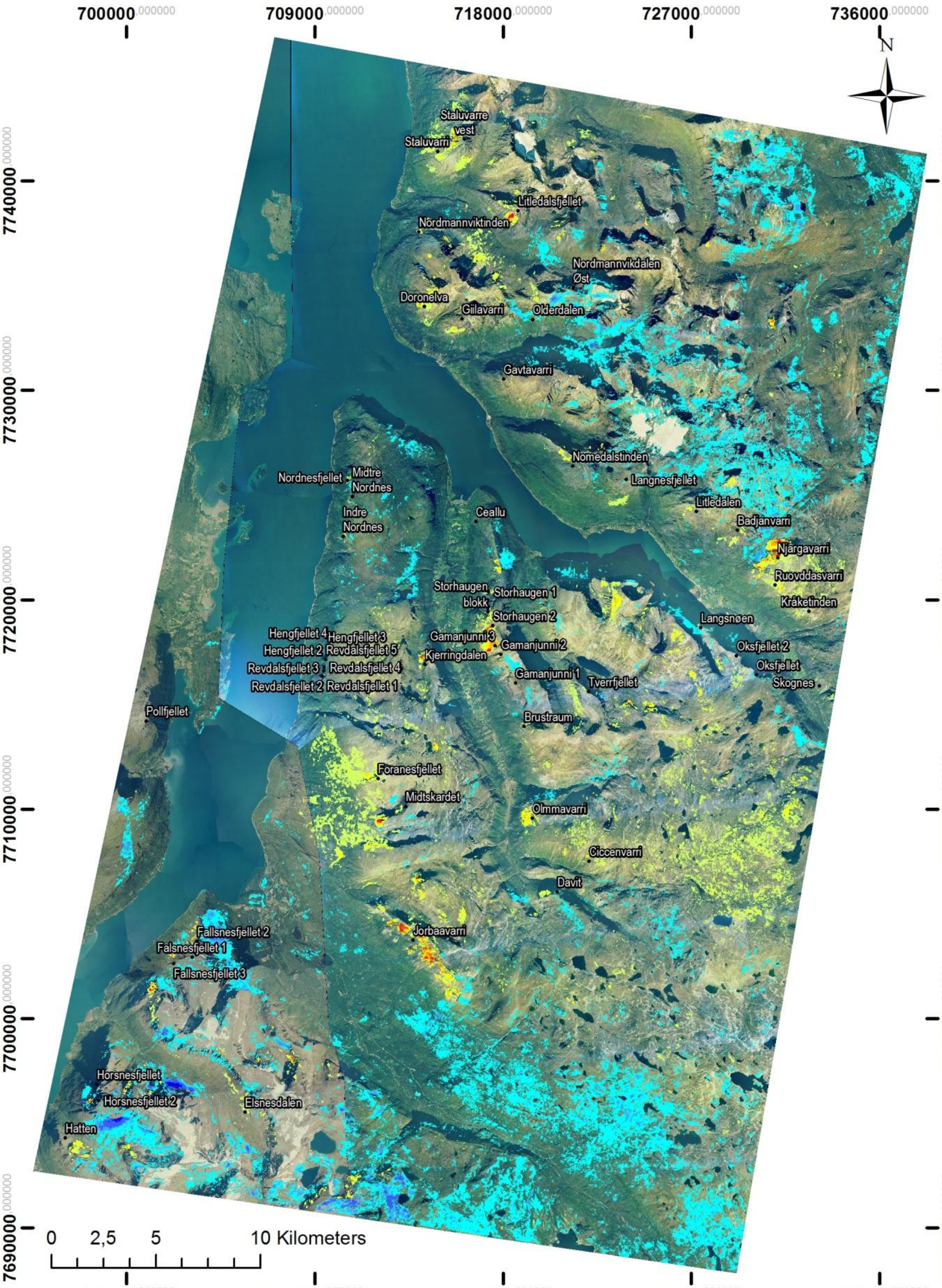

Fig. 37 - Descending InSAR data in mm/y for 2009-2012 for the study area. Name and location of objects mapped and/or monitored supplied by NGU.

Legend

Displacement in descending LOS

- 🟥 -113 - -80
- 🟧 -79 - -60
- 🟧 -59 - -40
- 🟨 -39 - -20
- 🟩 -19 - -10
- ⬜ -9 - +10
- 🟦 +11 - +20
- 🟦 +21 - +30
- 🟦 +31 - +60
- 🟦 +61 - +80

3.3 Displacement patterns at selected localities

In this Section results are presented in map view and as plots with data from selected profiles. Displacement patterns found in the InSAR- and calculated 2D InSAR data from the different localities are discussed. Patterns will be compared with geological- and geomorphological structures from other sources and observation from the field. In addition slope gradient maps produced based on DEM-data will be used in the discussion. A discussion of the limitations and possibilities of the InSAR technique has been emphasized throughout this Section. See Section 2.1 for an overview of the reference system and conversions used.

3.3.1 Nordnes Rockslide

3.3.1.1 Results

Orthophoto in (Fig. 38) show the outline of the Nordnes rockslide with back scarp and two profiles AA’ and BB’. The location of the profiles was selected to include location of well documented areas of the slide, interesting patterns from InSAR- and 2D InSAR data, GPS stations, large fault blocks, lineaments, back fractures, open fractures, slide fronts and – scarps.

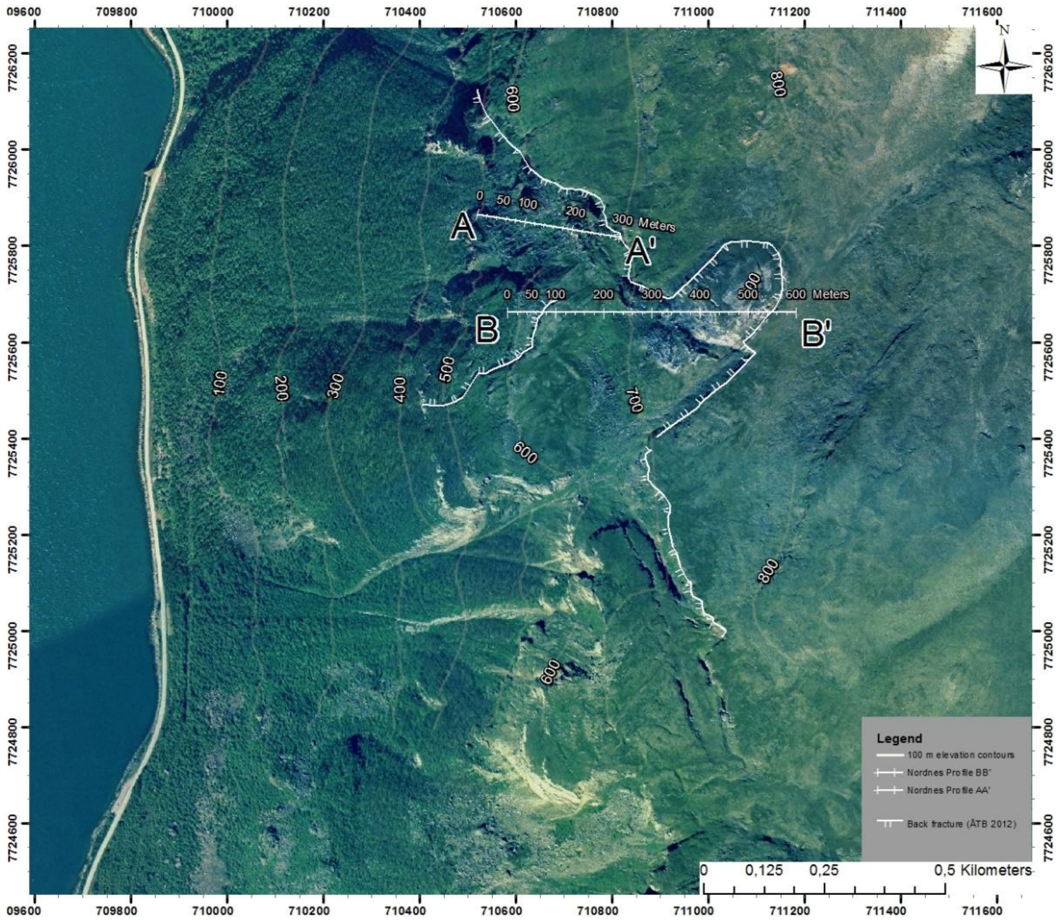

Fig. 38 – Orthophoto of the Nordnes Rockslide (Jettan) showing, structures from Åknes Tafjord Beredskap (ÅTB).

The common reference point for the ascending- and descending geometry was selected after study of orthophotos, slope gradient maps and coherence data. It is placed above the back scarp in an area with a slope angle of 13° and high mean coherence value from the SAR-images (Red cross in Fig. 39 A).

InSAR- and 2D InSAR data from two profiles, AA' and BB', was extracted. Results are presented in map view (Fig. 39 B to G) and as plots in (Fig. 43, Fig. 44, Fig. 45 and Fig. 46) Displacement values are generally positive (towards radar) in ascending LOS direction for both profiles. The ascending data in profile BB' has high ascending values peaking at ~280 m with ~37 mm/y.

The descending data show lower values, more displacement away from radar, when crossing over the back scarp and fractures separating large blocks from more stable areas (~265 m in AA' and ~100 m in BB').

2d InSAR data show horizontal displacement in the whole AA' profile with two maximums; at ~95 m and at ~195 m. In profile BB' the horizontal displacement towards West has a small negative maximum at ~70 m and a long section from ~240 m to ~450 m with high negative values.

Vertical displacement data is varying between ~6 and ~12 mm/y in profile AA’. In profile BB’, the vertical displacement data indicates downwards movement from 0 m to ~100 m and then upward displacement in the center of profile BB’.

Total displacement data, show the absolute value of the combined ascending- and descending displacement, and indicates most displacement in the middle of profile AA’ and BB’. The dip angle of the total displacement in profile AA’ is mimicking the pattern of the vertical displacement. Dip angle data have large sections with angles between 0 and -45 degrees. There are also small sections with angles between 0 and 45 degrees dip.

The slope gradient map (Fig. 39 H) shows the morphology of the profile. For profile AA’, the gradient is varying with the steepest parts (~ 50˚) in the middle of the profile (~150 m). In the BB’ profile, the morphology consist of terraces (< 25˚ slope angle) and slopes (>25˚ slope angle) with a general trend from steep (~45˚) to level terrain (~5˚).

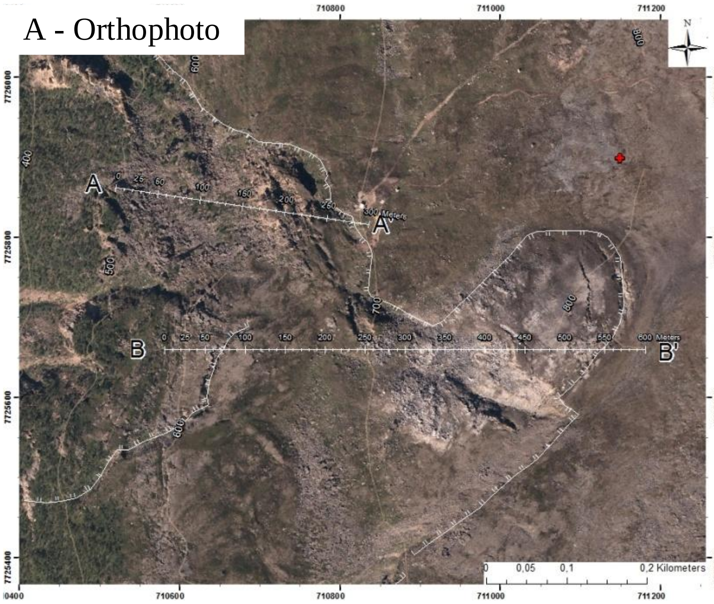
A - Orthophoto

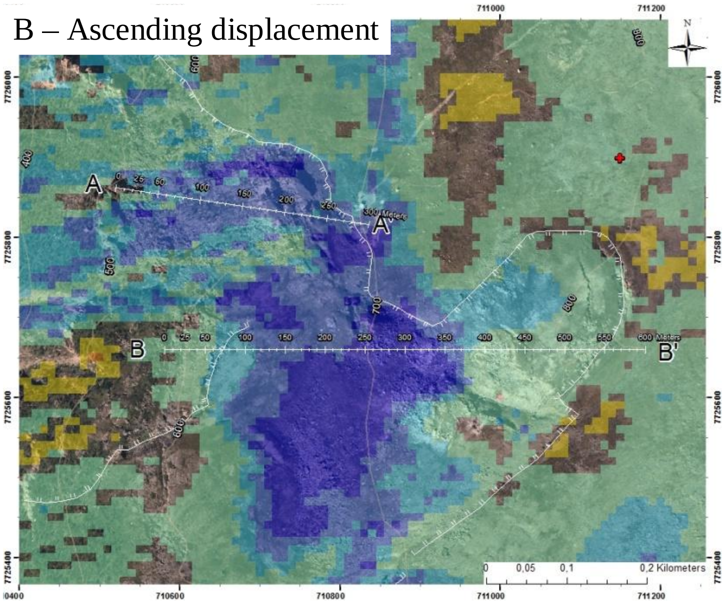
B – Ascending displacement

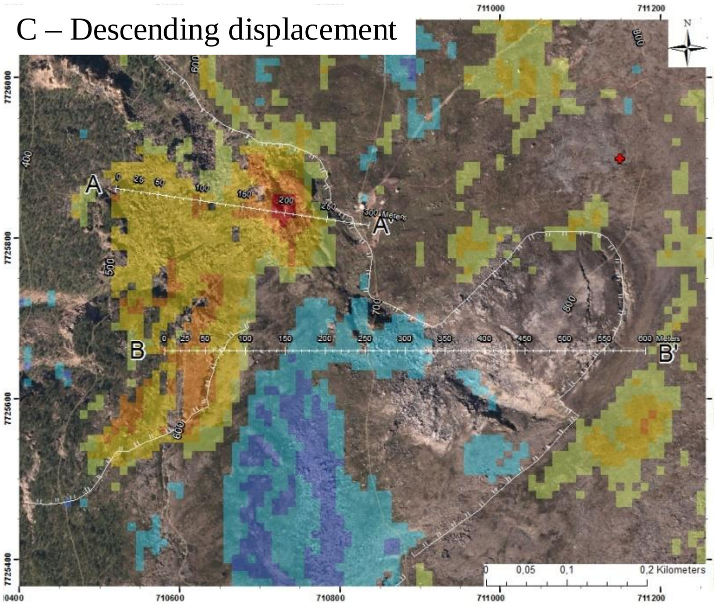
C – Descending displacement

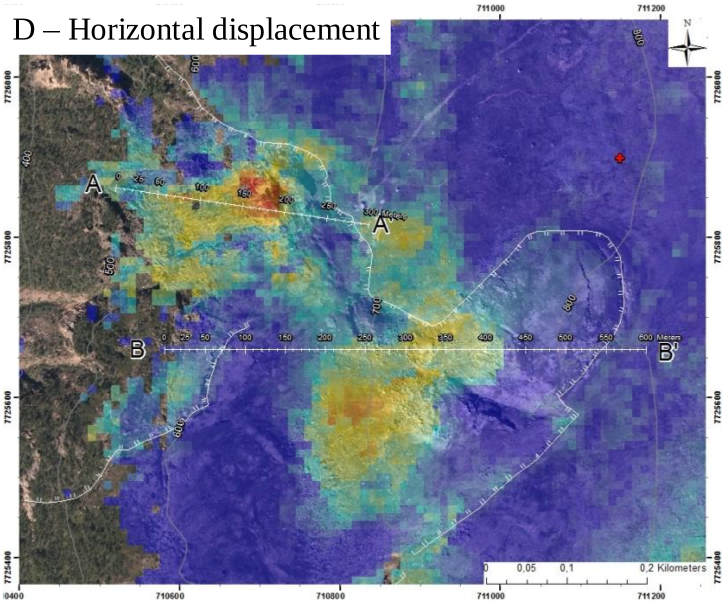
D – Horizontal displacement

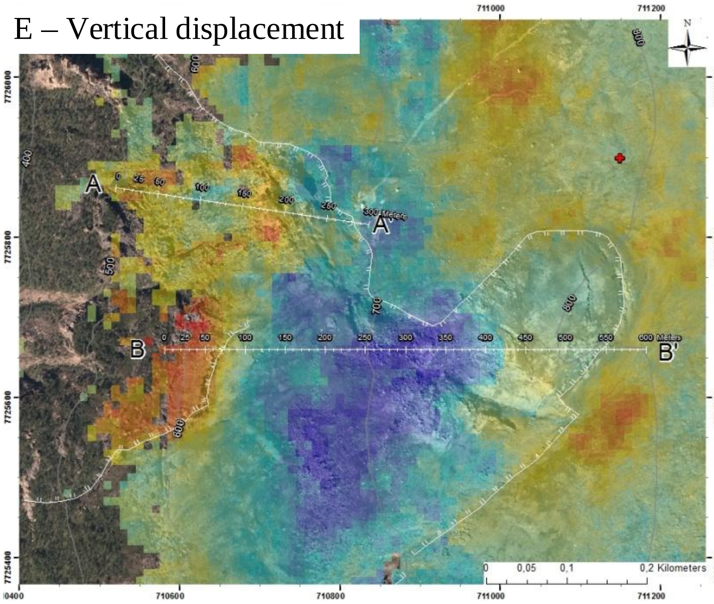
E – Vertical displacement

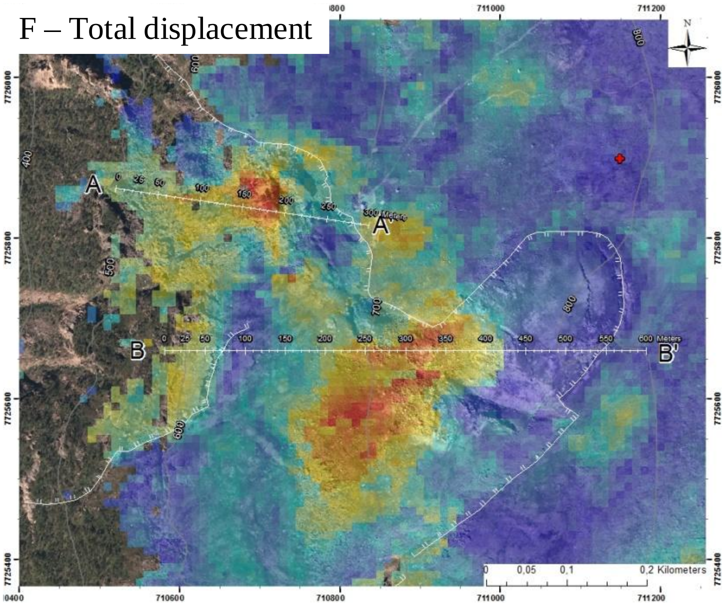
F – Total displacement

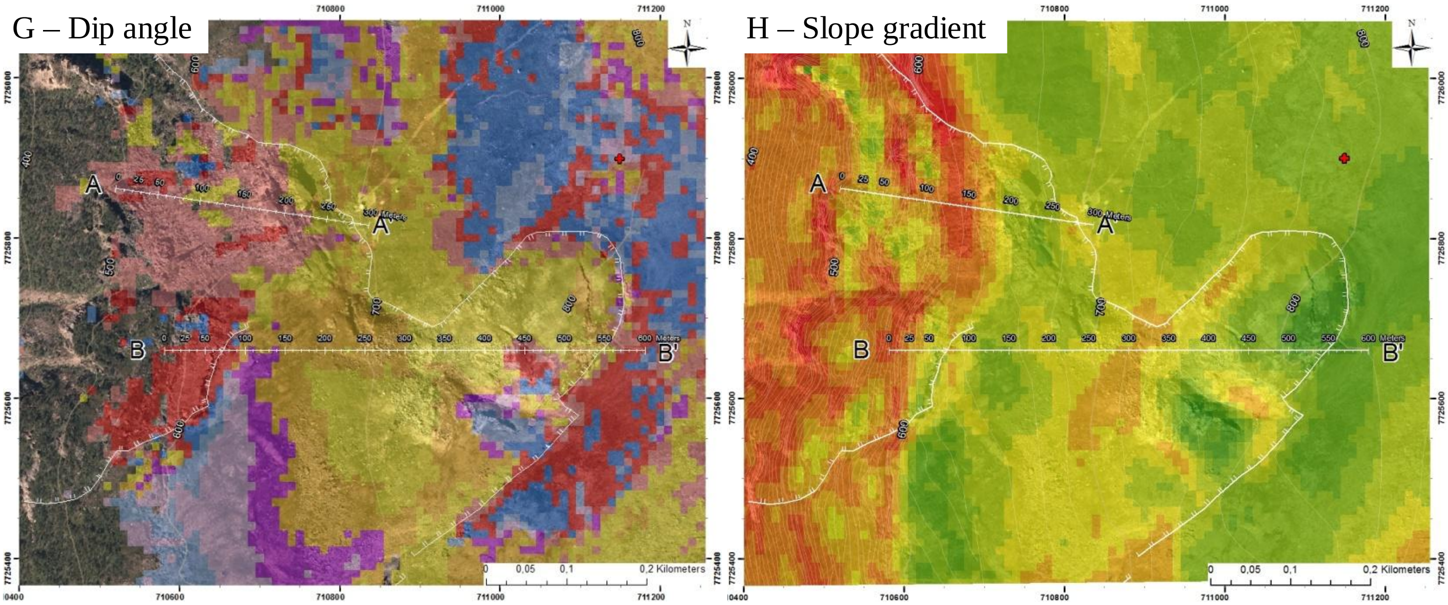

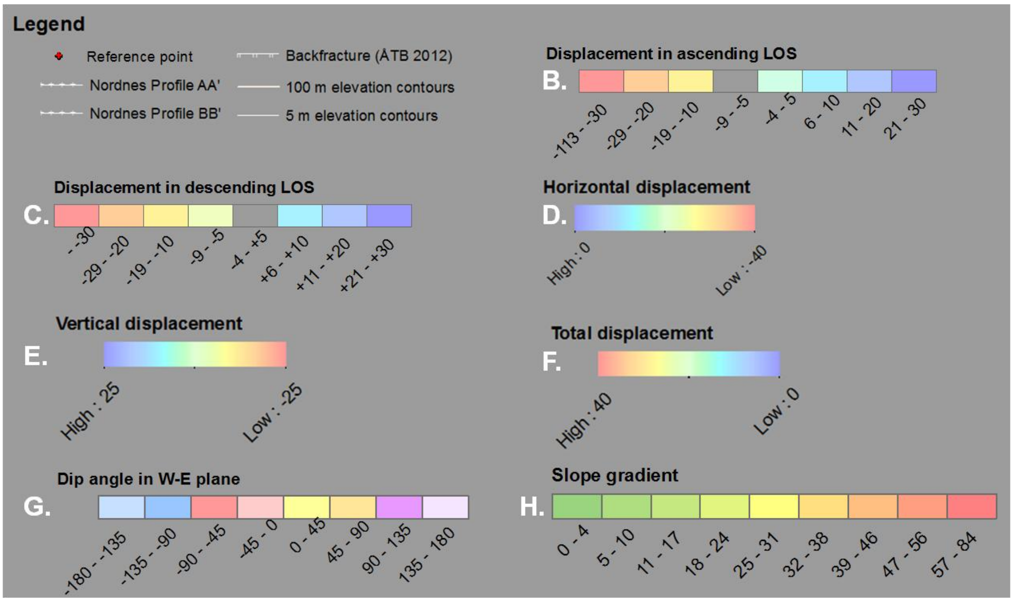

Fig. 39 - A. Orthophoto of Nordnes rockslide.
B. Ascending TSX data from 2009-2012.
C. Descending TSX data from 2009-2012.
D. Horizontal displacement in W-E direction.
E. Vertical displacement.
F. Total displacement vectors length.
G. Dip angle of total displacement vector in W-E plane.
H. Slope gradient map.

Mean yearly displacement rates in mm for 2011 from GPS stations at the Nordnes rockslide (Tab. 3) (NNFO, 2012) are included in the discussion in Section 3.3.1.2. dN is displacement in North–South direction, dE is displacement in East-West direction and dN is displacement in North–South direction.

From GPS data, strike, dip and length (mm/y) of total displacement vector have been calculated. This is plotted together with the location of the GPS station in (Fig. 40). Length of arrows indicates displacement rate.

Tab. 3 – Mean yearly displacement in North-South (dN)-, East-West (dE)- and Up-Down (dH) direction from GPS stations at the Nordnes rockslide from 2011 (NNFO, 2012). In addition strik, dip and total displacement vectors length calculated from GPS data is listed.

GPS	dN	dE	dH	Strike	Dip	Displacement
GPS YN 1	0,000	0,000	0,000	355	49	0
GPS YN 2	2,445	-7,788	-1,448	287	11	8
GPS YN 3	-8,153	-39,033	-13,816	258	19	42
GPS YN 4	3,232	-14,598	-11,218	282	38	19
GPS YN 5	3,558	-15,467	-11,434	283	36	20
GPS YN 6	5,833	-12,487	-12,020	295	44	18
GPS YN 7	2,999	-3,864	-4,092	308	47	6
GPS YN 8	4,836	-17,127	-1,127	286	4	18
GPS YN 9	4,454	-16,295	-6,269	285	21	18
GPS YN 10	7,544	-6,237	4,144	320	34	11
GPS YN 11	0,584	-1,984	-1,984	286	45	3

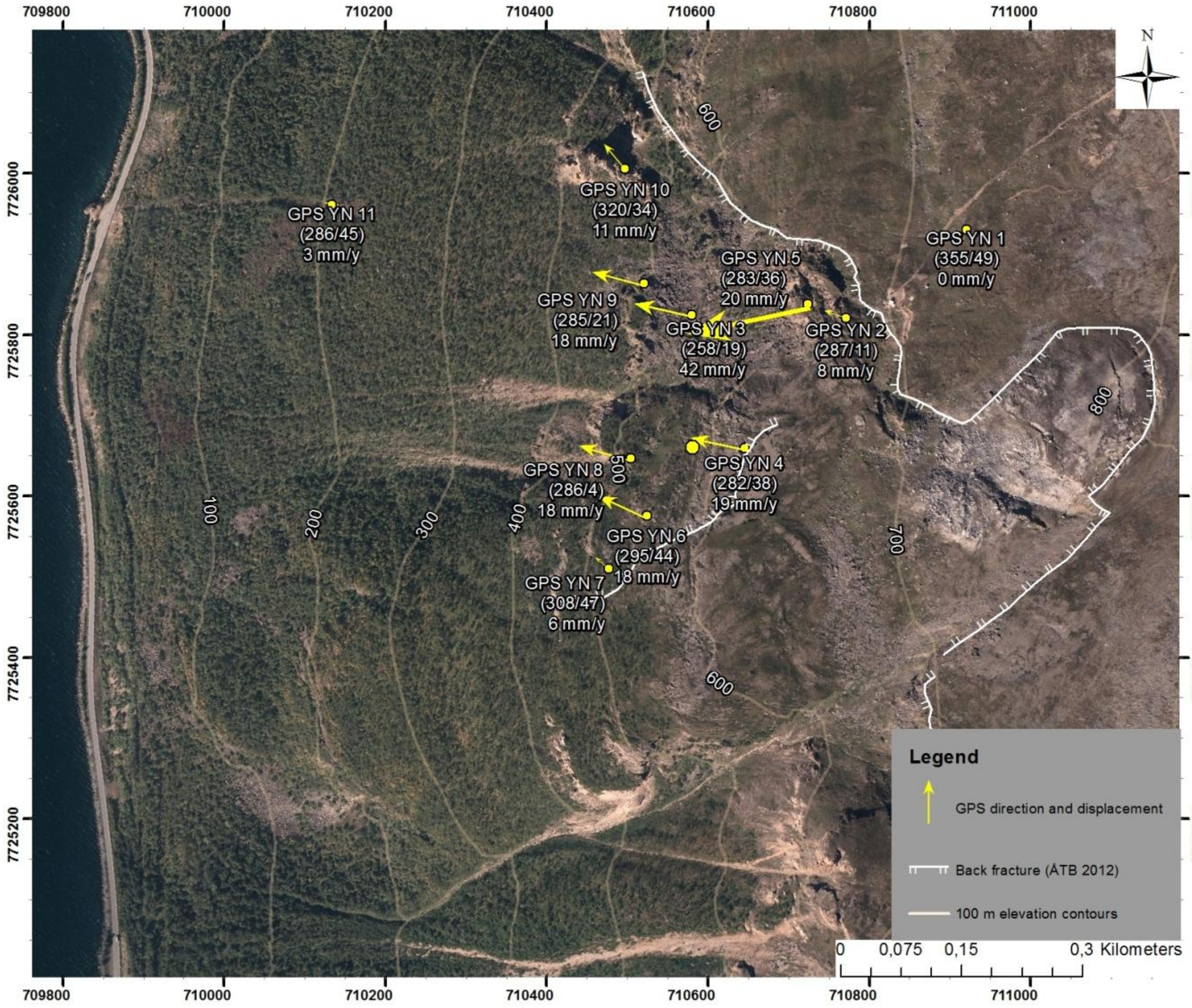

Fig. 40 - Location of GPS stations with calculated mean displacement- direction and magnitude data from 2011 (NNFO, 2012)

3.3.1.2 Discussion

In the following section elements like large fault blocks, lineaments, back fracture, open fractures, slide fronts and –scarps, identified in field and mapped by Åknes/Tafjord Beredskap, are related to patterns in the InSAR- and 2D InSAR data for the Nordnes rockslide. See (Fig. 41) for an overview of elements, profile lines and GPS stations used in the discussion.

Profile AA'

Comparison of structural- and morphological elements together with GPS data with to InSAR- and 2D InSAR data from profile AA' show that low points in the total displacement data in profile AA' are close to slide scarps at ~135 m and back scarp at ~300 m (Fig. 43). Total displacement values increase below these scarps, indicate a segmentation of slide material that correlating with mapped scarps. The peak of the total displacement values is at ~195 m, close to Block 2. This is a hinge point in the topographic profile (Fig. 43). An example of the same pattern is visible at ~95 m. The correlation between hinge points in the slope gradient and peaks in the total displacement values indicates a displacement pattern controlled by the slope gradient.

Dip data for the AA' profile shows a negative-positive pattern where some section of the profile are rising (positive dip angles) and some are subsiding (negative dip angles) (Fig. 44). Rising area can be toe-zone compression uplifting the front of a fault block. Similar patterns have been documented by (Braathen et al., 2004; Henderson et al., 2011). An example of this is the section from the highly fractured area around GPS station YN2 at ~250 m until ~90 m. There are negative dip angle from ~250 m to ~135 m, then positive values down to ~90 m. Another explanation of this negative-positive dip pattern can be rotation of fault blocks, caused by a listric detachment fault as found in passive continental margin developing during extension regimes (Lister et al., 1986; Lister et al., 1991), see red stippled line on (Fig. 44). This explanation is supported by observation of fault blocks in the slide area with foliation dipping to the East, in contrast to the overall foliation dipping gently to the West, as observed in the North lateral scarp and documented by (Braathen et al., 2004) and models proposed by (Blikra, 2012) (Fig. 42).

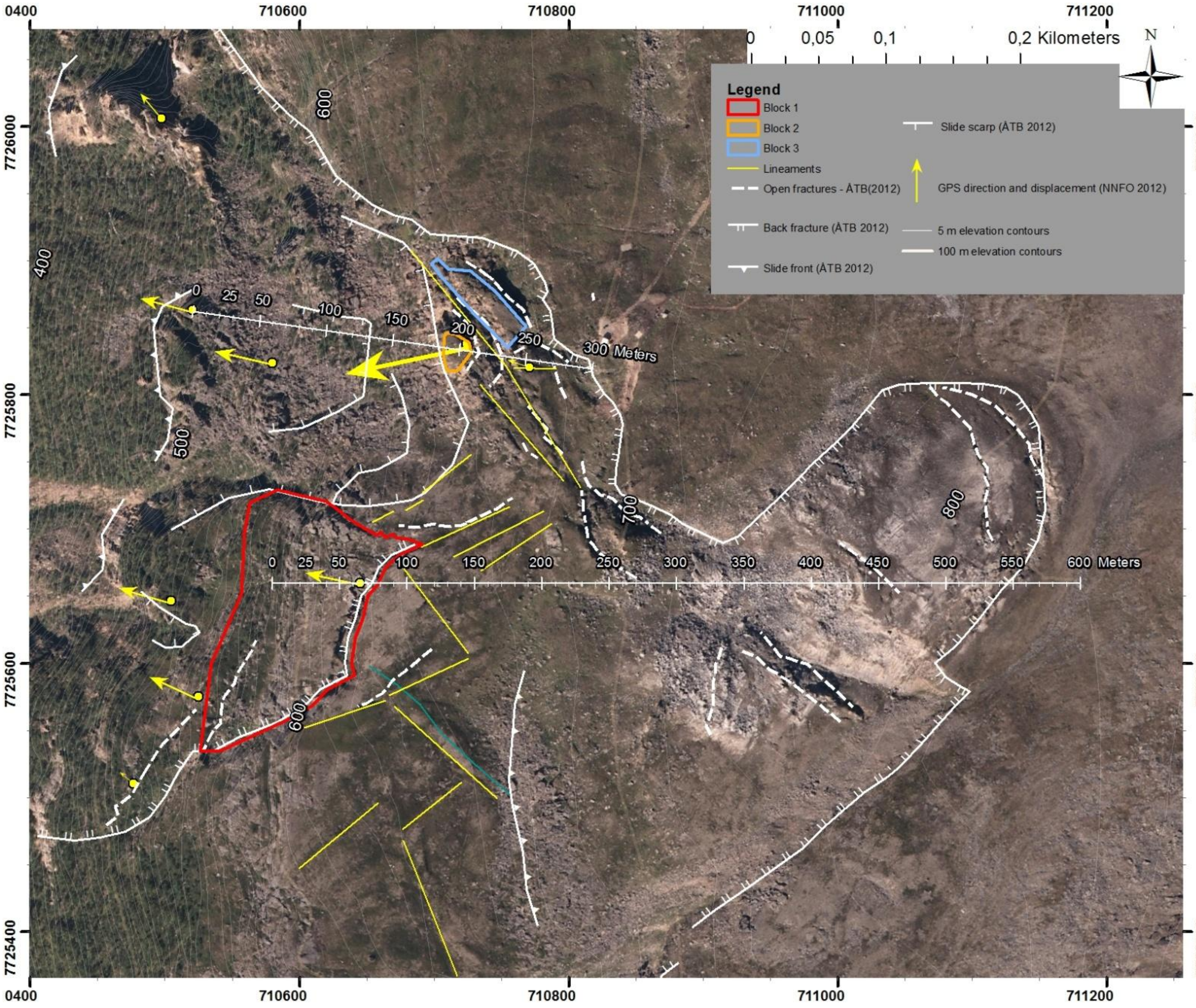

Fig. 41 - Structural- and geomorphological elements at Nordnes rockslide. From Åknes/Tafjord Beredskap, field observations and orthophoto studies.

Fig. 42 - East dipping fault blocks in the slide. Yellow lines indicate dip of foliation. Photographed from the North lateral scarp of the slide.

At ~35 m to ~45 m in profile AA’, ascending data show a sudden increase from ~-8 mm/y to ~+8 mm/y (Fig. 43). Downslope of profile AA’, the slope gradient goes down to ~50˚ (Fig. 39 H). If assuming that most longtime displacement generally follows the slope gradient, the ascending data has a low sensitivity to the displacement in this area. The change from negative to positive values could be an example of a change in dip direction with a more or less constant displacement rate close to the bind plane of the ascending geometry (see Section 2.4 and (Fig. 28)). An incidence angle of the ascending geometry of ~44˚ gives a dip of the blind plane of ~44˚ (180/44). This observed pattern can be explained by the change from displacement scenario D2 to D5 in (Fig. 27). Supporting this theory is the fact that this sudden increase in displacement velocity should be detected by descending data, and is not. The incidence angle of the descending geometry is ~37˚. This gives a blind plane of (000/37), and a good sensitivity to displacement in at the Nordnes rockslide.

The deviation between displacement measured by GPS stations in profile AA’ (GPS YN 2, GPS YN 3, GPS YN 5 and GPS YN 9) (Tab. 3) and 2D InSAR data from the profile line (Fig. 43) have been calculated and summarized in (Tab. 4). GPS displacements are marked with green dots (vertical displacement) and purple dot on the GPS lines in (Fig. 43).

Tab. 4 - Deviation between displacements measured by GPS stations in profile AA' and 2D InSAR data from the profile line

Compared displacement	**Deviation in mm/y**
GPS YN 2 East-West displacement (dE) against horizontal 2D InSAR data	6
GPS YN 2 vertical (dH) against vertical 2D InSAR data	5,5
GPS YN 3 East-West displacement (dE) against horizontal 2D InSAR data	5
GPS YN 3 vertical (dH) against vertical 2D InSAR data	4
GPS YN 5 East-West displacement (dE) against horizontal 2D InSAR data	8,4
GPS YN 5 vertical (dH) against vertical 2D InSAR data	9,6
GPS YN 9 East-West displacement (dE) against horizontal 2D InSAR data	3,7
GPS YN 9 vertical (dH) against vertical 2D InSAR data	3,7

For profile line AA' the mean deviation between the 2D InSAR data and GPS data for all the GPS stations was 5,7 mm/y horizontally and 5,7 mm/y vertically. Profile line AA' is in a highly fractured area where displacement patterns are expected to be complex. Considering this, and the fact that InSAR data are the average of many reflectors from a pixel (9,7 x 7,5 m) while GPS data are point measurements, there is quite good consistency between 2D InSAR- and GPS data.

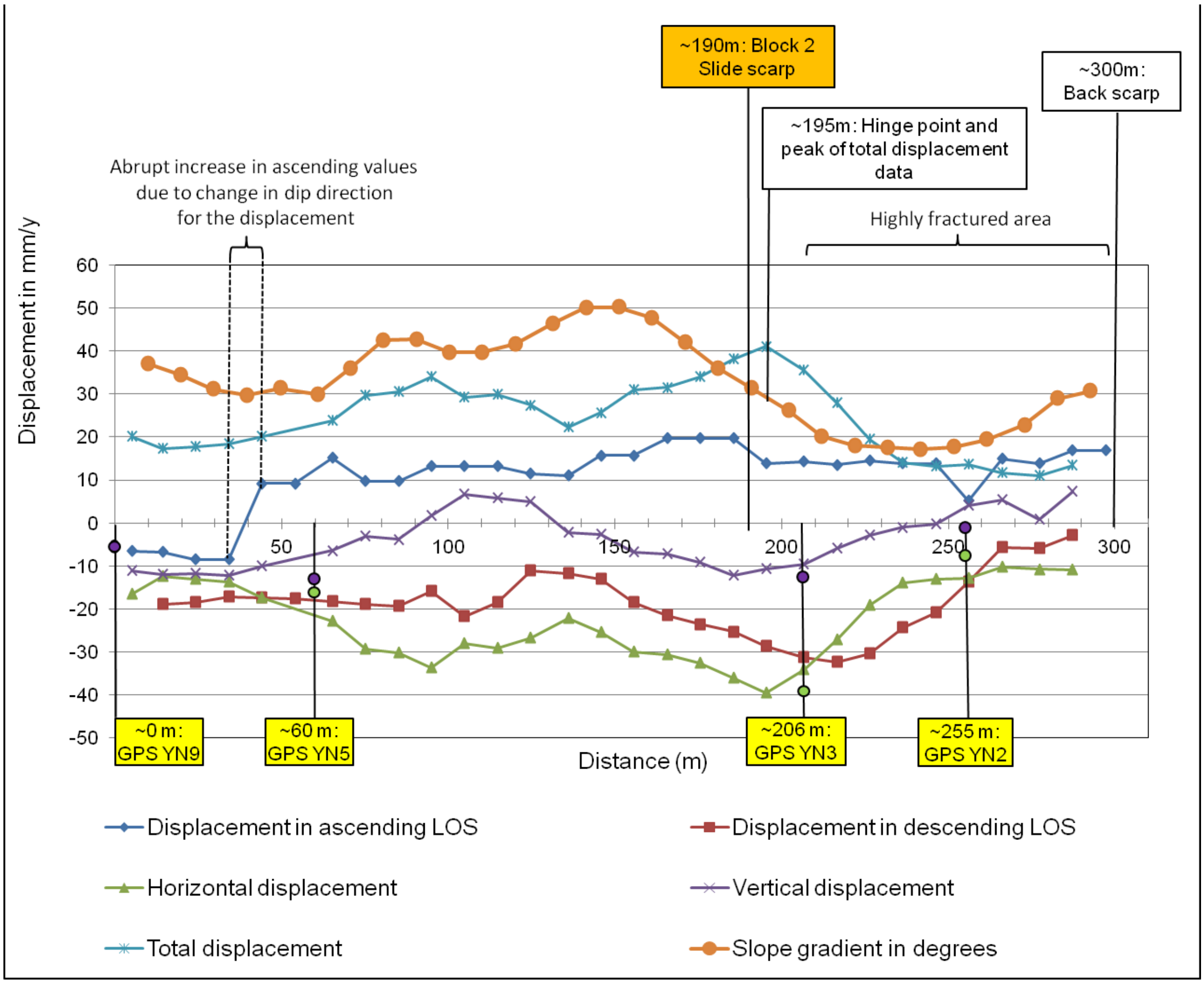

Fig. 43 - InSAR and 2D InSAR data for Nordnes profile AA' with GPS stations, fault blocks, slide- and back scarp. GPS displacement is marked with green dots (vertical displacement) and purple dot on the GPS lines.

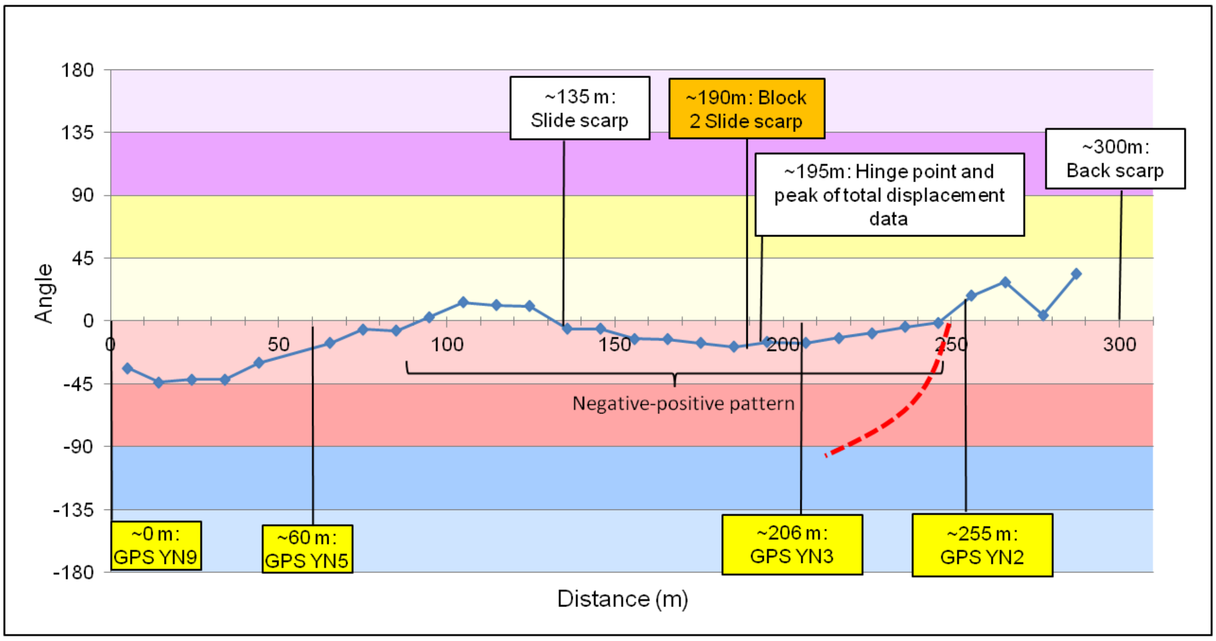

Fig. 44 - Dip angle for total displacement in Nordnes profile AA' in East-West plane with geological structures and negative-positive pattern. Stippled red line indicate location of possible listric detachment.

Profile BB’

In (Fig. 45 and Fig. 46) the structural- and morphological elements together with GPS data from the Nordnes rockslide are compared to the InSAR- and 2D InSAR data from profile BB’. The fracture separating Block 1 (~70 m) is visible as large changes in horizontal- and vertical displacement, and a dramatic fall in total displacement. The same is the case for the large fractures starting at ~425 m. These changes are not so localized to the fractures in the ascending and descending data. The dip angle data show dramatic changes in the same areas (Fig. 46). The displacement rate in the area of the back fracture (~550 m) is not large, but the vertical displacement changes from positive to negative values close to the back fracture (~550 m). The back fractures are easier to spot in the dip angle data. For this profile 2D InSAR data correlates with the structural elements. The constant increase in ascending data peaking at ~280 m, followed by a decrease, and a sudden fall at ~370 m together with positive descending data give decomposed result of almost 30 mm/y vertical upward displacement and ~-25 mm/y westward horizontal displacement. 2D InSAR data show that the section between ~100 m and ~425 m have an upward and westward displacement. This trend is visible as ~45˚ upward dip angles for the total displacement vector in the same area. The slope gradient for profile BB’ has the same trend as the total displacement vector indicating that the displacement is dependent on the topography.

Ongoing work at Nordnes has found patches of permafrost and a correlation between displacement rates, temperature and snow melt (Blikra and Christiansen, 2012). They have postulated a theory explaining the increase in displacement velocities in May, with a decrease in shear strength in ice-filled crack. This is induced by a temperature increase due to drainage of melt water warming the ice above the pressure melting point. Let’s assume there is permafrost present in fracture systems below the lifting area between ~150 m and ~425 m in profile BB’. Then the question is if freezing and expansion of melt water in the spring draining through fractures, and of groundwater during the summer, coming in contact with permafrost, can create the displacement patterns we are observing. Further research is necessary before this question can be answered.

The deviation between displacement measures by GPS YN4 and the 2D InSAR data from the profile line was 7 mm/y in the horizontal direction and 0,6 mm/y in the vertical direction (Tab. 3) and (Fig. 46). Horizontal displacement GPS displacement (dE) is marked with green dots and vertical displacement is marked with purple dot on the GPS line in (Fig. 45). Reasons for the deviation in profile BB’ are the same as discussed for profile AA’.

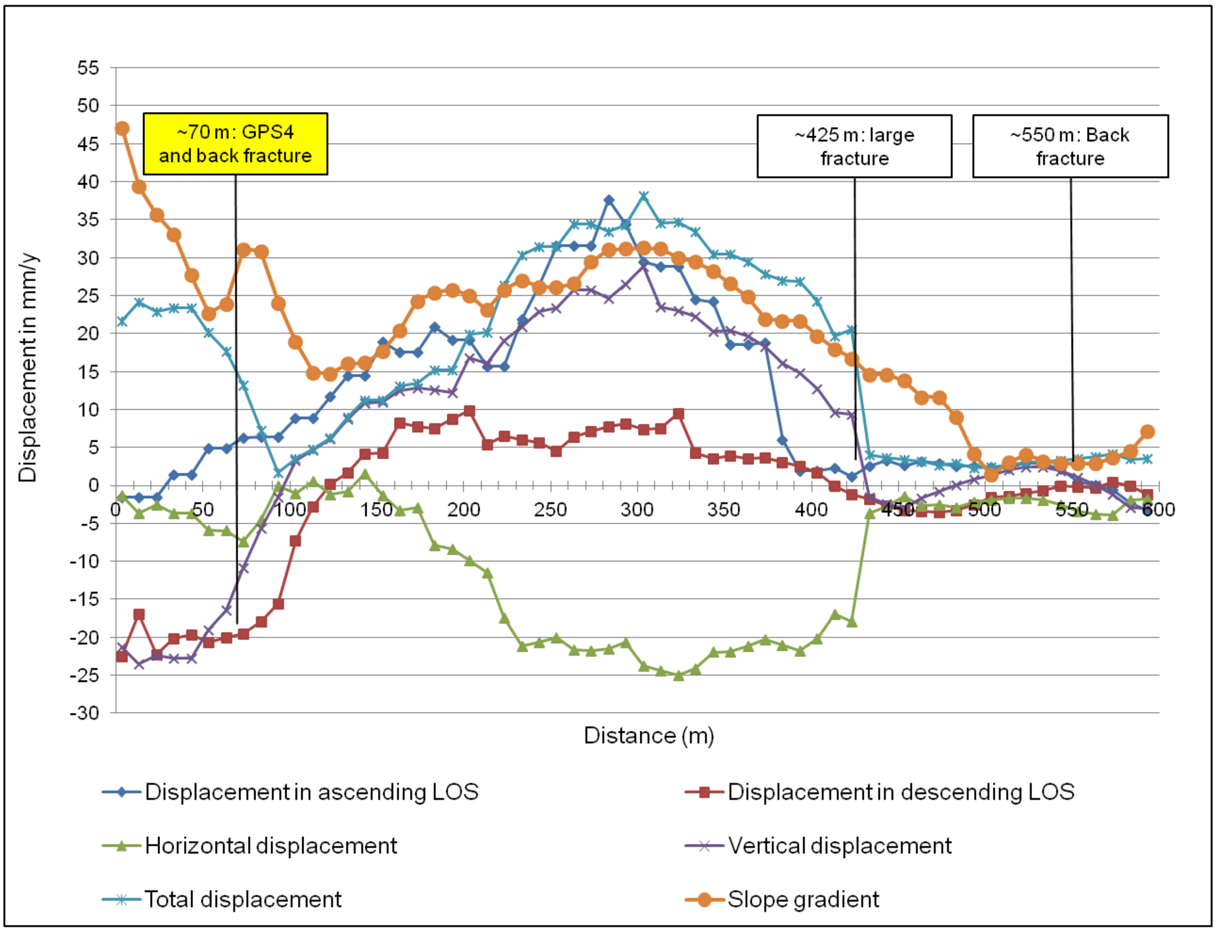

Fig. 45 - InSAR and 2D InSAR data for Nordnes profile BB' in East-West plane with geological structures pinpointed. Displacement measured at GPS station YN4 is marked with green dots (horizontal displacement) and purple dot (vertical displacement) on the GPS lines.

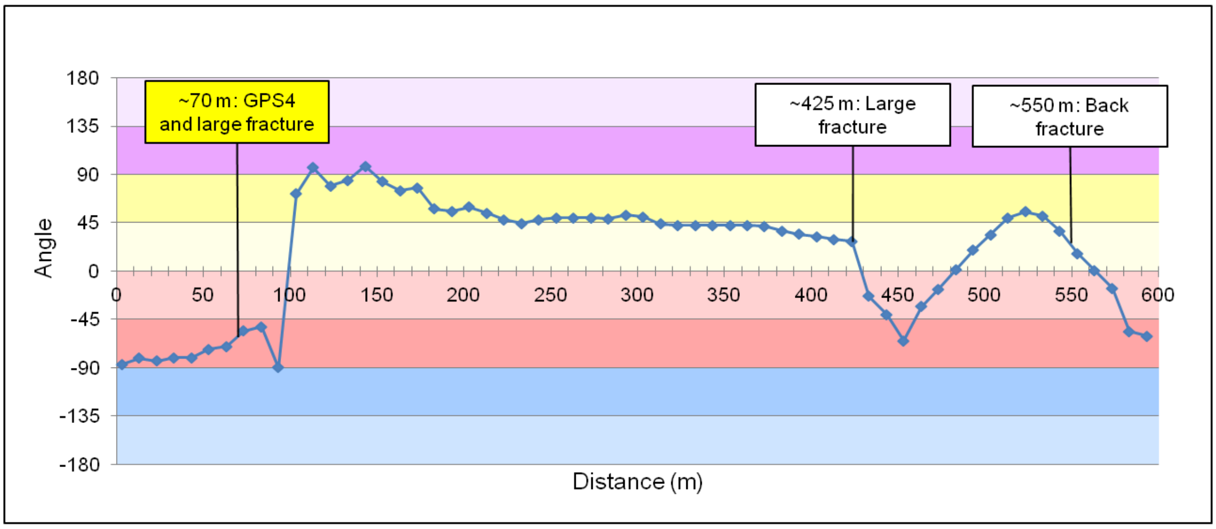

Fig. 46 - Dip angle for total displacement in Nordnes profile BB' in East-West plane with geological structures pinpointed.

From profile AA’ and BB’ the slide can be divided into two areas, a northern and a southern, with overall different displacement patterns. The northern area covered by profile AA’ has a terrace-slope-terrace topographic profile with large horizontal component and smaller varying vertical component. The dip angle of total displacement is varying indicating rotation of fault blocks, or an active thrust duplex. Observed displacement patterns from 2D InSAR supports work by (Blikra, 2012; Braathen et al., 2004) that Nordnes is a complex slide with listric fault detachment. This is supported by GPS data from GPS stations GPS YN 2, GPS YN 3, GPS YN 5 and GPS YN 9.

The southern area is transected by the lower parts of profile BB’, from the fracture separating Block 1 (~70 m) and further down. This area has a large vertical component and a smaller horizontal component in 2D InSAR data, giving steeper dip angle of total displacement. This is supported by GPS station YN4.

3.3.2 Gamanjunni3 rockslide in Manndalen

3.3.2.1 Results

Orthophoto in (Fig. 47) show the outline of the lateral borders, back fracture of the Gamanjunni3 rockslide. The common reference point selected for ascending- and descending data is also marked.

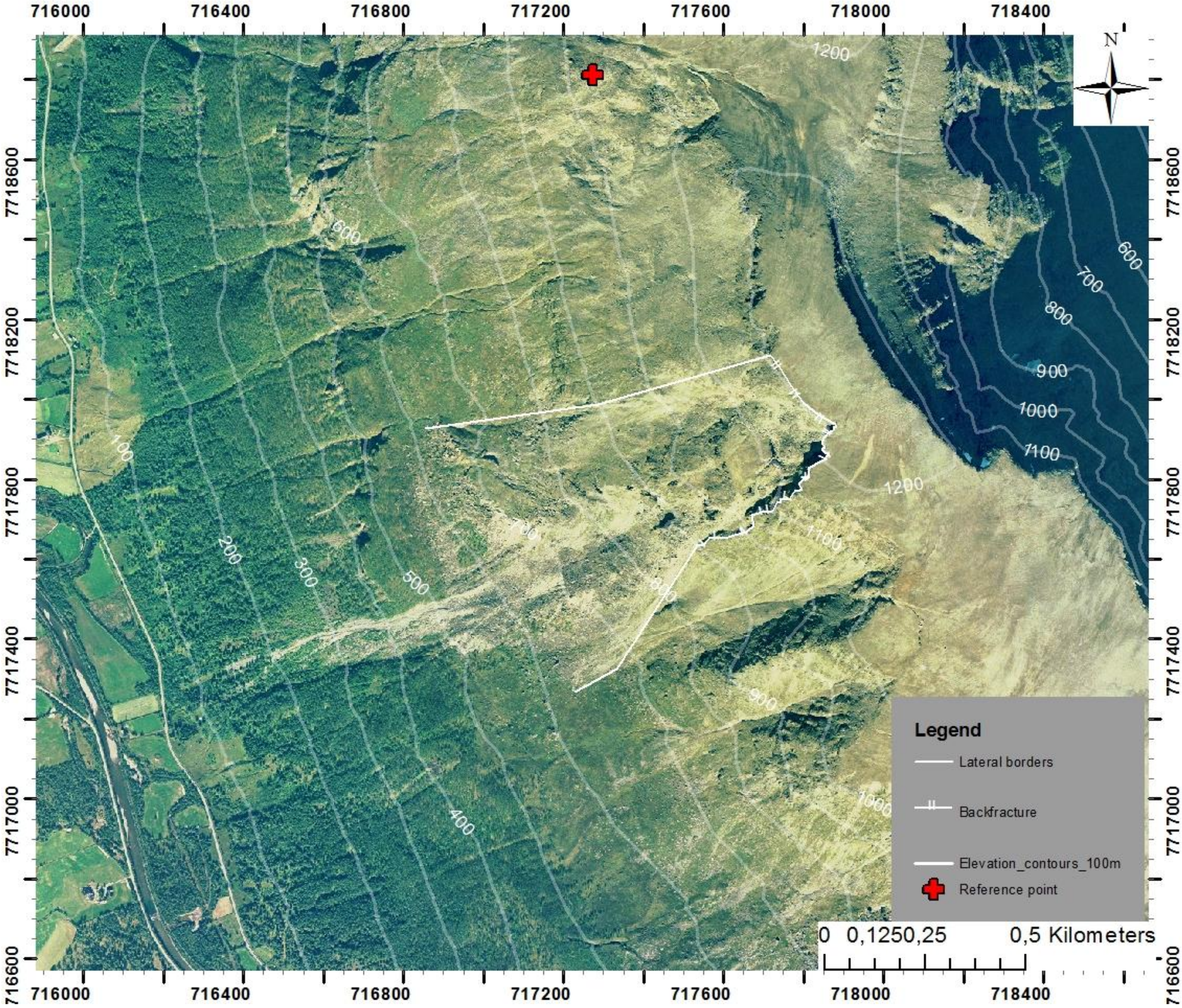

Fig. 47 - Orthophoto of Gamanjunni3 rockslide.

The common reference point was placed in terrain with a slope gradient of 23˚ with high coherence, looking like stable bedrock from orthophoto study. Preferably a reference point should be selected close to the object you would like to study. In this case the area on the sides and above Gamanjunni3 had low coherence values. The distance is still reasonably short (< 1 km) and atmospheric contribution influence on a larger scale.

InSAR- and 2D InSAR data from two profiles, AA' and BB', was extracted. Results are presented in map view (Fig. 48 B to G) and as plots of data from the profile AA' and BB' (Fig. 51, Fig. 52, Fig. 54 and Fig. 55).

Ascending data is varying between ~20 mm/y and ~-20 mm through the AA' profile and between ~60 mm/y and ~-10 mm/y in the BB' profile. In profile AA', there are positive values (displacement towards the radar) from 0 - ~400 m and low and varying values from ~400 m and out. In profile BB' ascending data rises from 0 – ~60 mm/y displacement from 0 m until ~180 m. Then the values are declining towards ~400 m and leveling out at the end of the profile.

The descending data in profile AA' increases from ~5 mm/y displacement to ~-90 mm/y from 0 m to ~950 m. Then there is an abrupt decrease in displacement. In profile BB' there is a high displacement (~ -180 mm/y) between ~160 m and ~275 m. From ~300 m to ~675 m the displacement are between ~60 and 80 mm/y. At 675, there is an abrupt decrease in velocity. Calculated 2D InSAR horizontal displacement data resemble the ascending data in both profiles. This is also the case with the vertical displacement data, but here the values are more damped. The dip angle of the total displacement in profile AA' shows upward dip from 0 to ~100 m, then varying dip angles to ~300 m, then an increase and a quite stable dip from ~-45 to ~950 m. Close to the back fracture the dip angle is very varying. Dip angle in the BB' profile show upward dip in lower area of the slide, dip between ~-20 and ~-45 in the middle section and vertical varying dip in the upper part.

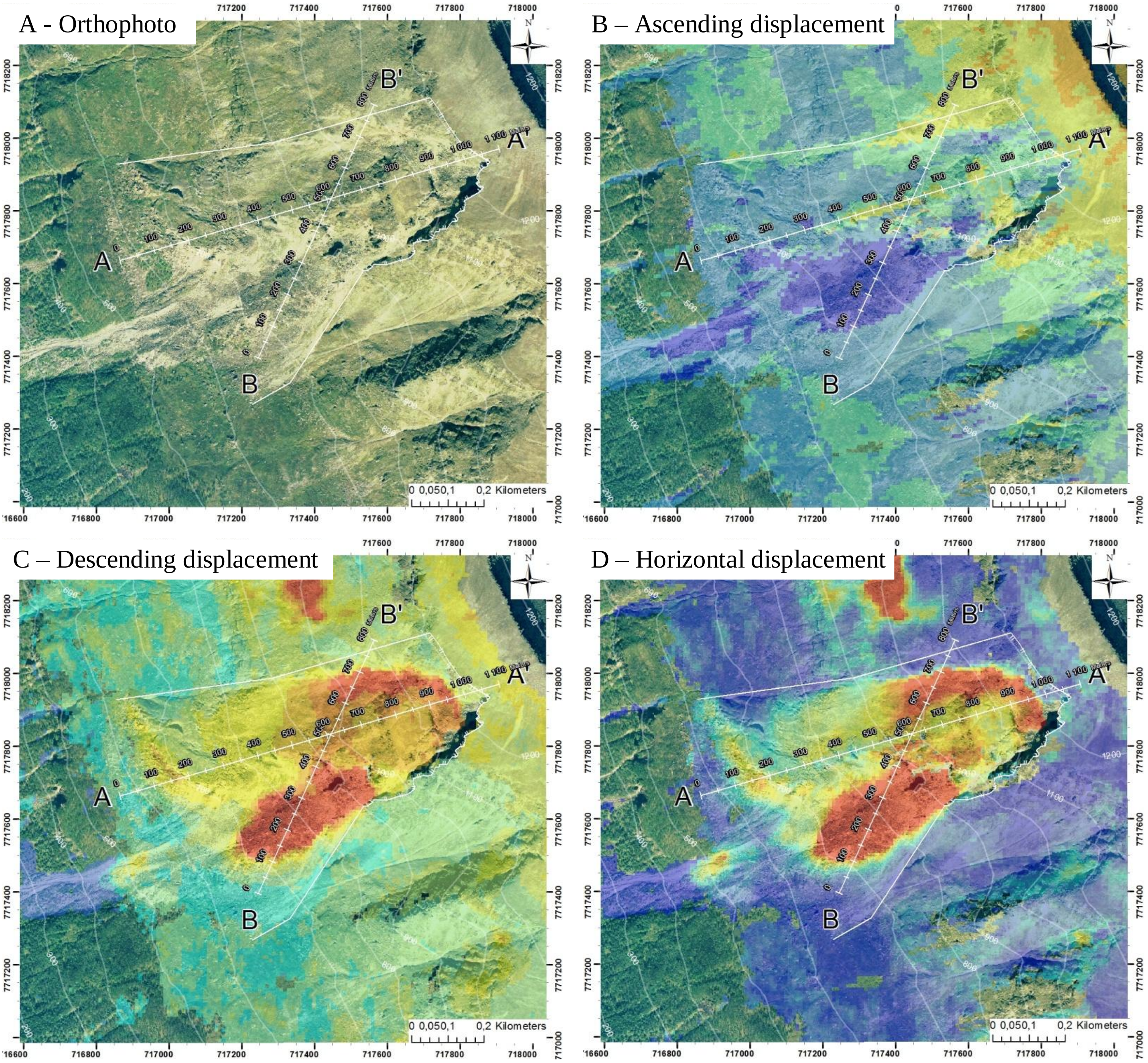
A - Orthophoto
B – Ascending displacement
C – Descending displacement
D – Horizontal displacement
A
A'
B
B'
0 0,050,1 0,2 Kilometers
716600
716800
717000
717200
717400
717600
717800
718000
7717000
7717200
7717400
7717600
7717800
7718000
7718200

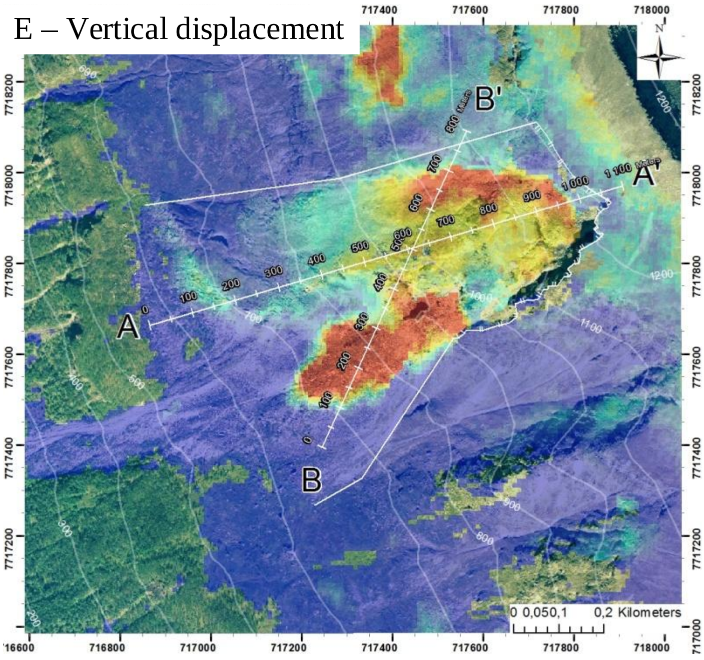

E – Vertical displacement

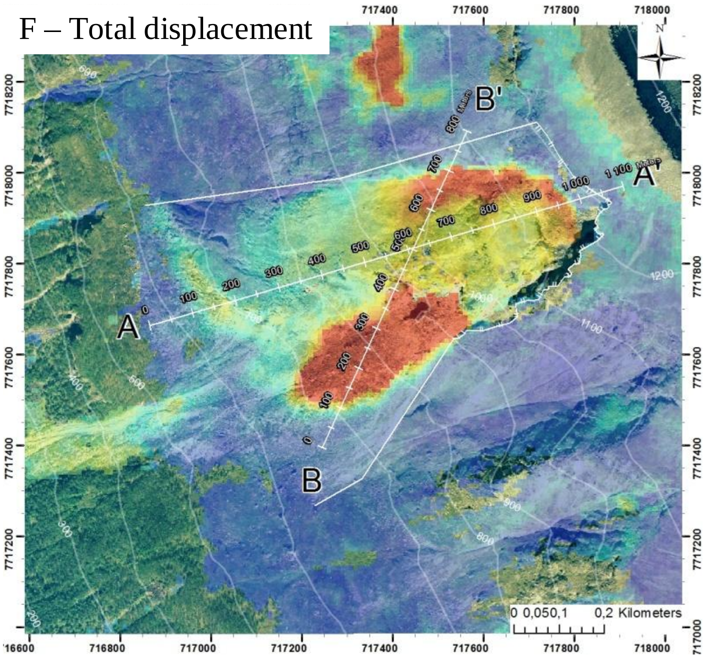

F – Total displacement

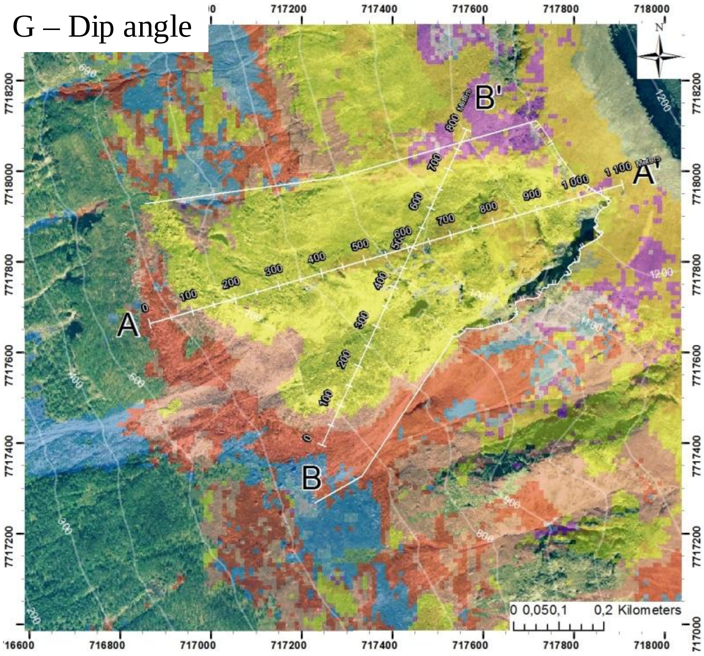

G – Dip angle

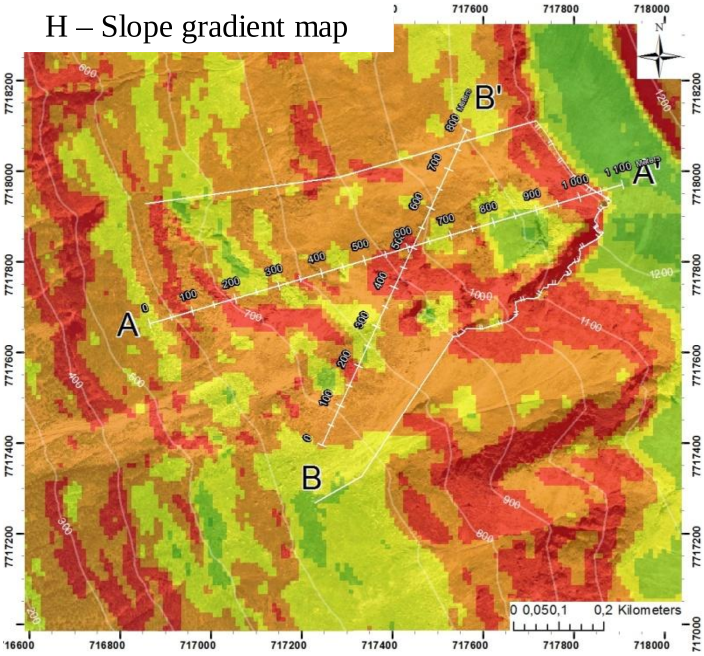

H – Slope gradient map

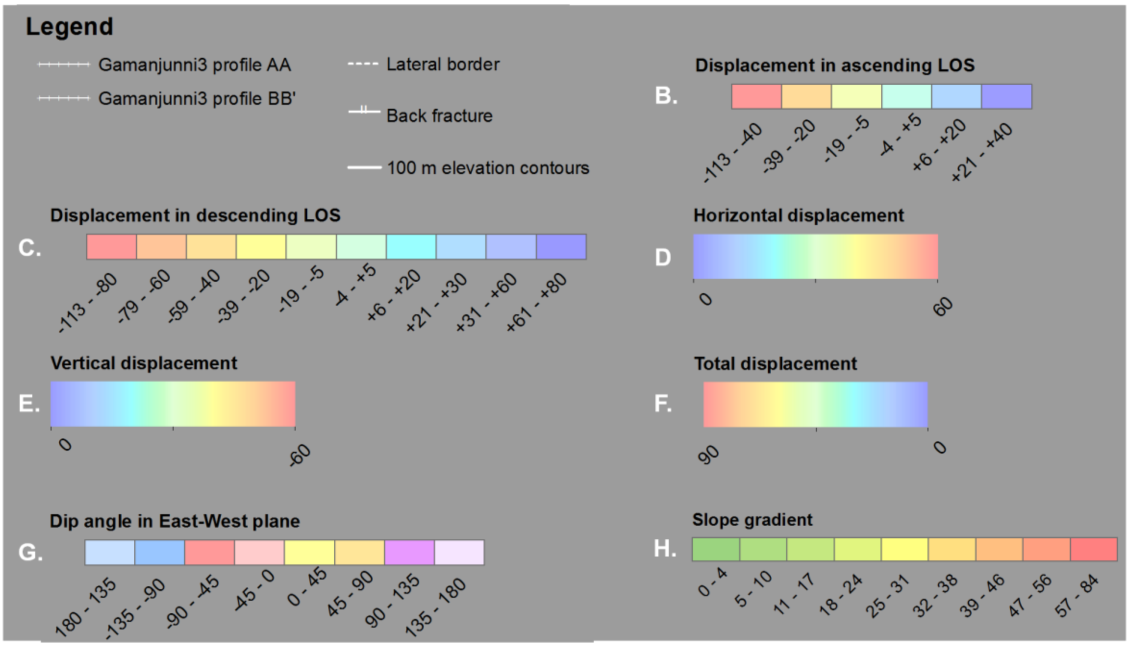

Fig. 48 - A. Orthophoto of Gamanjunni3. B. Ascending TSX data from 2009-2012. C. Descending TSX data from 2009-2012. D. Horizontal displacement in W-E direction. E. Vertical displacement. F. Total displacement vectors length. G. Dip angle of total displacement vector in W-E plane. H. Slope gradient map.

3.3.2.2 *Discussion*

As an overview (Fig. 49 A) show photographs of the Gamanjunni3 rockslide with mapped lateral borders, backs carps and toe zone (Bunkholt, 2013). Displacement of the fault block and minor back-rotation of the fault block has been documented by (Bunkholt et al., 2011) (Fig. 49 B).

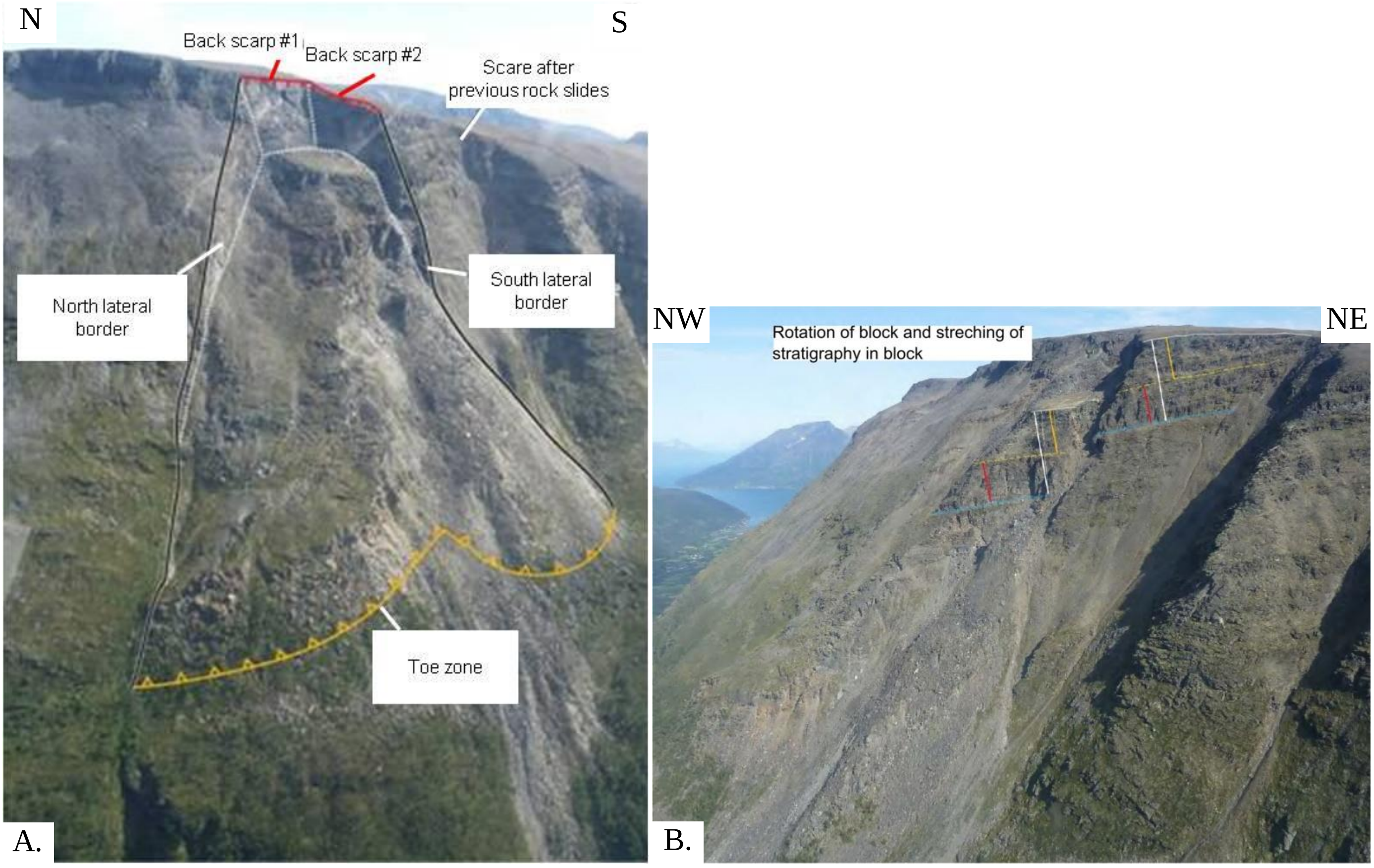

Fig. 49 – A. Overview of Gamanjunni3. Modified after (Bunkholt, 2013) B. Correlation of unstable block with stable ground (Bunkholt et al., 2011).

Location of structural- and geomorphological elements at the Gamanjunni3 rockslide referred to in this discussion can be found in (Fig. 50).

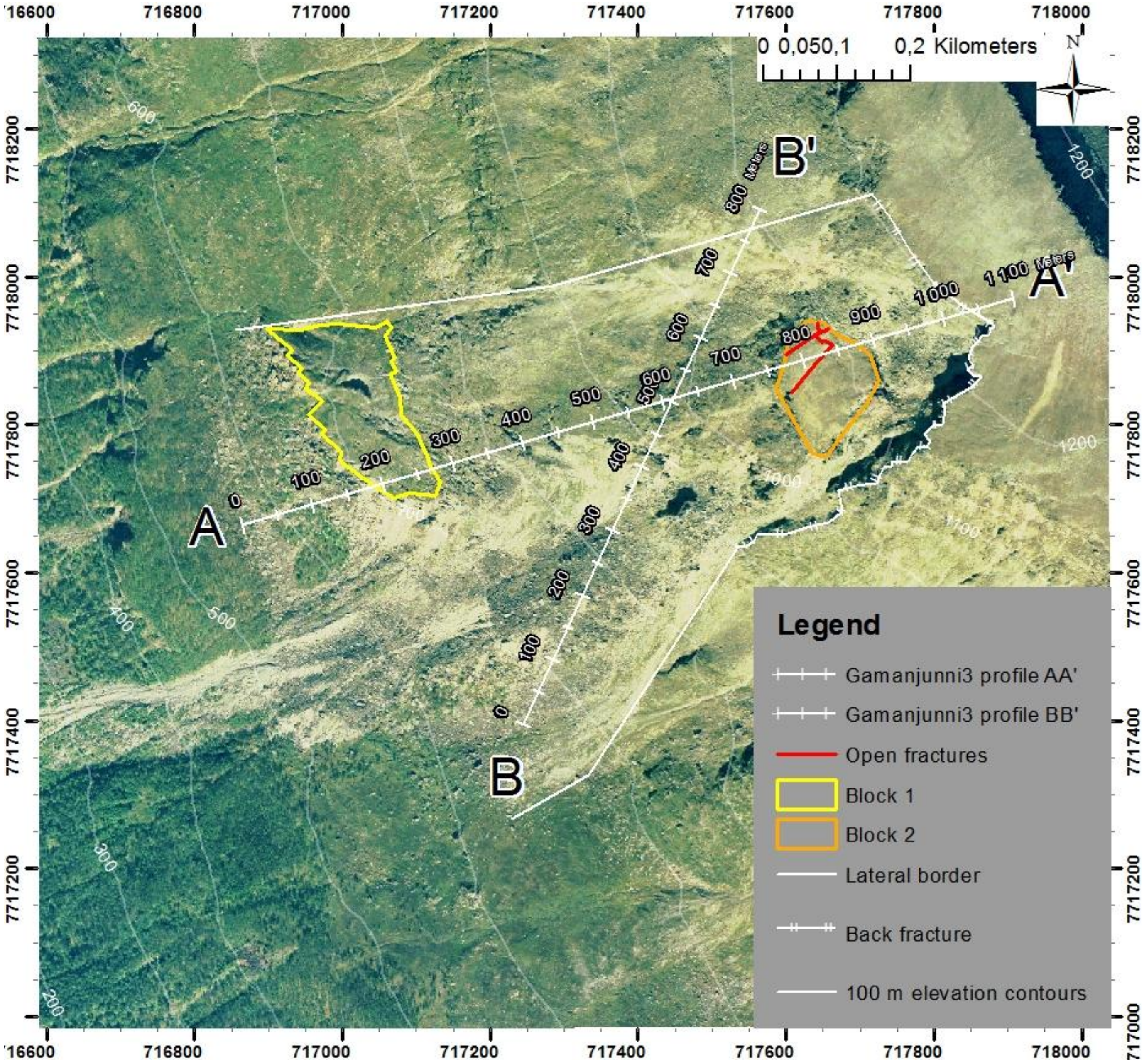

Fig. 50 - Structural- and geomorphological elements at Gamanjunni3 rockslide.

For the Gamanjunni3 rockslide, the general slope gradient for the slide is calculated to be ~33˚ (distance from the road in the valley to the back scarp) with dip towards West. Similar to the Nordnes rockslide, sensitivity to displacement in the Gamanjunni3 rockslide is higher in the descending- than the ascending InSAR data.

In the profile AA' the general trend of the Gamanjunni3 rockslide is increasing displacement from the toe zone to the back scarp. From ~100 m to ~225 m, there is a section with peaking descending- and stable ascending data (Fig. 51). This gives high 2D InSAR displacement values with total displacement dip angle of ~-25˚ and velocity of ~55 mm/y. The section from 0 m to ~100 m shows upward dip of total displacement (~55˚) but lower velocities. This gives a negative – positive dip angle pat tern (Fig. 52) as observed in the Nordnes Rockslide in profile AA' and discussed in Section 3.3.1.2. For the Gamanjunni3 rockslide as for the Nordnes rockslide, this pattern could be a consequence of rotation of fault blocks or the development of a thrust duplex in the toe-zone. Considering the high abundance of rock glaciers in the region (Frauenfelder et al., 2008; Tolgensbakk, 1988), the negative-positive pattern of the dip angel of total displacement in this section could be explained by a downslope flow of a small rock glacier. The slope gradient in the section is higher than upslope (Block 1) and the largest displacement in this section appears downslope of the topographic hinge-point at ~205 m.

Block 1 (~190 to ~270 m) has a constant slope gradient of ~30˚ and generally constant displacement rates. This indicates no rotation and that the block is moving like one body. From ~ 600 m to ~ 300 m, there is a decrease in displacement velocities. This is interpreted as a slowing down of slide material pushing on from behind. Supporting this interpretation is the fact that the dip angel changes from ~-45˚ to ~0˚ from ~400 m to ~300 m, indicates compression and relative upward displacement in this section.
The middle section (~600 m to ~875 m) consists of fragmented bedrock separated by large fractures. It has generally constant displacement velocities and the dip angels of the total displacement have minor variations. This indicates that the slide material in the middle of profile AA' moves as a homogenous body.

Block 2 in the upper part of the slide (~760 m to 870 m), has a quite stable displacement trend in the upper part of the block. In the lower part of the block, from ~815 m to ~760 m, there are variations in the displacement. The 2D InSAR data indicate an increase downward in vertical displacement and a steeper dip angel of total displacement towards the lower border of the block. This is interpreted to be an accelerating displacement on a shallow detachment due to increase in slope gradient towards the lower part of the block. Open fractures indentified from orthophoto support this fragmentation of Block 2 (Fig. 50).
A most probable sliding direction of (250/47) have been found for the Gamanjunni3 rockslide from kinematic stability tests performed by NGU. Their results are supported by Differential Global Navigation Satellite System (dGNSS) data from 2013 and TSL LIDAR (Bunkholt, 2013) (H. Bunkholt, personal communication, 2013), and matching 2D InSAR dip angle direction calculated in this thesis (see red dot in Fig. 52).

From Block 2 to the back scarp, the slope gradient is increasing from ~15˚ to ~40˚. This is the area with highest displacement rates in the profile. At ~ 950 m, there is an abrupt decrease in displacement. This is interpreted to be related to the back scarp.

In general, the slope gradient for profile AA’ resemble the total displacement data. This shows that the displacement rates are controlled by the slope gradient. Sensitivity to displacement in Gamanjunni3 is different in ascending- and descending geometry. This can be seen from ~325 m up to the back scarp, where ascending data have low and varying displacement rates. An explanation can be that a change in the overall dip angle of the total displacement, are approaching the blind plan of the ascending geometry. The calculation of 2D InSAR data by combining displacement from ascending- and descending InSAR data, has made it possible to extract more details about the displacement patterns in the Gamanjunni3 rockslide.

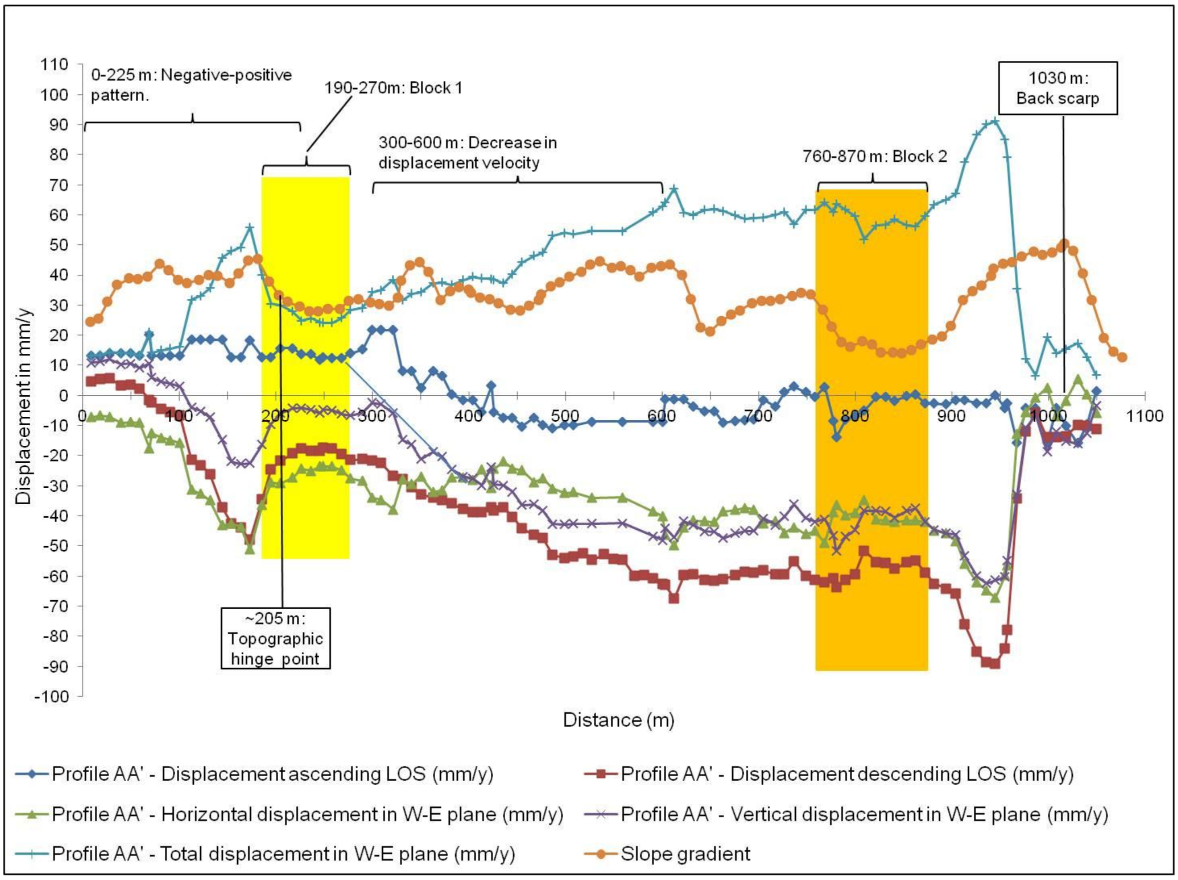

Fig. 51 - InSAR and 2D InSAR data for Gamanjunni3 profile AA' with structures and displacement patterns from 2D InSAR data.

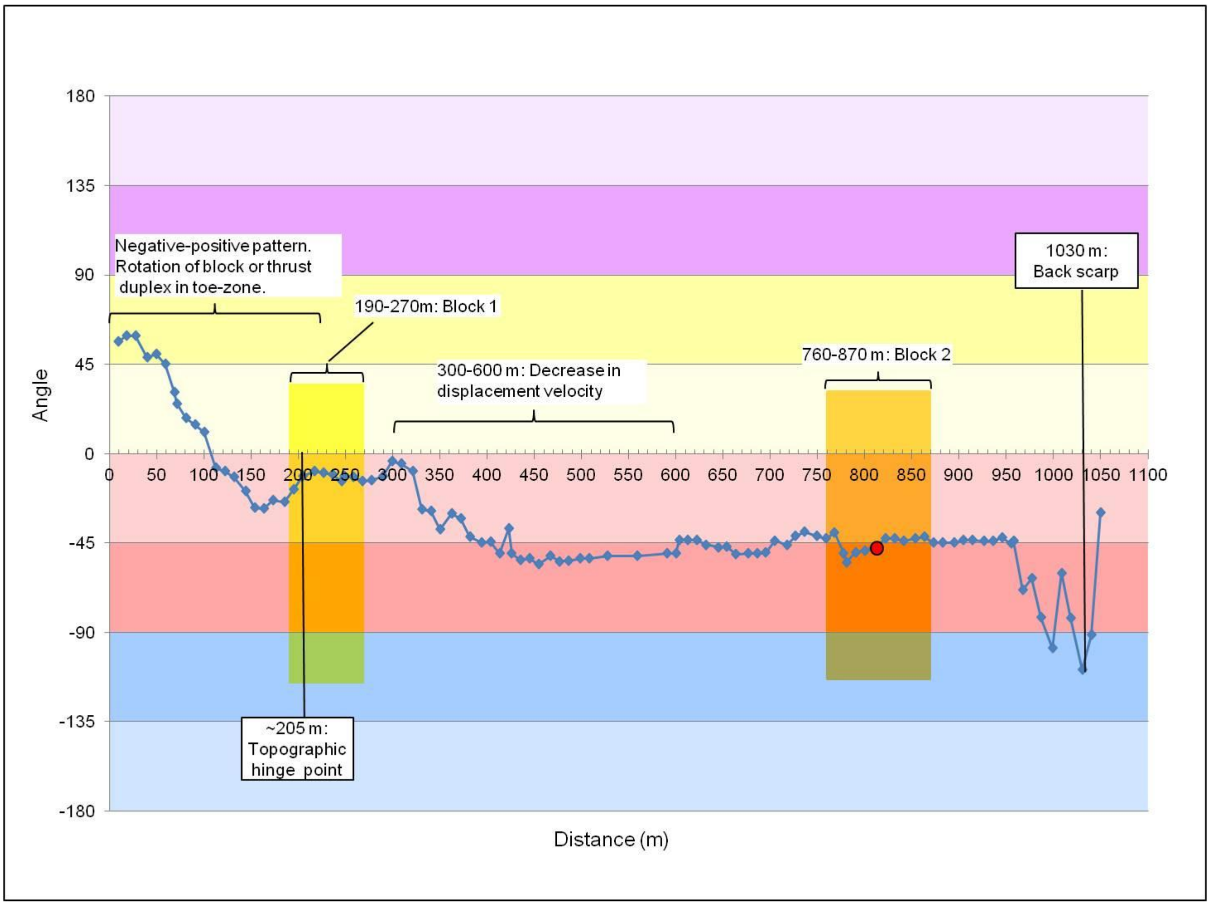

Fig. 52 – Dip angle of total displacement in Gamanjunni3 profile AA' with geological structures and displacement patterns from 2D InSAR data. Most probable sliding direction (250/47) for Block 2 from (Bunkholt, 2013) is marked with red dot.

Profile BB’ can be divided into three parts based on displacement rate and -pattern from 2D InSAR data; a high velocity area, a central area of the slide with lower velocities and a lateral zone with high displacement velocity. The high velocity area (~75 m to 300 m) has large displacement rates (Fig. 54) and stable values for the dip angle of total displacement (Fig. 55) indicating a flowing motion. Observation of this high velocity area indicates that this is an active rock glacier (Fig. 53). It is tongue shaped, has a steep front and no sign of vegetation indicating ongoing mass-wasting.

Fig. 53 - Rock glacier in high velocity area in profile BB'.

The central area (~300 m to ~550 m) has varying dip angle of total displacement and 2D InSAR data. It has the same undulating pattern as observed in the middle of profile AA' (Fig. 51). These variations in both profile AA' and profile BB' suggest that the middle part of the slide is built up of smaller and larger blocks interacting in a complex pattern. The lateral zone with high velocity (~550 m to 675 m) show the same characteristics in 2D InSAR data as the interpreted rock glacier in the high velocity area. It has large displacement rates (Fig. 54) and stable values for the dip angle of total displacement (Fig. 55), indicating the same flowing motion. No tongue shaped forms can be found on the orthophoto and further investigations are needed before concluding about the driving forces behind the measured displacement velocities.

Using definitions after (Braathen et al., 2004), the Gamajunni3 rockslide can be defined as a complex field with a planar fault geometry. Field observations and orthophoto interpretation indicating large fractures and large fault blocks with minor rotations support this. In addition 2D InSAR data show stable angles of total displacement in the majority of the slide (Fig. 52). For the profile BB', the dip angle of total displacement together with total displacement were very valuable and made it possible to distinguish between the rockslide and the rock glacier just by inspecting the 2D InSAR data.

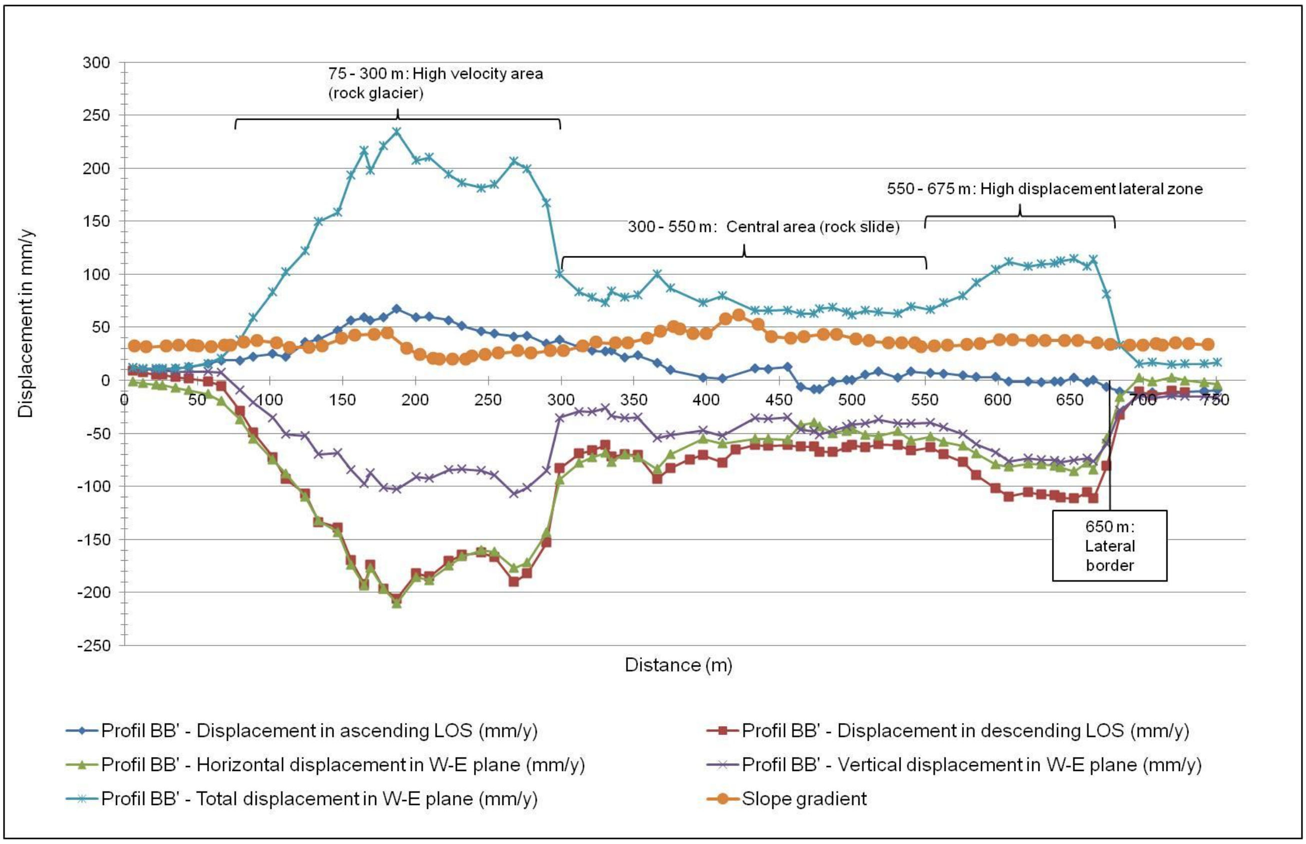

Fig. 54 - InSAR and 2D InSAR data for Gamanjunni3 profile BB'.

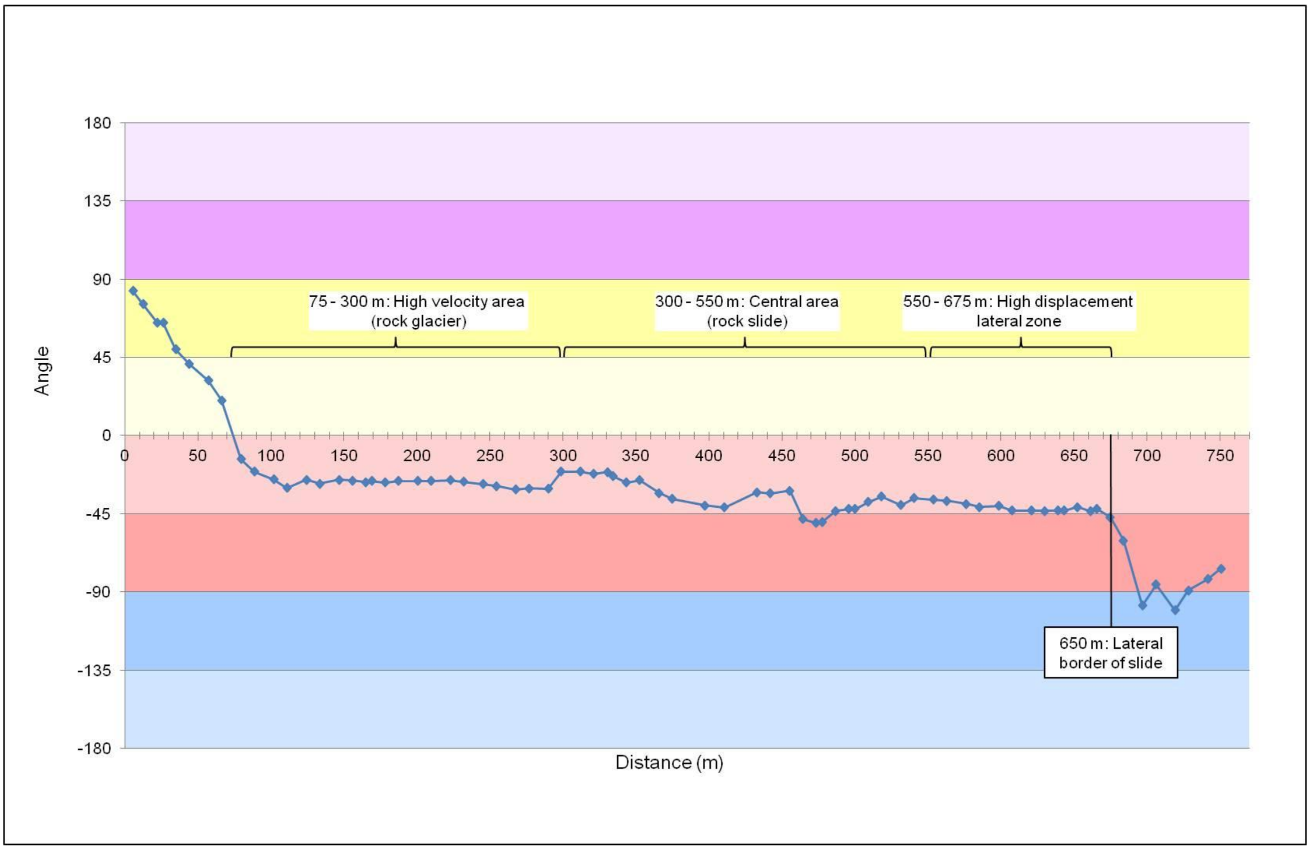

Fig. 55 - Dip angle of total displacement in Gamanjunni3 profile BB'.

3.3.3 Rock glacier in Helvetesdalen on Nordmannviktinden

3.3.3.1 Results

The common reference point for ascending- and descending geometry was selected on the valley floor in front of the rock glacier. It is in an area with high coherence and a slope gradient of 6˚. It was selected after orthophoto and slope gradient map study. Original ascending and descending TSX data from 2009-2012 and decomposed 2D InSAR data are presented in (Fig. 56). Profiles AA’ and BB’ intersects the rock glacier in NW-SE and W-E direction. The 2D InSAR data for the profiles is presented in (Fig. 61, Fig. 62, Fig. 63 and Fig. 64). The displacement of the rock glacier measured from the ascending LOS is small and negative in the AA’ profile. In the BB’ profile ascending data is varying; positive laterally and negative in the middle of the rock glacier. Descending displacement show a larger displacement both in the AA’ and the BB’ profile and coincide well with the lateral extent of the rock glacier. 2D InSAR data (horizontal-, vertical- and total displacement) coincide with the descending data. The dip angle varies between ~-40˚ and ~-50˚ in profile AA’ and between ~-25 and ~-50 in profile BB’.

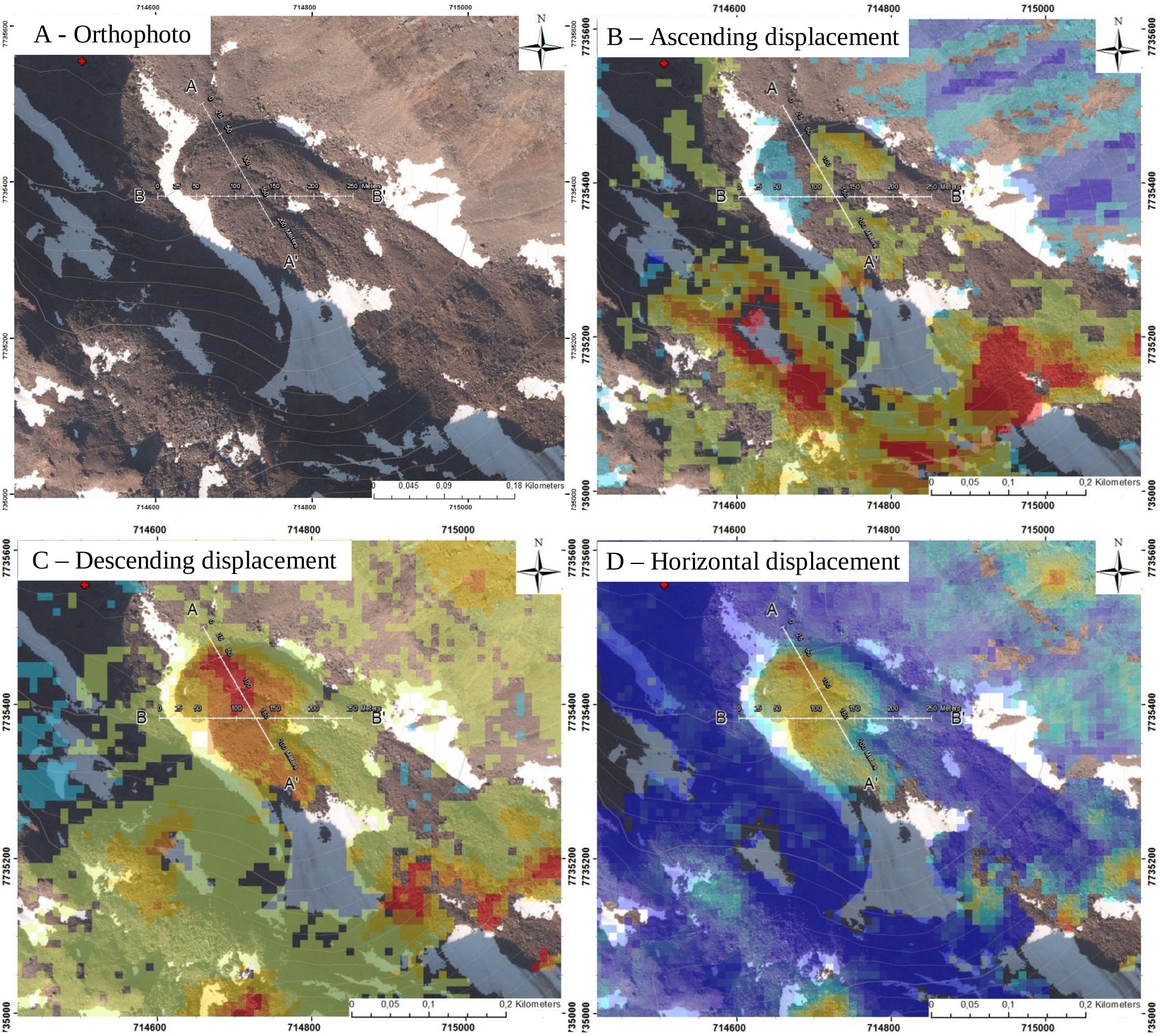
A - Orthophoto
B – Ascending displacement
C – Descending displacement
D – Horizontal displacement
N
A
A'
B
B'
0
25
50
100
150
200
250 Meters
200 Meters
714600
714800
715000
7735600
7735400
7735200
7735000
0 0,045 0,09 0,18 Kilometers
0 0,05 0,1 0,2 Kilometers

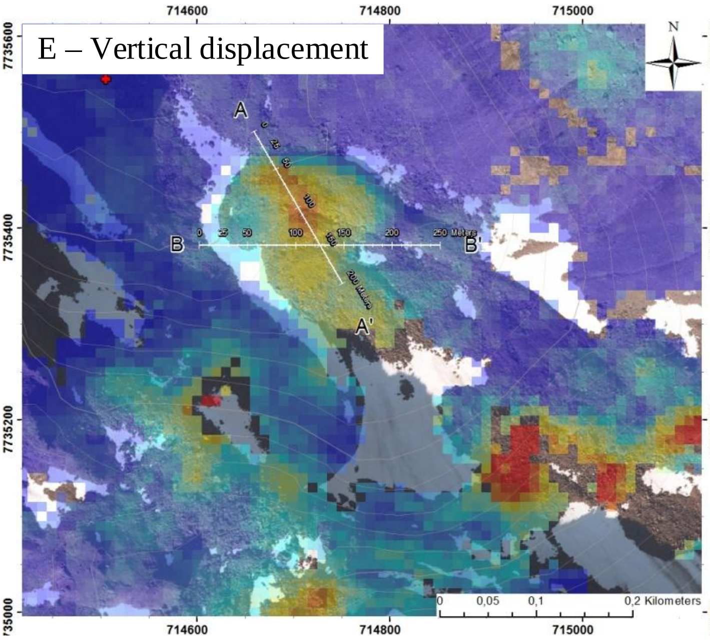

E – Vertical displacement

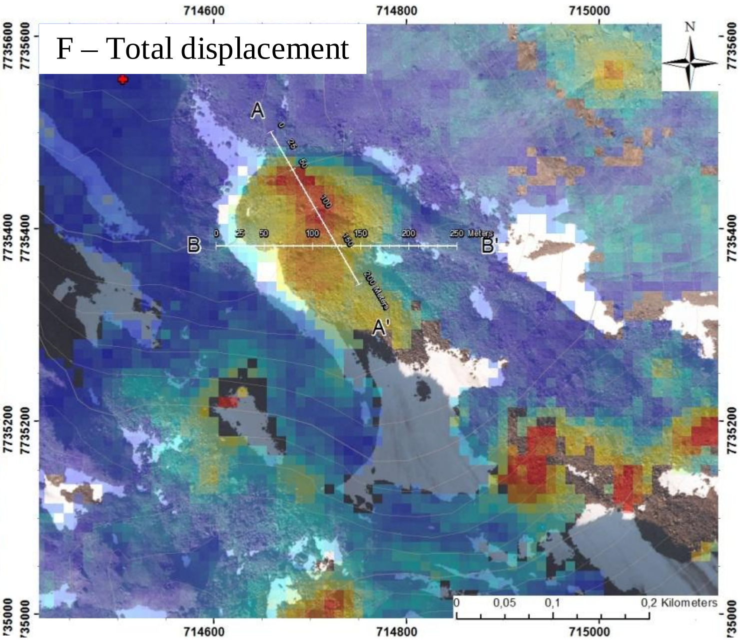

F – Total displacement

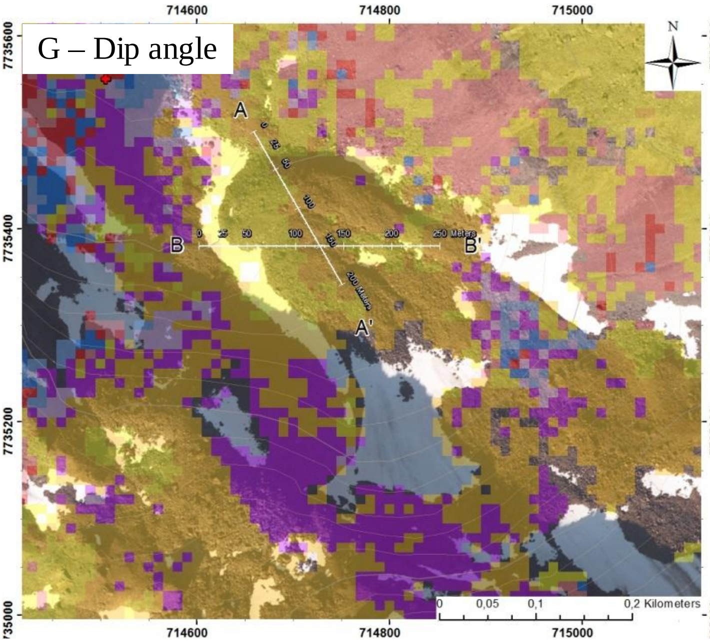

G – Dip angle

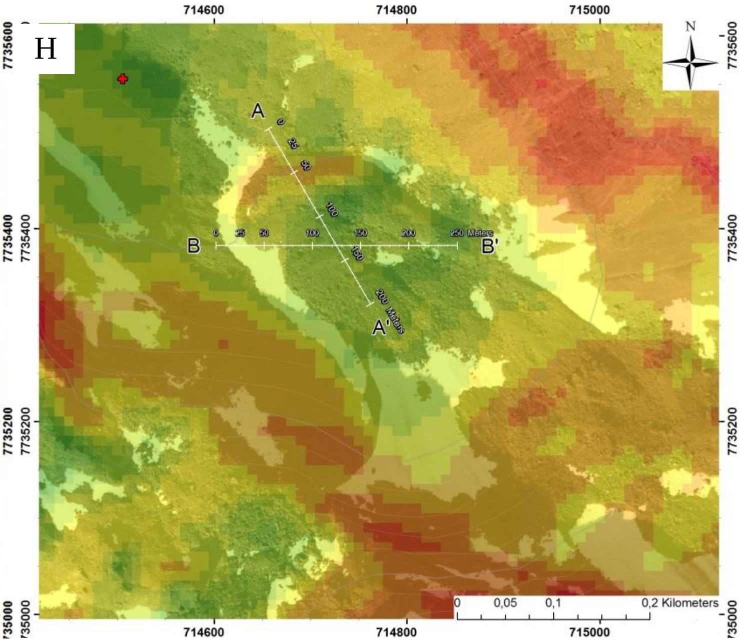

H

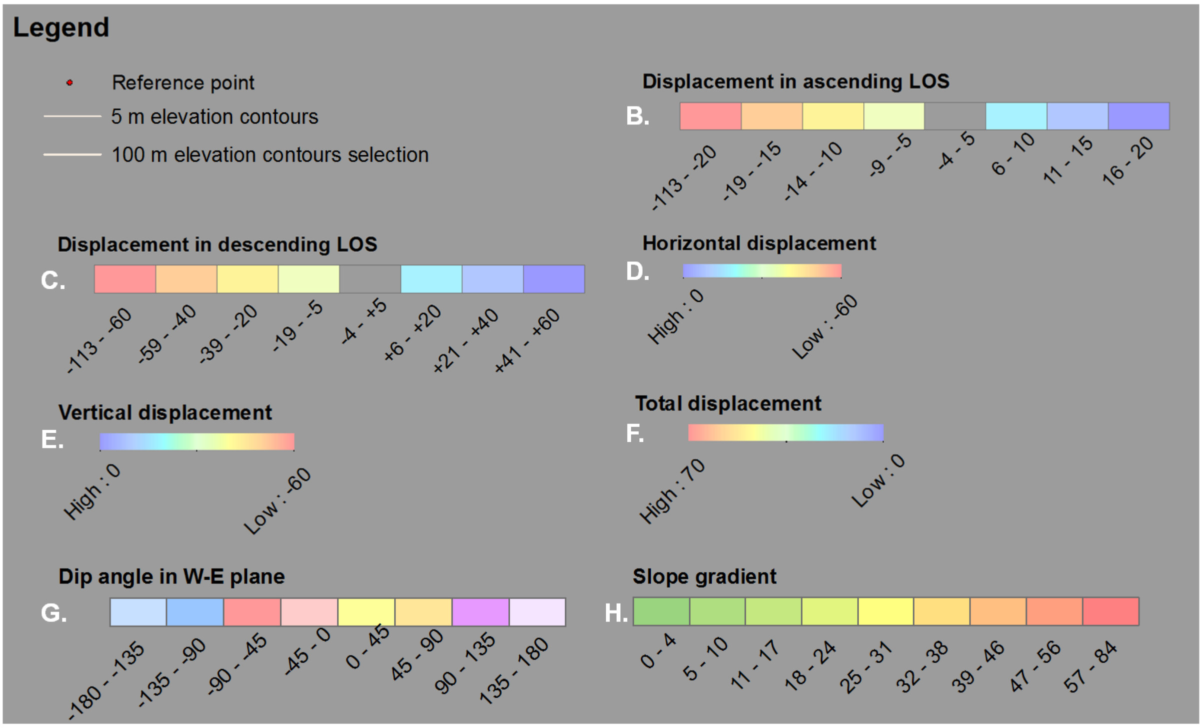

Fig. 56 - A. Orthophoto of rock glacier on Nordmannviktinden. B. Ascending TSX data from 2009-2012. C. Descending TSX data from 2009-2012. D. Horizontal displacement in W-E direction. E. Vertical displacement. F. Total displacement vectors length. G. Dip angle of total displacement vector in W-E plane. H. Slope gradient map.

3.3.3.2 Discussion

Based on field study and orthophoto interpretation, geomorphological elements of the rock glacier are summarized in (Fig. 57).

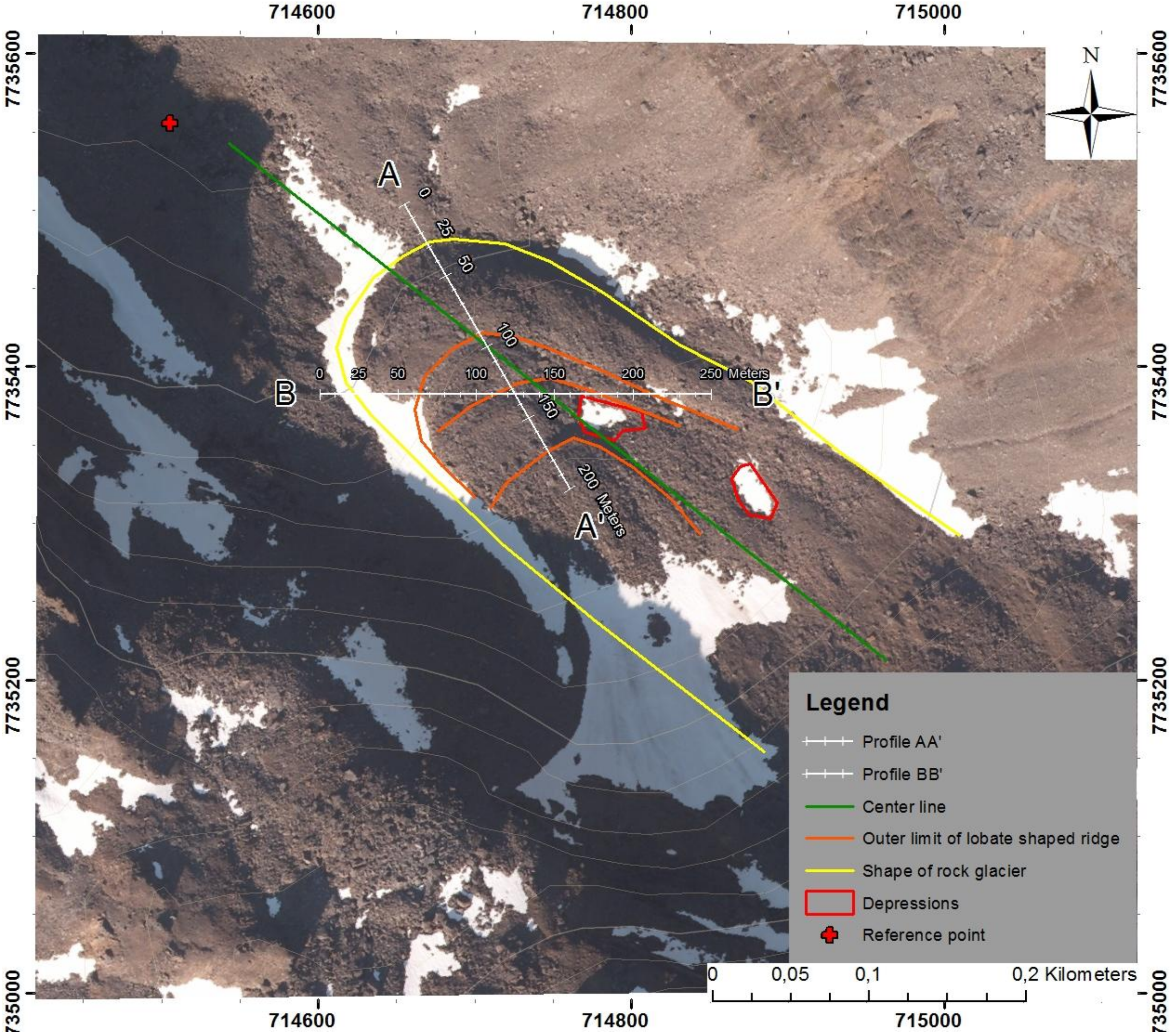

Fig. 57 – Rock glacier with morphological elements.

The increase in displacement velocities (~ 25 m) in profile AA’ correlates with the border between the valley and the rock glacier (Fig. 61). From profile AA’ and BB’ the highest total displacement rates are associated with the steepest part in the toe-zone (~50 m) and with the outer limits of the tongue shaped ridge on top of the rock glacier (~100 m) (Fig. 58 , Fig. 61 and Fig. 63). Further, there is a decrease in velocity in the upper part and on the sides of the rock glacier.

The lowest displacement in profile AA’ correlates with the outer limit of a tongue shaped ridge (~180 m).

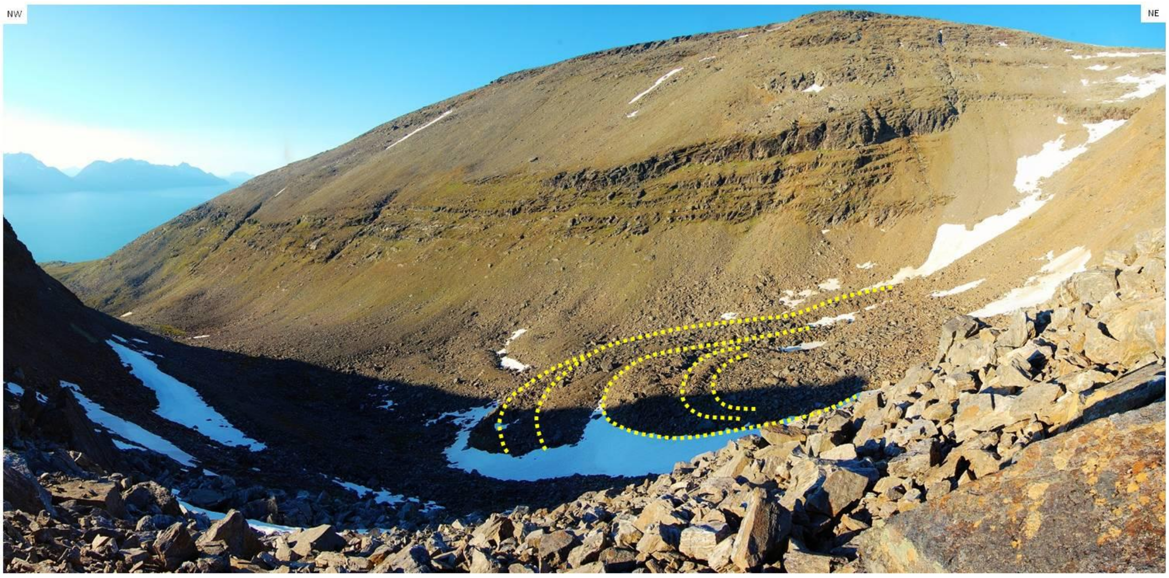

Fig. 58 - Rock glacier with tongue shaped ridges.

Observation from the field indicates resent mass-movement in front of rock glacier and minor lateral mass-movement. The front of the rock glacier consists of clast sizes from silty sand up to large boulders (~ 2 m) (Fig. 59).

Fig. 59 - A. Toe zone of rock glacier in profile with fresh mass-movement. B. Distal view of rock glacier

Using the DEM, the gradient of the strike and dip of the valley floor next to and distal to the rock glacier was calculated to be (315/12). The dip angle of the total displacement for profile AA’ is ~45˚ (Fig. 62). This is much steeper than expected if assuming a flow direction parallel to the valley floor. The large downward displacement measured, resemble displacement patterns documented for turf-banked solifluction lobes at Dovrefjell by (Harris et al., 2008). An explanation could be the fact that the InSAR data was collected during the snow free season. The interferograms has a temporal baseline of 33 day resulting in no linking of displacement between seasons. The mean yearly displacement produced, therefore overestimates the vertical displacement only showing the steep vertical downward displacement from the thawing sediments during summer. See Section 3.3.4.2 and (Fig. 71).

Another explanation could be that the actual displacement on the rock glacier is deflecting away from the center line as described by (Kääb et al., 2003) having a larger component towards North, not visible in InSAR and 2D InSAR data (Fig. 60). A large North component would result in a steeper measured dip angle of the total displacement and a shorter horizontal component. With this scenario, a change to more leveler values in the dip angel of total displacement data would be expected when profile AA' crosses the rock glaciers centre line (~105 m). Also an increase when moving away from the center line would be expected. When these are not the case, an explanation could be that the increase in displacement in the center of the rock glacier masks out this pattern. This is an example of an ambiguity that always has to be considered when interpreting InSAR- and 2D InSAR data; that a change in measured displacement rate could be the consequence of a change in direction (dip and/or strike).

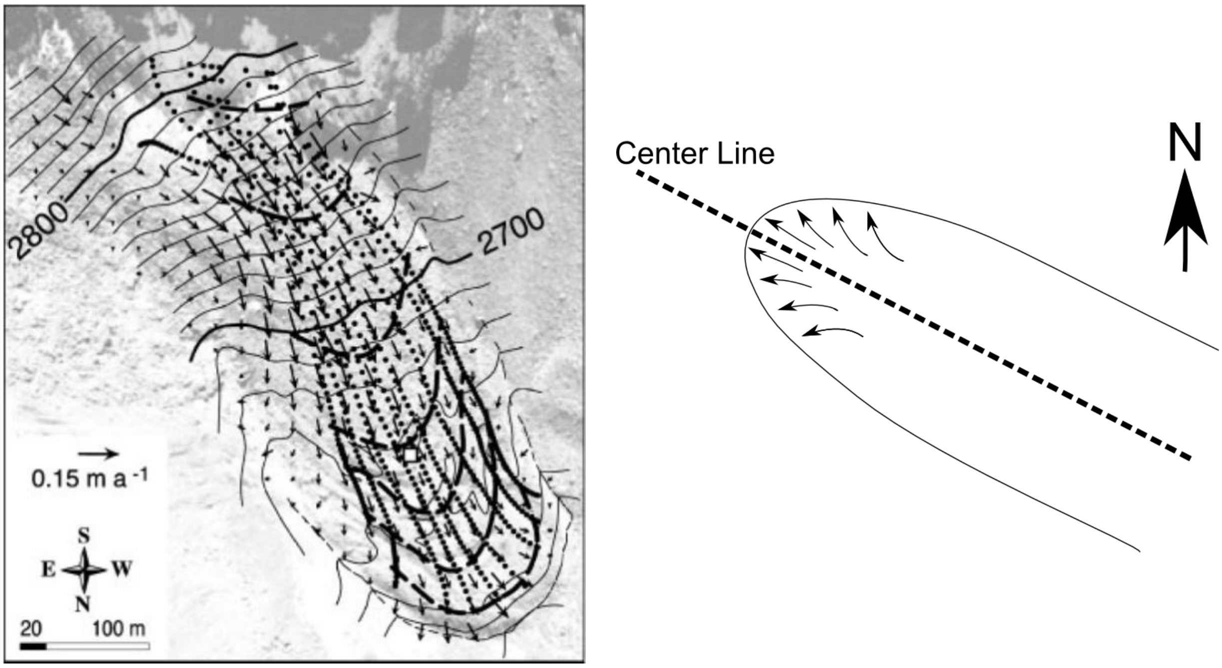

Fig. 60 - Left: Horizontal surface velocities on Murtèl rock glacier for 1987–1996. Right: Displacement pattern with displacement deflecting away from center line in rock glacier.

The outer edges of lobate shaped ridge on top of the rock glacier (~65 m and ~210 m) are seen as areas with lower dip angle of total displacement in profile BB' (Fig. 64). Dip angle increase when approaching the edges of the rock glacier.

2D InSAR data calculated coincidence with the SE lateral- and toe zone border of the rock glacier. The outer edge of tongue shaped ridges can be seen as areas with lower values in the dip angle of total displacement dataset. 2D InSAR data give an insight into the inner dynamics of the rock glacier. This is especially represented by the dip angel of the total displacement. Controlling factors for the displacement measured by InSAR are most likely freeze and taw processes.

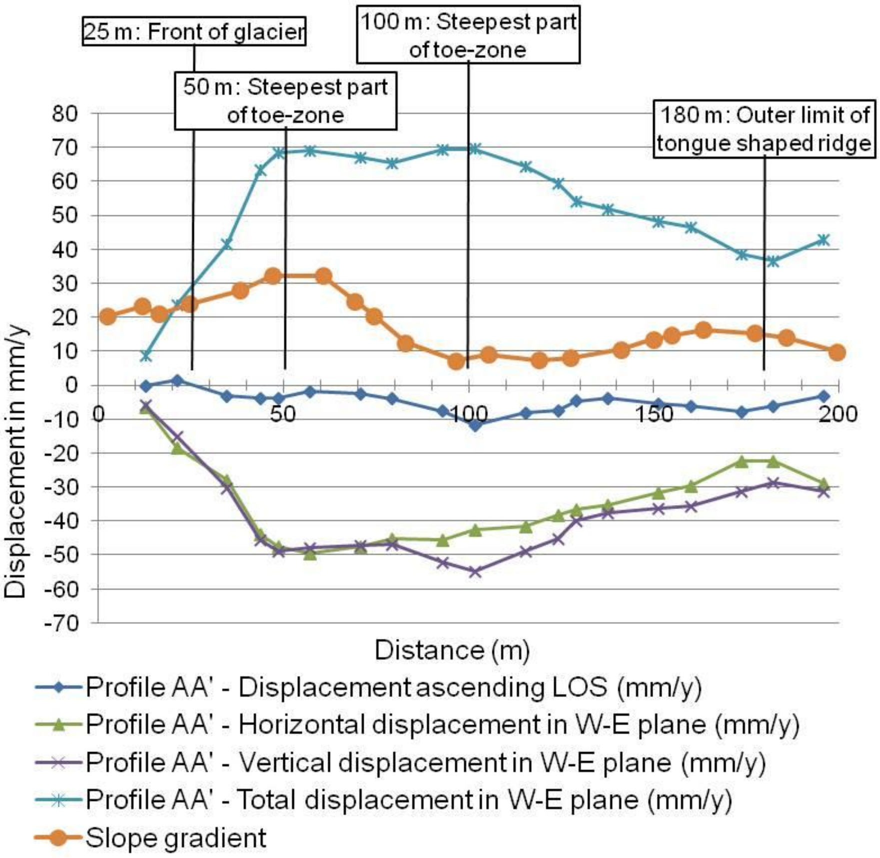

Fig. 61 - InSAR and 2D InSAR data for profile AA' of rock glacier.

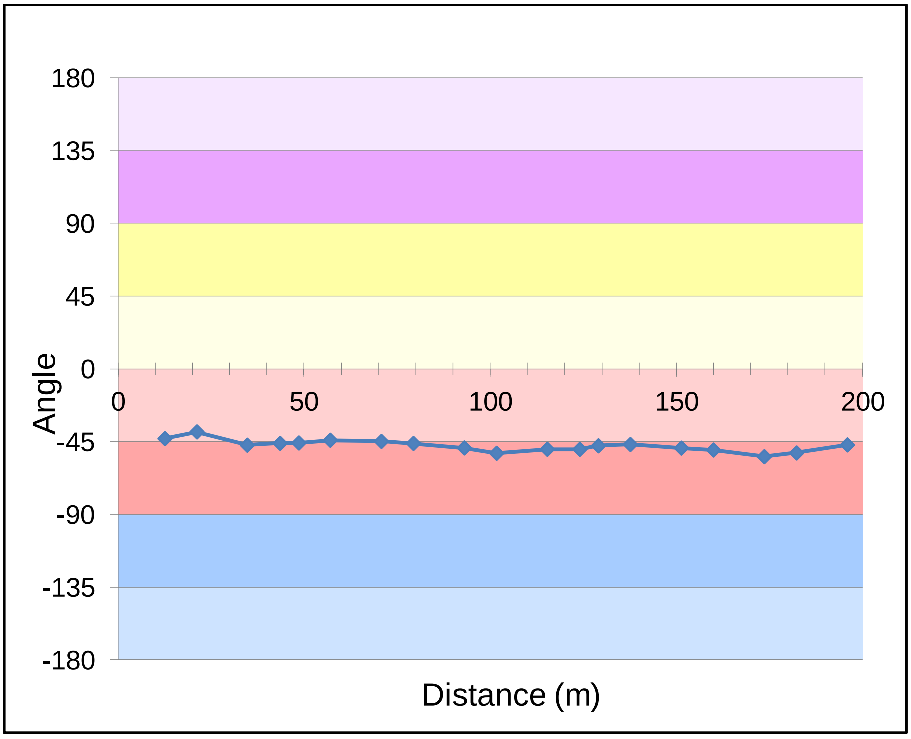

Fig. 62 - Dip angle of total displacement for profile AA' of rock glacier.

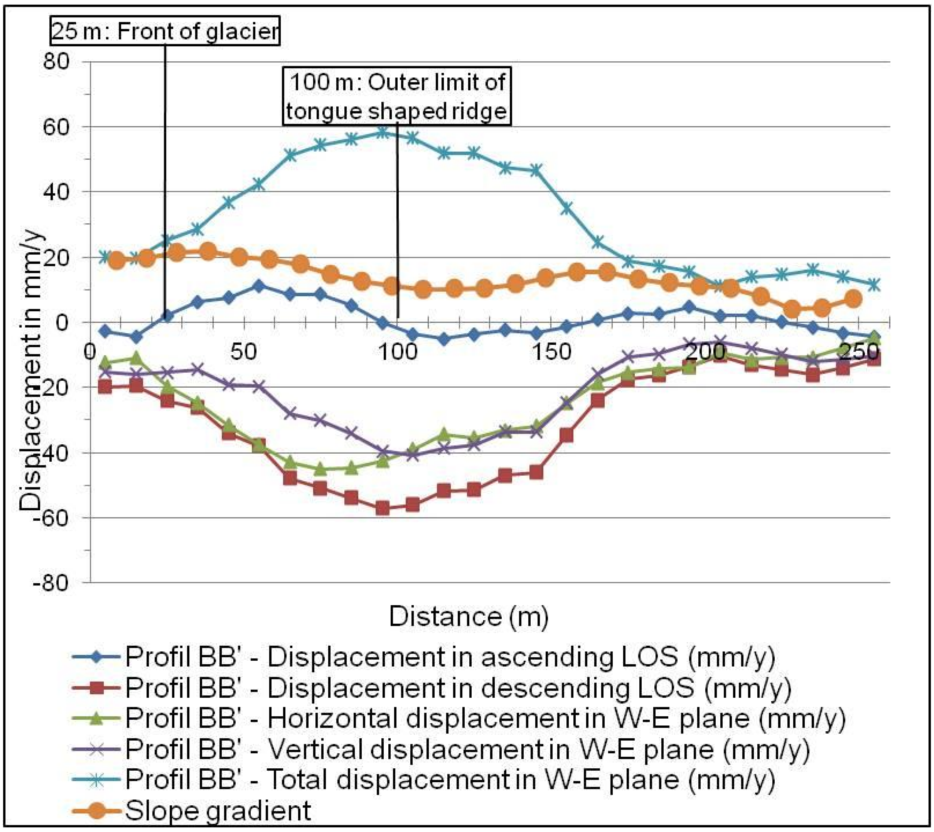

Fig. 63 - InSAR and 2D InSAR data for profile BB' of rock glacier.

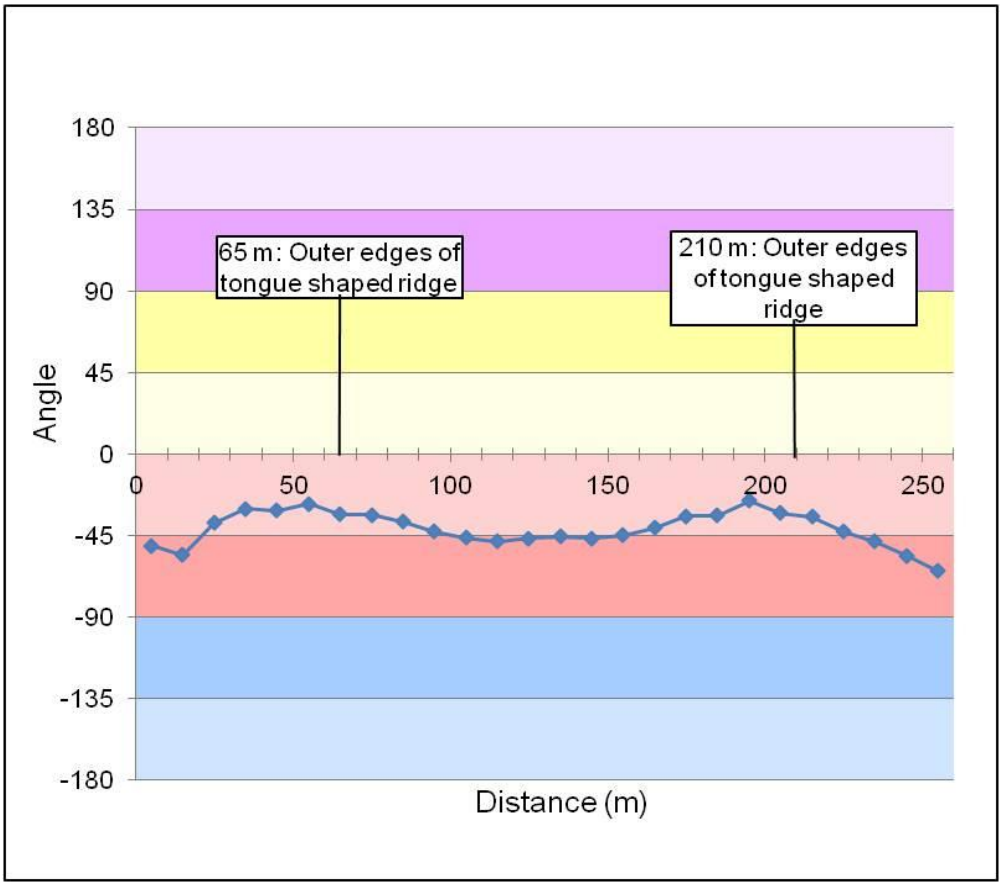

Fig. 64 - Dip angle of total displacement for profile BB' of rock glacier.

3.3.4 Joppolbakkan area with tongue shaped features on east side of Nordnes peninsula

Joppolbakkan is an East facing hill covered with hummus and sparse vegetation. Wavy tongue shaped features, are dominating the surface. They scale from 10s of cm to over 10s of m. The slope gradients in profiles are between ~0 and ~31 degrees. (Fig. 65) shows an overview of the Nordnes peninsula with location of Joppolbakkan, Nordnes rockslide and reference point used during InSAR processing.

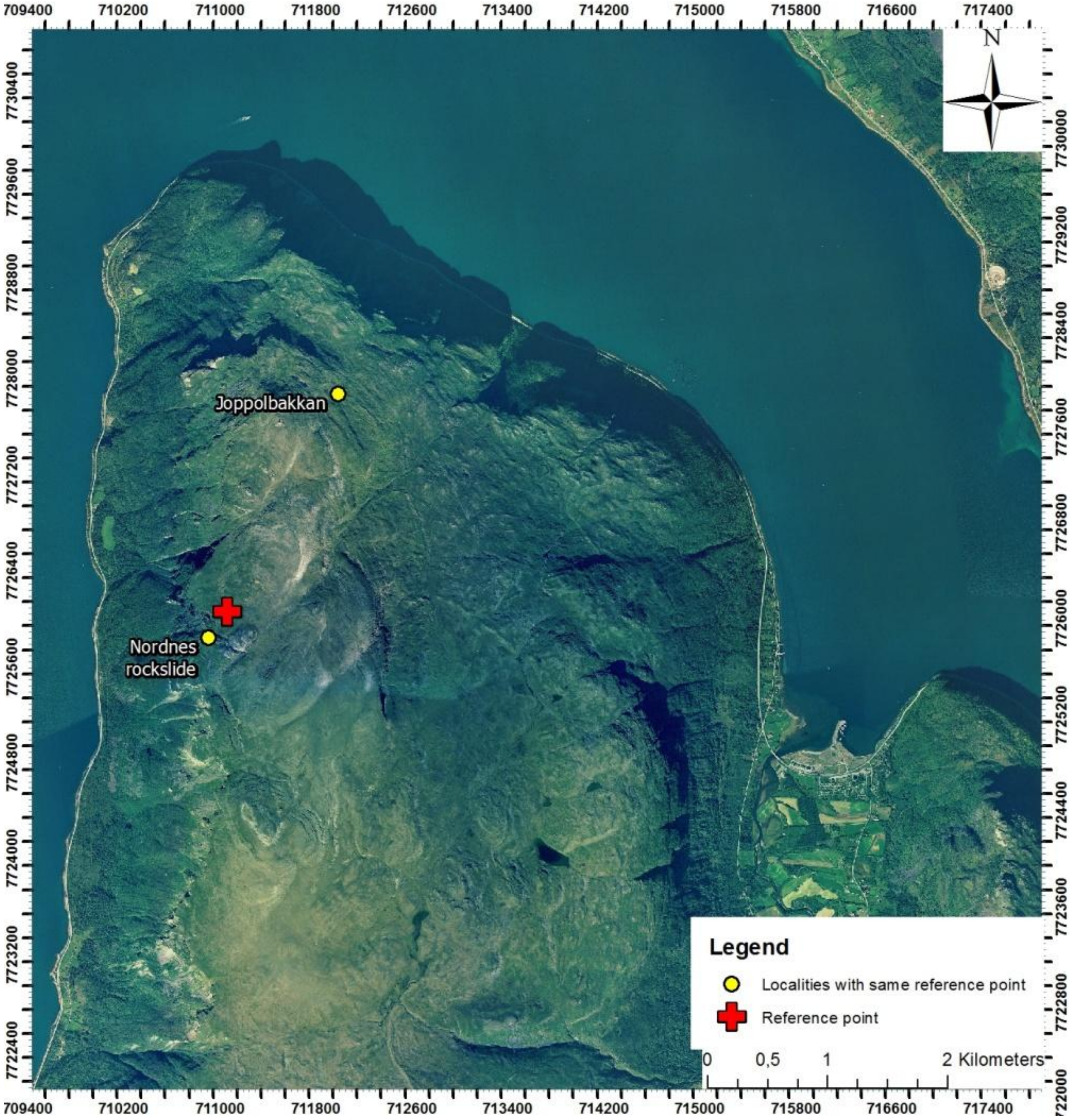

Fig. 65 – Overview of Joppolbakkan and reference point for InSAR processing.

3.3.4.1 Results

Data for the Joppolbakkan location is produced with the same reference point as for the Nordnes rockslide. The distance between Joppolbakkan and the reference point is still below 2 km and the atmospheric contribution should not affect the result considerably. InSAR- and 2D InSAR data for this location are presented in map view in (Fig. 66 B to G). Ascending data have and irregular repeating pattern, vary between ~-5 mm/y and ~-25 mm in profile AA' and BB' (Fig. 72 and Fig. 74). Descending data vary and between ~5 and ~-25 mm/y for both profiles, with the same irregularity. The horizontal data are varying between ~-10 mm/y and ~10 mm/y in profile AA' (Fig. 72). Profile BB' contains peaks of positive values (Eastward displacement) (Fig. 74). The vertical data are negative in both profiles, but as with other data, show a repetitive pattern. Dip angle data indicates down and eastward dip displacement in both profiles(Fig. 73 and Fig. 75).

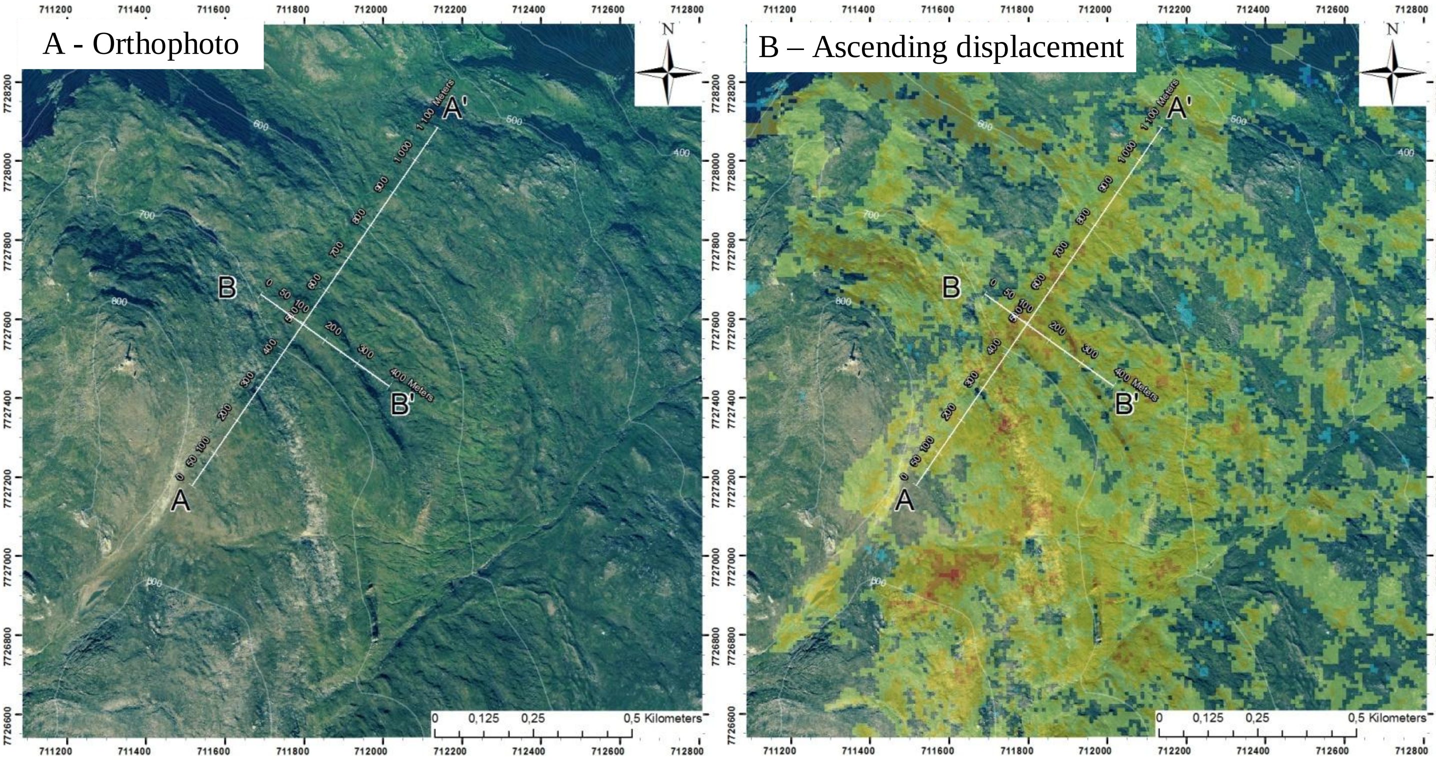

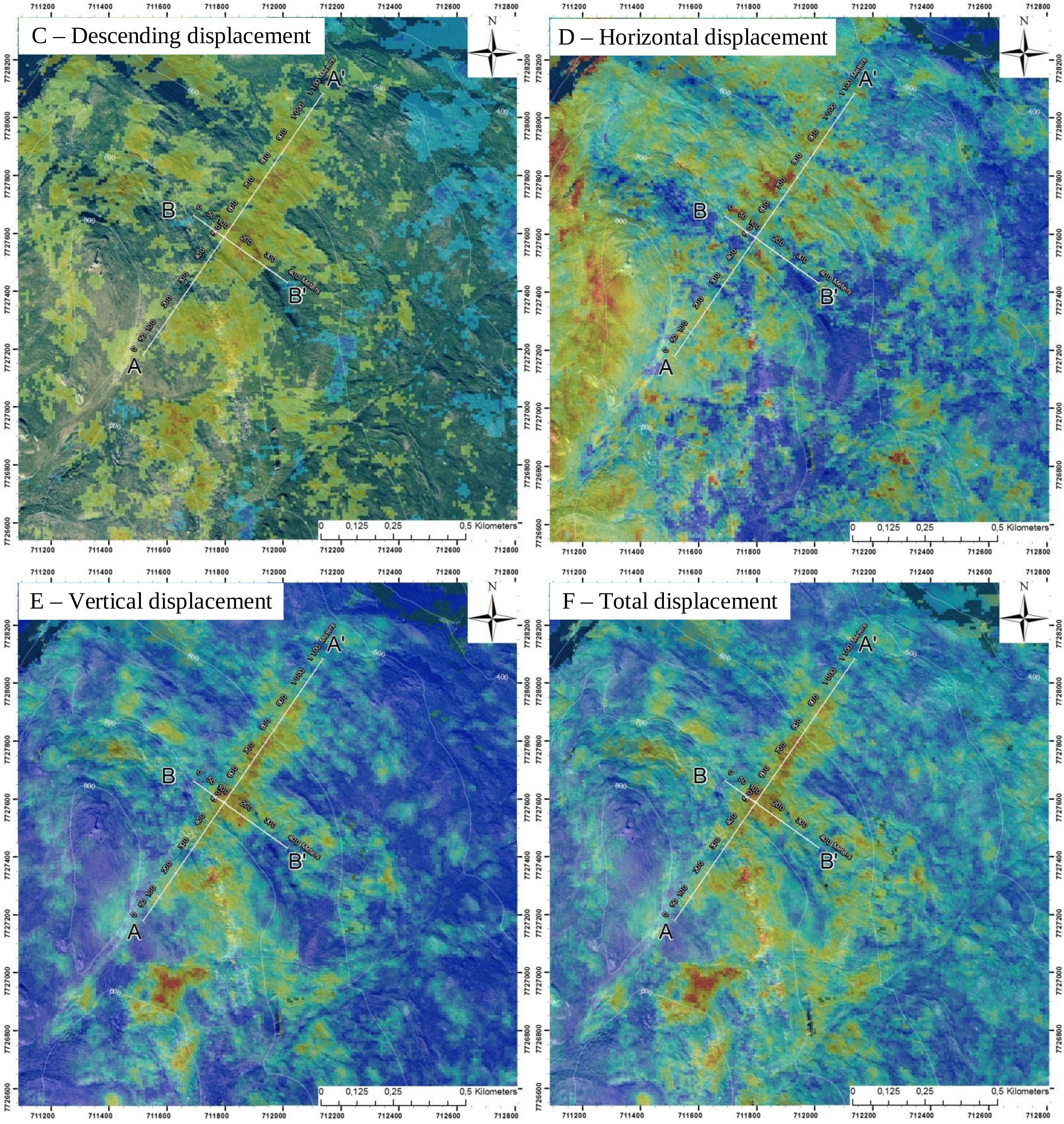
C – Descending displacement
D – Horizontal displacement
E – Vertical displacement
F – Total displacement
N
A
A'
B
B'
1.100 Meters
400 Meters
0 0,125 0,25 0,5 Kilometers
711200
711400
711600
711800
712000
712200
712400
712600
712800
7726600
7726800
7727000
7727200
7727400
7727600
7727800
7728000
7728200
600
700
800
400

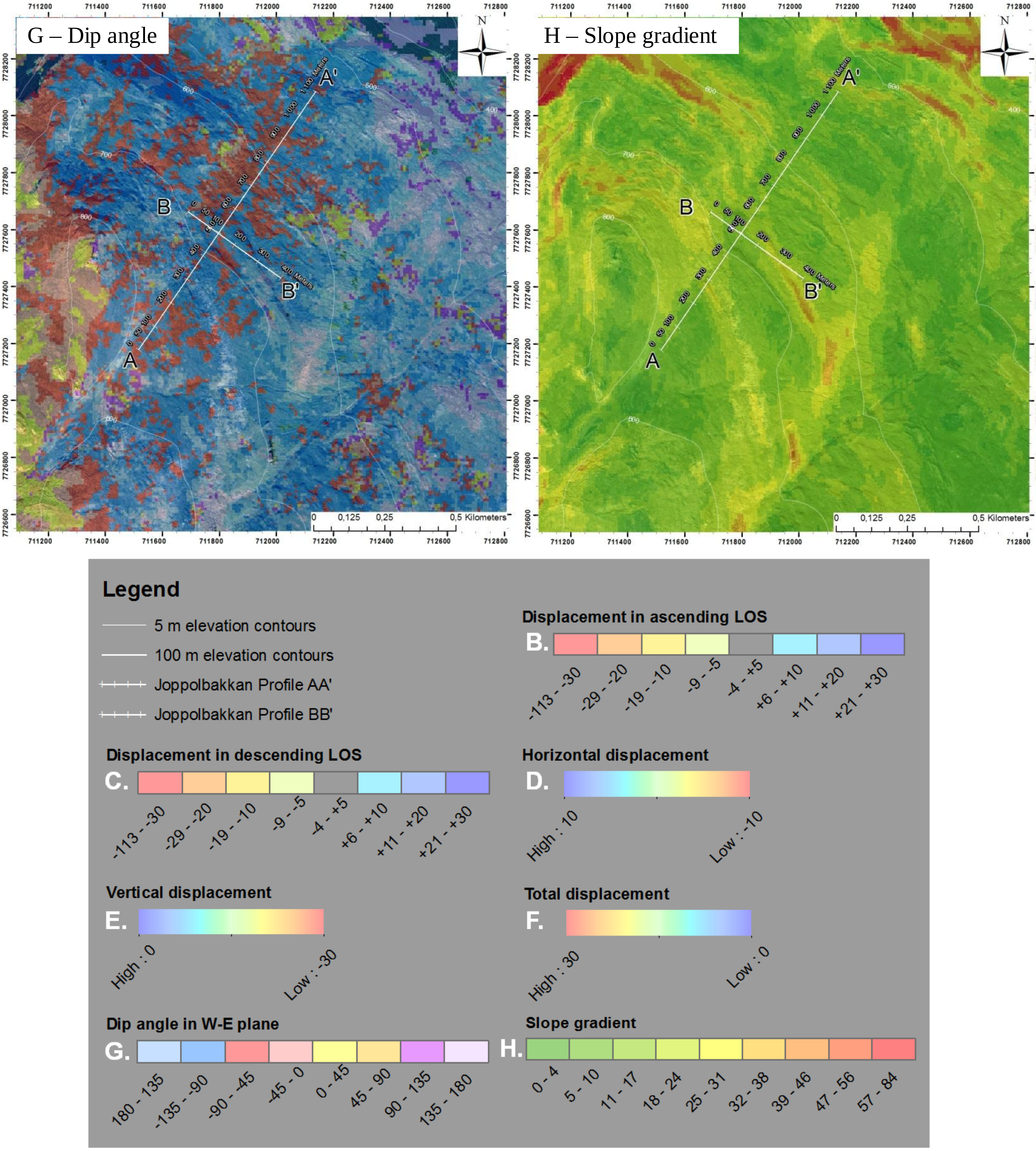

Fig. 66 - A. Orthophoto of tongue shaped formation at Joppolbakkan. B. Ascending TSX data from 2009-2012. C. Descending TSX data from 2009-2012. D. Horizontal displacement in W-E direction. E. Vertical displacement. F. Total displacement vectors length. G. Dip angle of total displacement vector in W-E plane. H. Slope gradient map.

3.3.4.2 Discussion

From orthophoto and field study, the inferred strike for the displacement of the tongue shaped features in the area is Northeast to Southeast direction. Profile AA (Fig. 66 A and H) covers a ravine-like formation possibly part of the local drainage pattern (Fig. 67 and Fig. 68). It is transecting a terrain with vegetated fine-grained tongue shapes formations, interpreted to be solifluction tongues, and tongue shaped formations without vegetation made up of coarser material (blocky). In the middle of the ravine, both coarse- and fine-grained material tongue shaped features are repeated in sets down the fall line. Profile BB (Fig. 66 A and H) are located in a flatter area with bog filled depression and drier ridges (Fig. 69).

Fig. 67 – Ravine formation with coarse material (blocky) tongue shaped features.

Fig. 68 – A. Close up of coarse material tongue shaped feature in profile AA’

E

Fig. 69 – Bog filled depression and dry ridges in profile BB’

In profile AA’ it is hard to link solifluction lobes mapped from orthophoto with the varying pattern in the InSAR- and 2D InSAR data. By solely looking at ascending- and descending data in profile BB’, it is hard to see any pattern that can be linked to the topography of morphology (Fig. 74). The horizontal 2D InSAR data on the other hand, show an interesting variation with alternation between stable section and section with displacement up to 10 mm/y against East. There is a quite good match between areas which contains solifluction lobes identified from orthophoto and areas with high horizontal displacement, see ~50 m, ~135 m, ~230 m and ~250 to ~350 m in (Fig. 70) and (Fig. 74). These solifluction lobes are visible as section with more level dip angels for the total displacement in these sections (Fig. 75). The vertical displacement is not localized in the same manner to these lobes, but is highest in the middle of the section. Even though the middle section of profile BB’ has the lowest gradient, this part show most displacement in both the InSAR- and 2D InSAR dataset. The intersection of profile AA’ and BB’ is located in an area with both vertical displacement down and horizontal displacement towards East.

As with the displacement for the rock glacier on Nordmannviktinden (Section 3.3.3.2), the dip angels of the total displacement are steeper here than for a flow parallel to slope gradient. In both profiles the angels vary around vertical downwards (~90˚), except for areas with solifluction lobes having a higher horizontal displacement, as discussed above. The steep angle could be explained by the short temporal baseline of 33 days resulting in InSAR data not linked between years. Observed displacement from InSAR- and 2D InSAR therefore will only show displacement happening in the summer. The thaw of the sediments produces a displacement with dominating downward vertical direction. This is supported by monitoring of solifluction lobes at Dovrefjell by (Harris et al., 2008). They document a displacement pattern with heave in the autumn and thaw (gelifluction/creep) in the spring and summer (Fig. 71).

For this locality 2D InSAR data represented by horizontal displacement and dip angle of total displacement, show a pattern that resembles the spatial distribution of solifluction lobes and course grained lobate features.

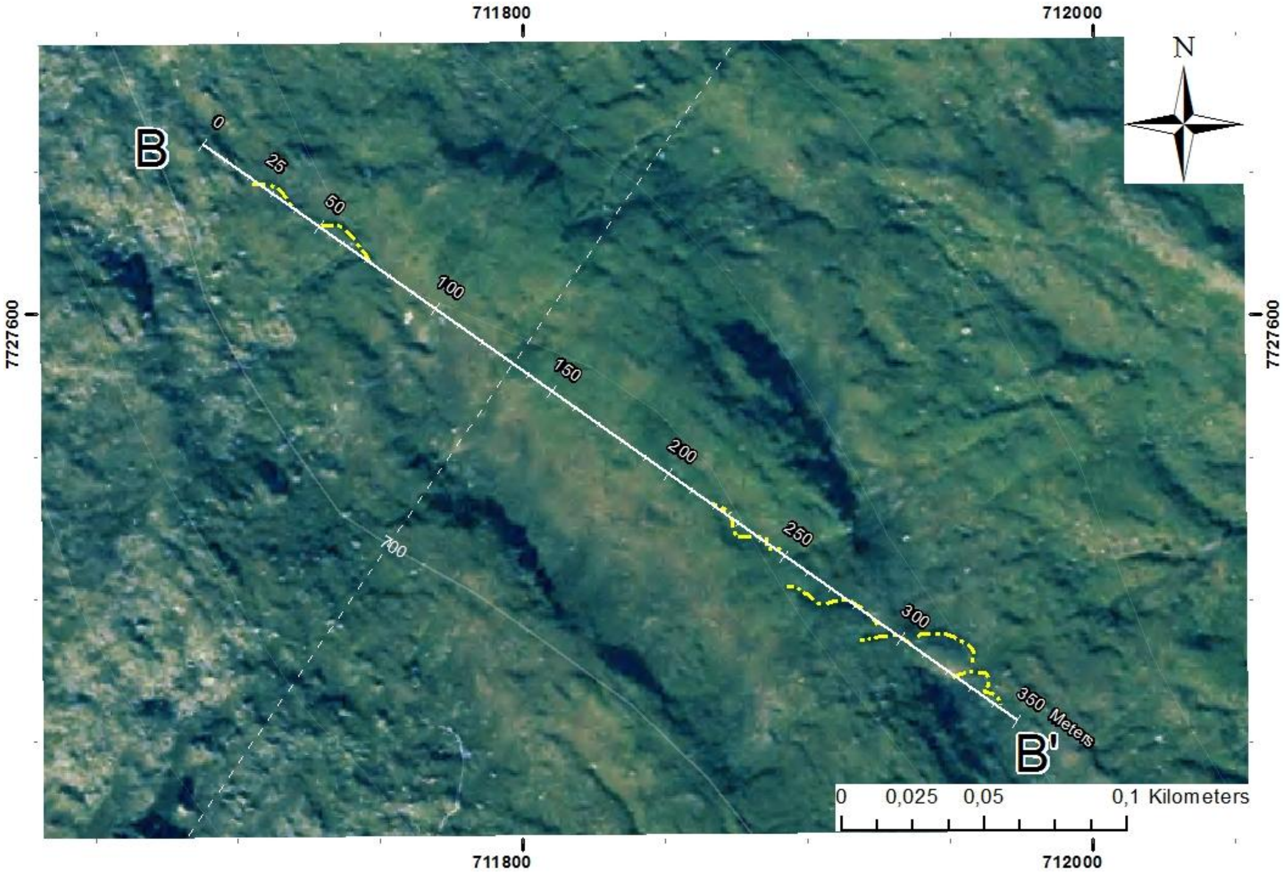

Fig. 70 - Area intersected by profile AA' and BB'. Solifluction tongues near profile line BB' marked with stippled yellow line.

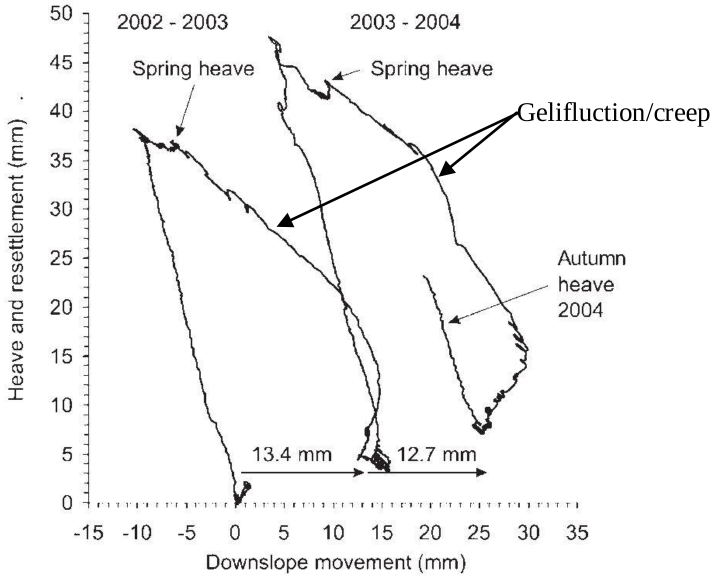

Fig. 71 - Vectors of surface movement from Dovrefjell. Modified after (Harris et al., 2008).

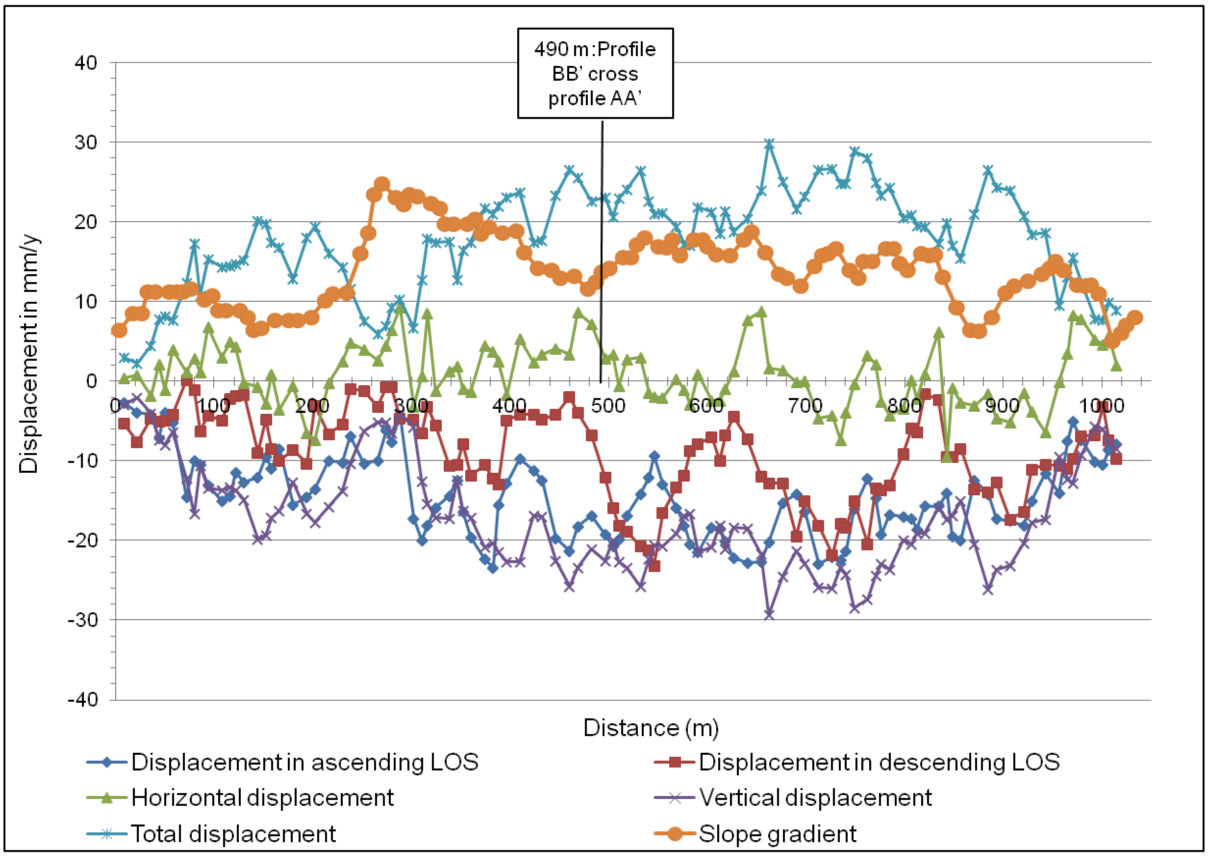

Fig. 72 - InSAR and 2D InSAR data for profile AA' from Joppolbakkan.

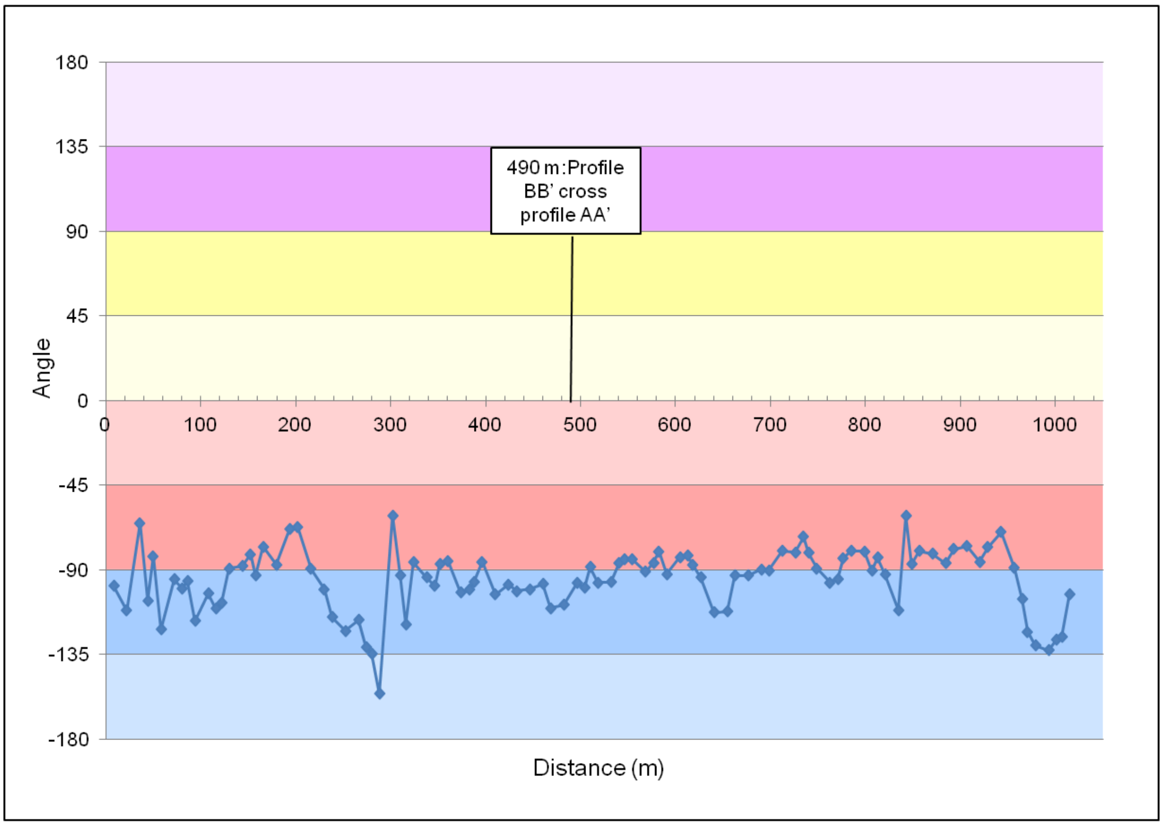

Fig. 73 - Dip angle of total displacement for profile AA' from Joppolbakkan.

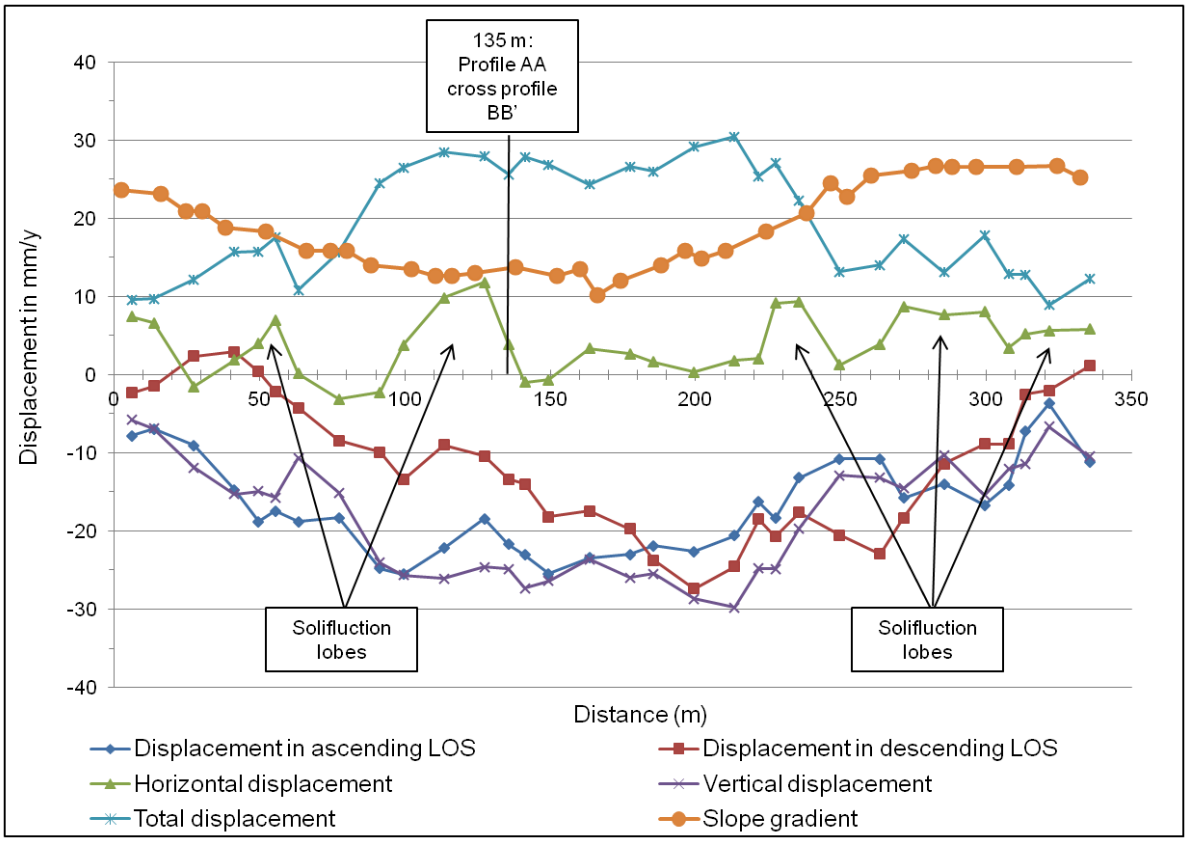

Fig. 74 - InSAR and 2D InSAR data for profile BB' from Joppolbakkan.

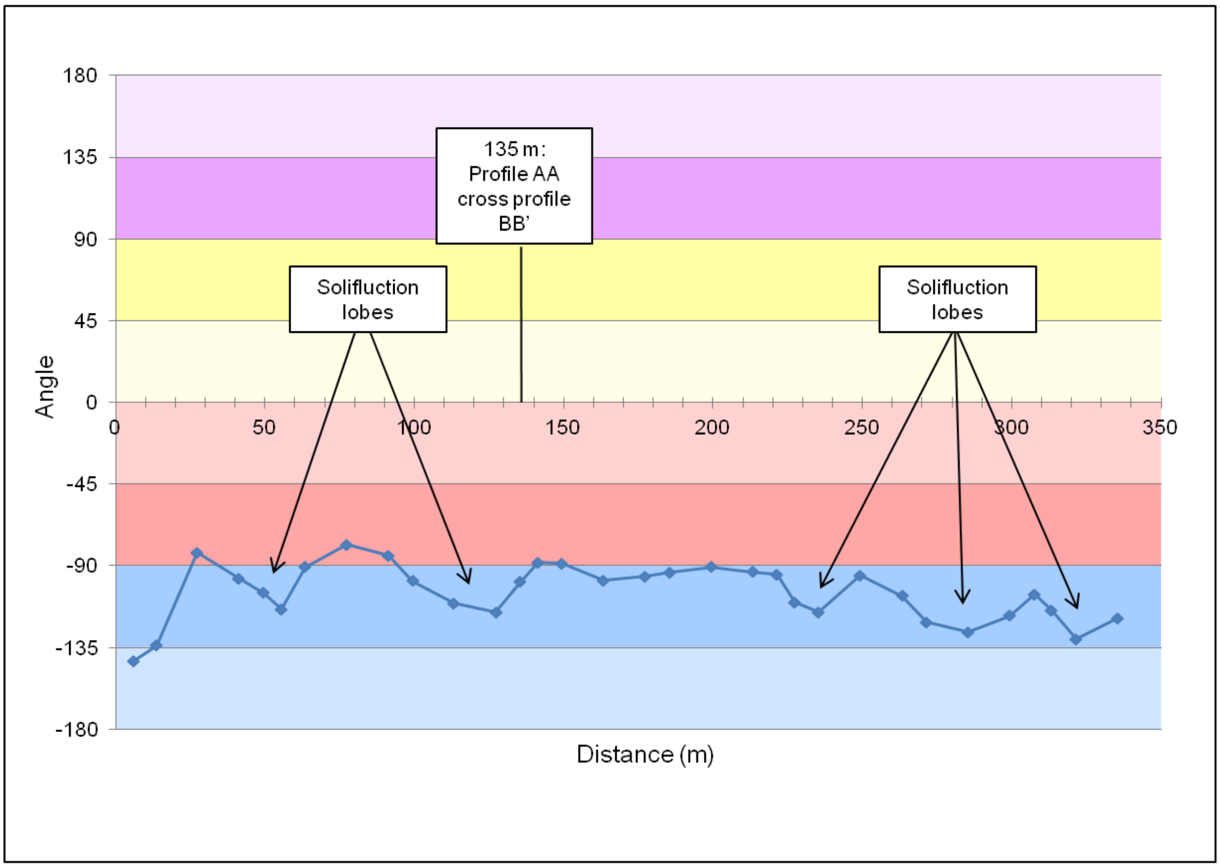

Fig. 75 - Dip angle of total displacement for profile BB' from Joppolbakkan.

4 Summary and conclusions

The main goal of this thesis has been to produce 2D InSAR data (horizontal-, vertical-, total displacement and dip angle of total displacement data) by combining data from two different satellite geometries and discuss if 2D InSAR data can give a more adequate and comprehensible presentation of displacement. This has been done by producing InSAR data for different localities, verifying results against data from GPS stations situated at the Nordnes rockslide, and finally relating InSAR and 2D InSAR data to different forms of slope processes in the field area.

Processing of InSAR data was done using the GSAR application from Norut. This was not trivial, and some of the processing steps require caution when selecting input parameters. Employees from Norut, were very helpful in this process. After processing InSAR- and 2D InSAR data, the verification of the InSAR technique was done by comparing TerraSAR-X InSAR data from ascending- and descending geometry (the input to the 2D InSAR decomposition procedure) with GPS data. The results showed that the GPS data and the ascending- and descending InSAR data had good correlation. Calculations based on GPS- and InSAR data from 2011, showed deviations smaller 2,7 mm/y in the East-West direction and 2,8 mm/y in vertical direction. The errors were smaller than the displacement patterns of interest in this thesis, and the ascending- and descending InSAR datasets was found reliable in the area around GPS station YN3 at the Nordnes rockslide.
In addition, a verification of the 2D InSAR decomposition procedure was done. The input was the East-West components (dE) and the vertical components (dH) from GPS station YN3 data. The resulting horizontal- and vertical components resembled the input GPS data as expected, with a Pearson correlation of 1 in the East-West direction and of 0,99830439 in vertical direction. This verified that the 2D InSAR decomposition procedure was valid.

Further, GPS data from five GPS stations was used to verify 2D InSAR data from two profiles transecting the Nordnes rockslide. For profile line AA’, the mean deviations between the 2D InSAR data and GPS data for all the GPS stations were 5,7 mm/y horizontally and 5,7 mm/y vertically. For the BB’ profile, the deviations were 7 mm/y in the horizontal direction and 0,6 mm/y in the vertical direction. As with the verification of the 2D InSAR decomposition procedure, errors are smaller than the displacement patterns of interest in this thesis which is 10 mm/y. Based on this, slope processes from selected localities could be related to InSAR and 2D InSAR data with confidence.

Supporting the verification, is the fact that calculated 2D InSAR dip angle of total displacement for a large fault block in the Gamanjunni3 rockslide (Block 2) correlates with the most probable sliding direction found from kinematic stability tests performed by NGU. NGUs and the findings in this thesis are supported by dGNSS (Differential Global Navigation Satellite System) data from 2013 and TSL LIDAR data (Bunkholt, 2013) (H. Bunkholt, personal communication, 2013).

The different slope processes studied in this thesis, revealed interesting displacement patterns in the 2D InSAR data. Such as the correlation between slope gradient and the 2D InSAR total displacement data for the Gamanjunni3 rockslide. Here slope gradients resemble the total displacement data. This suggests that the displacement rates are controlled by the slope gradients in the Gamanjunni3 rockslide.

2D InSAR data have shown cases where the inner dynamics of rockslides has been unveiled. Sections from both the Nordnes- and the Gamanjunni3 rockslide show negative-positive patterns in dip angle of total displacement data. At the Nordnes rockslide, the patterns could origin from rotation of fault blocks, caused by listric detachment faults or toe-zone compression uplifting the front of the fault blocks (thrust duplex). At Gamanjunni3, in addition to the above-mentioned suggestions, the negative-positive pattern could be explained as creep in a small rock glacier.

In addition, 2d InSAR data have made it possible to make prediction if large blocks are fragmenting or moving as one body, based on the degree of variations in the 2D InSAR data from the block. 2D InSAR data from the uppermost block at the Gamanjunni3 rockslide (Block 2) indicate a fragmentation of the block. As opposed to the lowermost block (Block 2) which has generally constant displacement rates, indicating no rotation and that the block is moving as one body.

This technique, can be utilized when classifying rockslides. For example, can 2D InSAR displacement data with only small variation over large section of the slide, combined with constant angle of total displacement, suggest a slide with planar fault geometry. This is the case with the Gamanjunni3 rockslide. Here 2D InSAR data suggest that the middle part of the slide is built up of smaller and larger blocks, interacting in a complex pattern, but moving as a homogenous body on a planar detachment. The northern part of the Nordnes rockslide on the other hand, show large variation in displacement and dip angel of total displacement. This substantiate work of (Blikra, 2012; Braathen et al., 2004) and indicates that this part of the Nordnes rockslide show displacement pattern that can be related to a complex field with listric fault geometry controlled by deep-seated, low-angle detachments.

Furthermore, there are good indications that slide dynamics depending on topography can be revealed by combining the slope gradient with total displacement data. For the Nordnes Rockslide, the hinge points in the slope gradient and maximums in the total displacement data correlate. This indicates a displacement pattern controlled by the slope gradient.

Producing 2D InSAR data from ascending- and descending InSAR-data, has made it possible to measure the displacement rates on single solifluction lobes at Joppolbakkan. For the Joppolbakkan locality, 2D InSAR data (horizontal displacement and dip angle of total displacement) show a pattern that resembles the spatial distribution of solifluction lobes and course grained lobate features.

2D InSAR data from the rock glacier at Nordmannviktinden give insight into the inner workings of slope processes confined by a valley. Here the dip angel of the total displacement data were the most valuable, correlating with the outer edges of the rock glacier and the outer edges of tongue shaped ridges part of the rock glacier.

Visualization of the 2D InSAR data in three dimensions (3D) has not been elaborated to any extent in this thesis. 3D presentation of 2D InSAR data, is expected to become an important tool in the future when the working out the inner dynamics of slope processes. To exemplify this a 3D representation of the dip angle of total displacement from the Nordnes rockslide have been developed using Arc Scene (Fig. 76). Varying colors and direction of black arrows show the calculated dip for the total displacement (TerraSAR-X InSAR data from 2009-

2012). GPS data from 2011 (NNFO, 2012) show the mean yearly displacement direction.

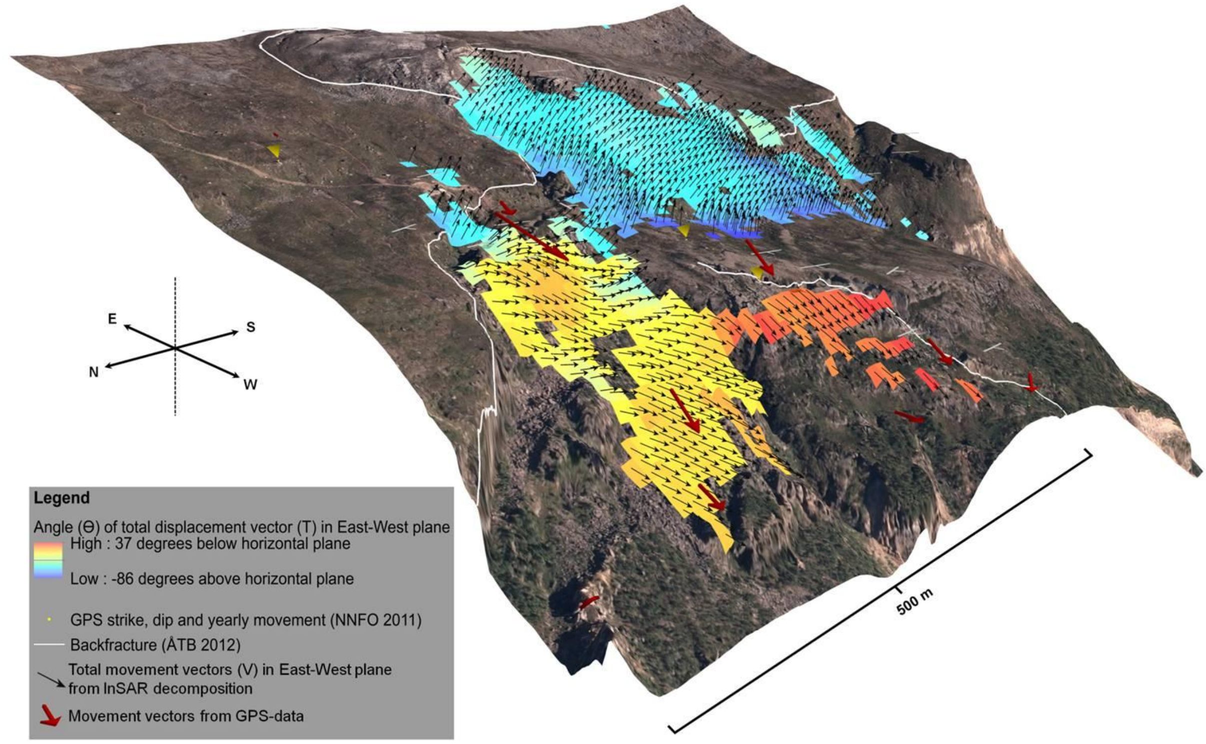

Fig. 76 - 3D representation of the dip angle of total displacement from the Nordnes rockslide.

The use of 2D InSAR data gives a more adequate and comprehensible presentation of displacement in slope processes due to the fact that the user does not, to the same extent, have to consider the sensitivity of the InSAR satellite. In advance, the combination of data from different geometries captured with different LOS (Line Of Sight) supplement each other, increasing the sensitivity to displacement. For example are patterns visible in 2D InSAR data not so easy to find in ascending- and descending data.

One of my motivations in this thesis was to investigating the possibility to use TerraSAR-X data to map new unknown rockslides threatening settlement and infrastructure. TerraSAR-X data has limited ability when it comes to mapping a large area for slope processes with slow displacement rates. This is due to the sensitive to atmospheric variations and variations in the dielectric properties of the ground. Because of frequent acquisitions, TerraSAR-X data are much more useful detecting high-displacement objects and monitor displacement, at all rates, in a limited area.

Summary

- The use of 2D InSAR data give a more adequate and comprehensible presentation of displacement in slope processes than TerraSAR-X InSAR data from ascending and descending geometries. Combination of TerraSAR-X InSAR data 2009-2012 from different ascending- and descending geometries increase the sensitivity to displacement.
- Verification of the produced ascending- and descending InSAR datasets found them reliable when investigating slope processes in the vicinity of the InSAR reference point.
- 2D InSAR decomposition procedure is verified as valid.
- Produced 2D InSAR data show numerous examples of correlation between geomorphological- and structural elements and pattern observed in the 2D InSAR data.

  For example:
    - are back fractures easy to identify from the dip angle of total displacement data,
    - and fractures separating blocks are visible as large changes in horizontal- and vertical displacement, together with dramatic fall in the total displacement and the dip angle of total displacement data.
- Displacement patterns from 2D InSAR data has made it possible to make prediction if large blocks are fragmenting or moving as one body.
- Both for the Nordnes- and the Gamanjunni3 rockslide, abrupt variations in 2D InSAR data have been related to the back scarp and other open fractures.
- By combining the slope gradient with total displacement data, the areas of a slide depending on topography can be revealed. A correlation between slope gradient and the 2D InSAR total displacement data has been found for the Gamanjunni3 rockslide.
- The northern parts of the Nordnes rockslide show displacement pattern that can be related to a complex field with listric fault geometry controlled by deep-seated, low-angle detachments. The correlation between hinge points in the slope gradient and peaks in the total displacement values in the northern part of the Nordnes rockslide indicates a displacement pattern controlled by the slope gradient.
- The total displacement increase below scarps, indicate a segmentation of the slide material correlating with mapped scarps for the Nordnes rockslide.

- Negative-positive pattern in dip angle of total displacement data for the Nordnes- and Gamanjunni3 rockslide, could origin from rotation of fault blocks, caused by a listric detachment fault, a toe-zone compression uplifting the front of the fault block (thrust duplex) or the flow of a small rock glacier.
- Producing 2D InSAR data from InSAR data has made it possible to measure the displacement rates on single solifluction lobes. Patterns hard to see in InSAR data, appear more clearly in 2D InSAR data.
- 2D InSAR data give a valuable extended view of the inner dynamics of slope processes.
- 2D InSAR data can be utilized in the classification of rockslides and other slope processes.
- 2D InSAR data can contribute when evaluation the controlling factors of rockslides.

4.1 Suggestions to future work

- To make a more robust verification of 2D InSAR data for the Nordnes rockslide, the same verification procedure done for GPS station YN3 can been done for other GPS stations covered by both ascending- and descending InSAR data. This was omitted due to the amount of work required.
- Use InSAR data acquired from ascending- and descending geometry together with a DEM to generate a map that showing the sensitivity possible to achieve when producing 2D InSAR data. This is map can be an important contribution when doing a survey in order to know what kind of displacement rate what is possible to detect.
- Compare 2D InSAR data with theodolite displacement data from Sannjarriep'pi rock glacier from (Frauenfelder et al., 2008).
- Map and categorize different slope processes (rock glaciers, alluvial fans, rockslides, solifluction, ice core moraine) based on quaternary maps and 2D InSAR data.
- Use 2D InSAR data and data describing the extent of permafrost to investigate the if freezing and expansion of melt water in the spring and groundwater during the summer, coming in contact with patches of permafrost, can create the observed displacement patterns with vertical upward and westward displacement in the area between ~150 m and ~425 m in profile BB’ at the Nordnes rockslide.
- Map and categorize different mass-wasting mechanisms (rock glaciers, alluvial fans, rockslides, solifluction, ice core moraine) based on quaternary maps and InSAR data.
- Use 2D InSAR data based on InSAR data, processed with the SBAS algorithm, from ascending- and descending geometries to study displacement variations through the snow-free season for different displacement phenomenons. On way to visualize the data can be to make animations showing displacement over time in geological profiles.
- TerraSAR-X data from 2009-2012 show displacement and interesting patterns for the Addjet rockslide in Skiboten (marked as Jorbaavarri in (Fig. 36 and Fig. 37). This is an interesting locality that has been mapped by (Corner, 1973 (unpublished)), inviting to be studied.

5 Acronyms

2D InSAR – Decomposed InSAR data in East-West plane. This includes total displacement, horizontal-, vertical displacement components (mm/y) and dip of the total displacement vector (degree).

The name 2D InSAR, refer to the fact that all data are vectors in the East-West plane.

BP – Radiocarbon years before present. Present is defined as 1950 AD.
dGNSS – Differential Global Navigation Satellite System
DEM – Digital Elevation Model
D-InSAR – differential InSAR technique
DLR – German Aerospace Centre
ERS – European remote sensing satellite
GPS – Global Positioning System
IDL – Interactive Data Language
LIDAR – LIght Detection and Ranging
InSAR – Interferometric Synthetic Aperture Radar
LGM – Last Glacier Maximum
LOS – Line Of Sight
M.A.S.L – Meters Above Sea Level
ML – Marin Limit
NNFO – Nordnorsk Fjellovervåking
NMA – The Norwegian Mapping Authority
Norut – Northern Research Institute
RADAR – Radio Detection And Ranging
SAR – Satellite synthetic Aperture Radar
SB – Small Baseline method
SBAS – Small Baseline subset algorithm
SLC – Single Look Complex
TLS LiDAR – Terrestrial Laser Scanning Light Detection and Ranging
UIT – University of Tromsø
ÅTB – Åknes/Tafjord Beredskap IKS

6 Appendix 1 – Corner (in prep) – Storfjord – Quaternary geological map

This map is produced by (Corner, (in prep.)).

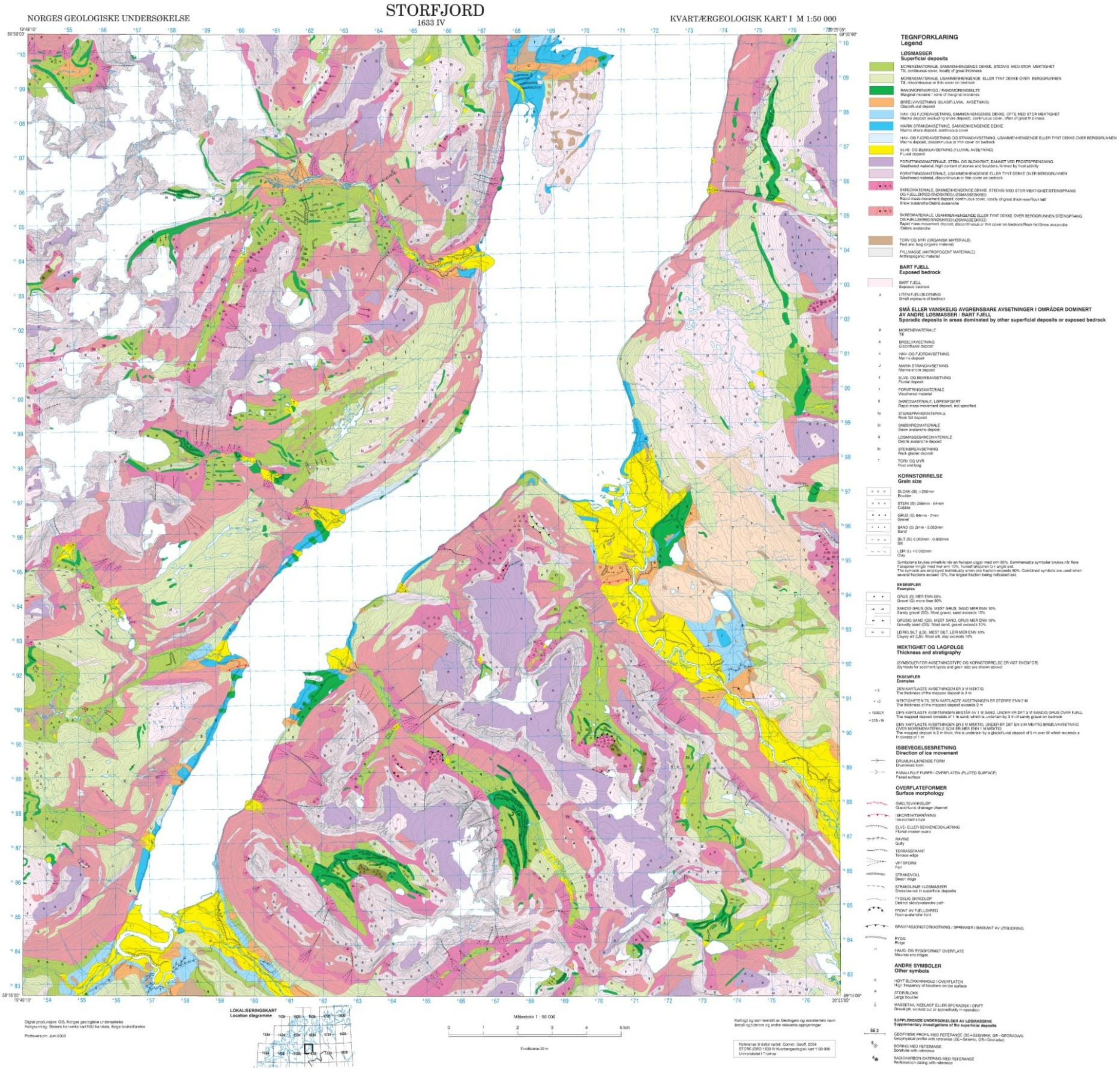

7 Appendix 2 – Tolgensbakk og Sollid (1988) – Kåfjord – Quaternary geological map

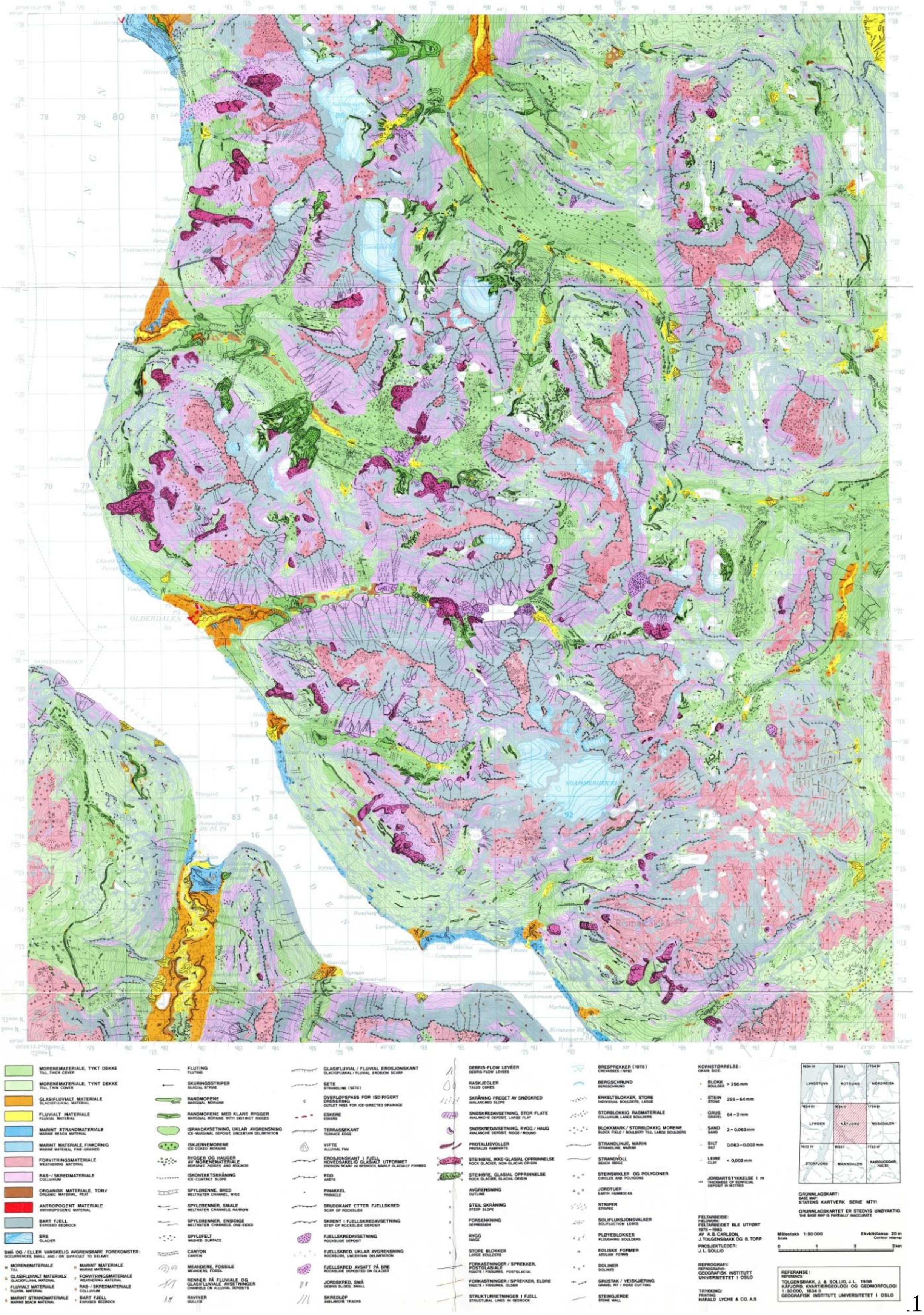

8 Appendix 3 – Calculation of horizontal and vertical displacement vectors from ascending and descending InSAR-data

Based on guidance, application code for producing 2D InSAR data and documentation from Yngvar Larsen (Norut), this appendix describe a method to calculate horizontal- and vertical displacement vectors from ascending and descending InSAR-data (Larsen).

Vectors, quantities having a magnitude and direction, will in the following text be formatted in bold.

It is necessary to have at least two interferograms of the area of interest. One processed from SAR-images taken from a satellite in descending orbit and the other processed from SAR-images taken from a satellite in ascending orbit.

The application calculates the two dimensional (2D) displacement components the plane made up of the ascending- and descending LOS-vectors (LOS-plane). As a simplification the following text will discuss how to decompose the displacement components belonging to a single pixel in the interferograms.

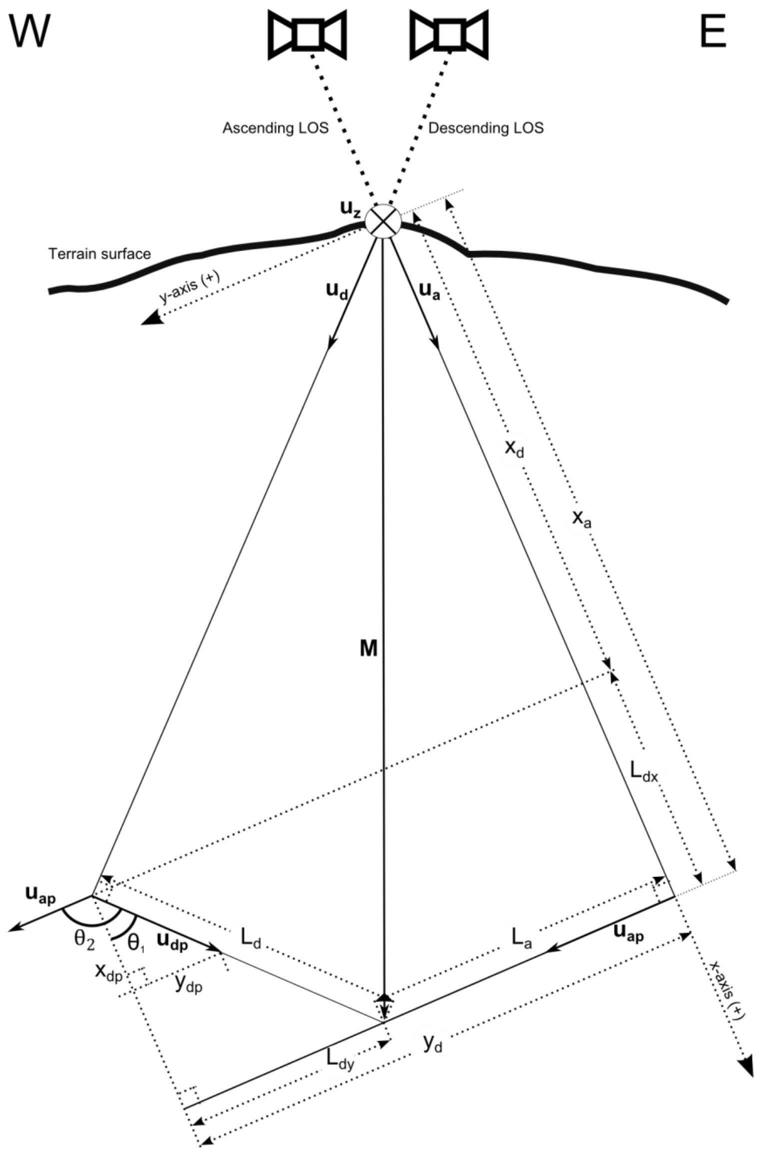

Figure 1: Geometric solution on calculation of horizontal and vertical displacement from ascending and descending InSAR-data

Using routines from the GSAR application and the ascending- and descending interferograms, the unit vector for every pixel in the interferograms pointing from the satellite to the target on the ground was found.

First the $\mathbf{u_z}$ vector is found. $\mathbf{u_z}$ is orthogonal to both the ascending unit vector $\mathbf{u_a}$ and the descending unit vector $\mathbf{u_d}$. $\mathbf{u_z}$ is pointing out of the paper plane. $\mathbf{u_z}$ is found by calculating the cross product of the $\mathbf{u_a}$ and $\mathbf{u_d}$ (Fig. 1 and Box 1).

$$\mathbf{u_z} = \mathbf{u_a}\ \mathrm{x}\ \mathbf{u_d}$$

By calculating the cross product of $\mathbf{u_z}$ and $\mathbf{u_a}$, the vector $\mathbf{u_{ap}}$ is found. $\mathbf{u_{ap}}$ is the unit vector perpendicular to the ascending unit vector ($\mathbf{u_a}$).

$$\mathbf{u}_{ap} = \mathbf{u}_{z} \text{ x } \mathbf{u}_{a}$$

Now a reference system to be used during the calculation can be defined using the calculated unity vectors $\mathbf{u}_{ap}$, $\mathbf{u}_{a}$ and $\mathbf{u}_{z}$. $\mathbf{u}_{ap}$ represent the x-axis, $\mathbf{u}_{a}$ the y-axis and $\mathbf{u}_{z}$ the z-axis (Fig. 3)

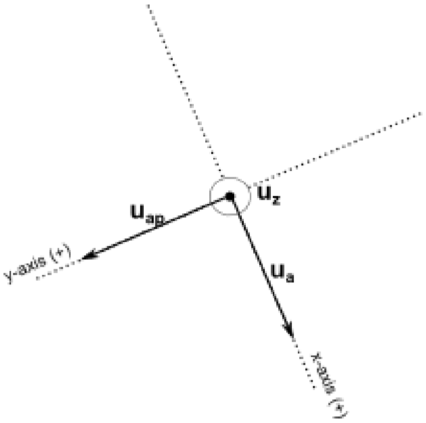

Figure 2: The reference system, constructed by vector u_a, u_{ap} and u_z, used during the calculation. u_z is pointing out of paper plane

Next the vector $\mathbf{u}_{dp}$ is found calculating the cross product of $\mathbf{u}_{d}$ and $\mathbf{u}_{z}$. $\mathbf{u}_{dp}$ is the unit vector orthogonal to both the $\mathbf{u}_{d}$- and the $\mathbf{u}_{z}$ vector.

$$\mathbf{u}_{dp} = \mathbf{u}_{d} \text{ x } \mathbf{u}_{z}$$

With a reference system in place, the next goal is to find the length of L_d projection on to the x-axis. This length is called L_{dx} (Fig 2.).

First the dot product, called x_{dp}, of vectors $\mathbf{u}_{dp}$ and $\mathbf{u}_{a}$ is calculated (Fig 4).

$$x_{\mathbf{dp}} = \mathbf{u}_{dp} \circ \mathbf{u}_{a}$$

$$x_{\mathbf{dp}} = |\mathbf{u}_{dp}|\ |\mathbf{u}_{a}| \cos \theta_1$$

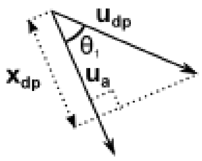

Figure 3: Geometric solution to x_{dp}

Since $\mathbf{u}_{dp}$ and $\mathbf{u}_{a}$ both are unit vectors with length 1, the dot product is the cosine of the angle between them

$$x_{\mathbf{dp}} = \cos \theta_1$$

From Fig. 2 it follows that

$$L_{dx} = L_d \cos \theta_1$$

$$L_{dx} = L_d\, \mathbf{x_{dp}}$$

Then the length of L_d projection on to the y-axis is calculated. This length is called L_{dy} (Fig. 2).

First the dot product, called $\mathbf{y_{dp}}$, of vectors $\mathbf{u_{dp}}$ and $\mathbf{u_{ap}}$ is calculated (Fig. 5).

$$\mathbf{y_{dp}} = \mathbf{u_{dp}} \circ \mathbf{u_{ap}}$$

$$\mathbf{y_{dp}} = |\mathbf{u_{dp}}|\ |\mathbf{u_{ap}}| \cos \theta_2$$

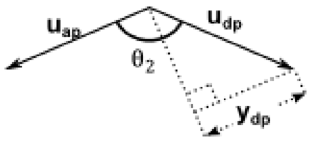

Figure 5: Geometric solution to y_{dp}

Box 1: Calculating the cross product of two vectors

The cross product of vectors **a** and **b** is a vector perpendicular to the vectors **a** and **b** in the direction of the unit vector **n** which is found by the right hand rule (Fig). |**a**| is the length of vector **a**. |**b**| is the length of vector **b**. θ is the smallest angle between vectors **a** and **b**.

$$\mathbf{a} \times \mathbf{b} = |\mathbf{a}|\ |\mathbf{b}| \sin \theta\ \mathbf{n}$$

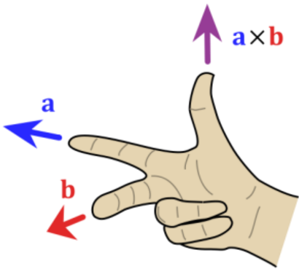

Same as for x_{dp} above, y_{dp} is the dot product is the cosine of the angle between $\mathbf{u_{dp}}$ and $\mathbf{u_{ap}}$

$$y_{dp} = \cos \theta_2$$

Further from Fig. 2 it follows that

$$L_{dy} = L_d \cos \theta_2$$

The scalar x_a (Fig. 2) is found by calculating the dot product of $\mathbf{m_a}$ and $\mathbf{u_a}$. $\mathbf{m_a}$ is the total displacement vector in the direction of line of sight (LOS) measured from the ascending satellite. Since $\mathbf{m_a}$ and $\mathbf{u_a}$ are parallel, $\theta = 0$ and $\cos 0 = 1$. Further $|\mathbf{ua}| = 1$, therefor $x_a = |\mathbf{m_a}|$

$$x_a = \mathbf{m_a} \circ \mathbf{u_a} \ \wedge \ \mathbf{m_a} \parallel \mathbf{u_a} \ \Rightarrow \ \theta=0$$

$$x_a = |\mathbf{m_a}|\ |\mathbf{u_a}| \cos \theta$$

$x_a = |\mathbf{m_a}|$

The scalar x_d is found by calculating the dot product of vectors $\mathbf{m_d}$ and $\mathbf{u_a}$. $\mathbf{m_d}$ is the total displacement vector in the direction of line of sight (LOS) measured from the descending satellite. x_d is the magnitude of the projection of $\mathbf{m_d}$ in the direction of $\mathbf{u_a}$ or the x-axis in the reference system (Fig. 2)

$$x_d = \mathbf{m_d} \circ \mathbf{u_a}$$

$$x_d = |\mathbf{m_d}|\ |\mathbf{u_a}| \cos \theta$$

Dot product of vectors $\mathbf{m_d}$ and $\mathbf{u_{ap}}$ gives the scalar y_d. y_d is the magnitude of the projection of $\mathbf{m_d}$ in the direction of $\mathbf{u_{ap}}$ or the y-axis in the reference system (Fig. 2)

$$y_d = \mathbf{m_d} \circ \mathbf{u_{ap}}$$

$$y_d = |\mathbf{m_d}|\ |\mathbf{u_{ap}}| \cos \theta$$

The goal now is to calculate the total displacement vector $\mathbf{M}$. From Fig. 2 it follows that

$\mathbf{M} = \mathbf{m_a} + L_a \mathbf{u_a} \quad (1)$

Where the displacement vector in ascending direction, $\mathbf{m_a}$, is added to the length L_a multiplied with the ascending unit vector $\mathbf{u_a}$. $\mathbf{m_a}$ and $\mathbf{u_a}$ is known but length L_a has to be calculated.

From Fig. 2 it follows that

$$x_a = x_d + L_{dx}$$

From before we know that

$$L_{dx} = L_d \, x_{dp}$$

Therefore

$$x_a = x_d + L_d\, x_{dp}$$

This again can be written

$$L_d = \frac{x_a - x_d}{x_{dp}} \quad (2)$$

Further Fig. 2 gives

$$L_a = y_d + L_d\, y_{dp} \quad (3)$$

Eq. (2) inserted into Eq. (3) gives

$$L_a = y_d + L_d\, y_{dp}$$

$$L_a = y_d + \frac{x_a - x_d}{x_{dp}}\, y_{dp} \quad (4)$$

Using Eq. (4) it is possible to calculate L_a. Then it is possible to solve Eq. (1), finding the total displacement vector **M**.

$$\mathbf{M} = \mathbf{m_a} + L_a\, \mathbf{u_a} \quad (1)$$

From vector **M** horizontal displacement is found calculating the dot product of **M** and a unit vector pointing directly against East. Further the vertical displacement is found calculating the dot product of **M** and a unit vector pointing upwards. From horizontal- and vertical displacement dip angle of the total displacement in East-West plane is found.

9 Appendix 4 – InSAR processing

This appendix lists the different parameter used in ,the GSAR application from Norut when processing the InSAR data for the different localities.

9.1 InSAR data used for verification against GPS at the Nordnes rockslide

Processing parameters for ascending data

Number of SLC files	11
Time period	2011
Multi-look factor in azimuth and range	5 x 4
Pixel size in m	9,7 x 7,5 m
Number of interferograms used	26 of 26
Temporal filter width	33 days
Spatial filter width	500 m
Reference point coordinates in UTM coordinates	34W 477511 7716633 UTM
Reference point coordinates in range and azimuth	209 1054
Coherence	0,7
Coherence threshold for pixel selection	0,2
Percentage threshold for pixel selection	0,5
Algorithm	SBAS

Processing parameters for descending data

Number of SLC files	13
Time period	2011
Multi-look factor in azimuth and range	5 x 4
Pixel size in m	7,5 m x 8,2
Number of interferograms used	14 of 14
Temporal filter width	33 days
Spatial filter width	500 m
Reference point coordinates in UTM coordinates	34W 477511 7716633 UTM
Reference point coordinates in range and azimuth	484 520
Coherence	0,75

Coherence threshold for pixel selection	0,2
Percentage threshold for pixel selection	0,5
Algorithm	SBAS

9.2 InSAR data related to geomorphological- and structural elements

Rock glacier on Nordmannviktinden 2009-2012

Processing parameters for ascending data

Number of SLC files	42
Time period	2009 -2012
Multi-look factor in azimuth and range	5 x 4
Pixel size in m	9,7 x 7,5 m
Number of interferograms used	88 of 94
Temporal filter width	33 days
Spatial filter width	600 m
Reference point coordinates in UTM coordinates	34W 481796 7725908 UTM
Reference point coordinates in range and azimuth	215 760
Coherence	0,745231
Coherence threshold for pixel selection	0,2
Percentage threshold for pixel selection	0,45
Algorithm	Mean velocity stacking

Processing parameters for descending data

Number of SLC files	46
Time period	2009 -2012
Multi-look factor in azimuth and range	5 x 4
Pixel size in m	9,7 x 7,5 m
Number of interferograms used	104 of 107
Temporal filter width	33 days
Spatial filter width	600 m
Reference point coordinates in UTM coordinates	34W 481799 7725912 UTM
Reference point coordinates in range and azimuth	726 993

Coherence	0,776129
Coherence threshold for pixel selection	0,2
Percentage threshold for pixel selection	0,35
Algorithm	Mean velocity stacking

Gamanjunni3 - 2009-2012

Processing parameters for ascending data

Number of SLC files	42
Time period	2009 -2012
Multi-look factor in azimuth and range	5 x 4
Pixel size in m	9,7 x 7,5 m
Number of interferograms used	92 of 94
Temporal filter width	33 days
Spatial filter width	500 m
Reference point coordinates in UTM coordinates	34W 482908 7708982 UTM
Reference point coordinates in range and azimuth	324 1489
Coherence	0,814753
Coherence threshold for pixel selection	0,20
Percentage threshold for pixel selection	0,45
Algorithm	Mean velocity stacking

Processing parameters for descending data

Number of SLC files	46
Time period	2009 -2012
Multi-look factor in azimuth and range	5 x 4
Pixel size in m	9,7 x 7,5 m
Number of interferograms used	75 of 75
Temporal filter width	22 days
Spatial filter width	600 m
Reference point coordinates in UTM coordinates	34W 482908 7708981 UTM

Reference point coordinates in range and azimuth	566 506
Coherence	0,73035
Coherence threshold for pixel selection	0,15
Percentage threshold for pixel selection	0,3
Algorithm	Mean velocity stacking

Nordnes rockslide and tongues shaped formation at Joppolbakkan – 2009-2012

Processing parameters for ascending data

Number of SLC files	42
Time period	2009 -2012
Multi-look factor in azimuth and range	5 x 4
Pixel size in m	9,7 x 7,5 m
Number of interferograms used	84 of 94
Temporal filter width	33 days
Spatial filter width	600 m
Reference point coordinates in UTM coordinates	34W 477511 7716633 UTM
Reference point coordinates in range and azimuth	209 1054
Coherence	0,7
Coherence threshold for pixel selection	0,2
Percentage threshold for pixel selection	0,35
Algorithm	Mean velocity stacking

Processing parameters for descending data

Number of SLC files	46
Time period	2009 -2012
Multi-look factor in azimuth and range	5 x 4
Pixel size in m	9,7 x 7,5 m
Number of interferograms used	107 of 107
Temporal filter width	33 days
Spatial filter width	600 m

Reference point coordinates in UTM coordinates	34W 477511 7716633 UTM
Reference point coordinates in range and azimuth	484 520
Coherence	0,75
Coherence threshold for pixel selection	0,2
Percentage threshold for pixel selection	0,35
Algorithm	Mean velocity stacking

10 References

Andersen, A., 1988, Caledonian terranes of Northern Norway and their characteristics: Trabajos de Geologia, no. 17, p. 103-117.

Berardino, P., Costantini, M., Franceschetti, G., Iodice, A., Pietranera, L., and Rizzo, V., 2003, Use of differential SAR interferometry in monitoring and modelling large slope instability at Maratea (Basilicata, Italy): Engineering Geology, v. 68, no. 1–2, p. 31-51.

Berardino, P., Fornaro, G., Lanari, R., and Sansosti, E., 2002, A new algorithm for surface deformation monitoring based on small baseline differential SAR interferograms: Geoscience and Remote Sensing, v. 40, no. 11, p. 2375-2383.

Blikra, L. H., 2012, Åknes notat: Geologisk grunnlag for boring og instrumentering: Åknes/Tafjord Beredskap, p. 11.

Blikra, L. H., and Christiansen, H., 2012, A field based model of the influence of snow and frozen ground on seasonal rockslide deformation in the Nordnes area, northern Norway (in review). Geomorphology.

Blikra, L. H., Henderson, I., Nordvik, T., 2009, Faren for fjellskred fra Nordnesfjellet i Lyngenfjorden, Troms: NGU Rapport 2009.026, p. 29.

Blikra, L. H., Longva, O., Braathen, A., Anda, E., Dehls, J. F., and Stalsberg, K., 2006, ROCK SLOPE FAILURES IN NORWEGIAN FJORD AREAS: EXAMPLES, SPATIAL DISTRIBUTION AND TEMPORAL PATTERN, *in* Evans, S., Mugnozza, G., Strom, A., and Hermanns, R., eds., Landslides from Massive Rock Slope Failure, Volume 49, Springer Netherlands, p. 475-496.

Boyd, R., Mikalsen, T., Minsaas, O. og Zwaan, K. B. , 1985, Berggrunnskart Storfjord 1633.4, M 1:50.000. Prelim. utgave: NGU.

Braathen, A., Blikra, L. H., Berg, S., and Karlsen, F., 2004, Rock-slope failures in Norway; type, geometry, deformation mechanisms and stability: Norwegian Journal of Geology, v. 84, p. 67-87.

Bunkholt, H., 2013, Fare og risikoklassifisering av det ustabile fjellpartiet Gamanjunni 3, Manndalen, Troms, in prep, v. NGU.

Bunkholt, H., Osmundsen, P. T., Redfield, T., Oppikofer, T., Eiken, T., L'Heureux, J.-S., Hermanns, R., and Lauknes, T. R., 2011, ROS fjellskred i Troms: status og analyser etter feltarbeid 2010: NGU Rapport 2011.031, p. 135.

Christiansen, H. H., Etzelmüller, B., Isaksen, K., Juliussen, H., Farbrot, H., Humlum, O., Johansson, M., Ingeman-Nielsen, T., Kristensen, L., Hjort, J., Holmlund, P., Sannel, A. B. K., Sigsgaard, C., Åkerman, H. J., Foged, N., Blikra, L. H., Pernosky, M. A., and Ødegård, R. S., 2010, The thermal state of permafrost in the nordic area during the international polar year 2007–2009: Permafrost and Periglacial Processes, v. 21, no. 2, p. 156-181.

Corner, G. D., 1972, Rockslides in North Troms, Norway. : Unpublished report, Tromsø Museum, p. 11.

Corner, G. D., 1973 (unpublished), Rasområder - Addjet/Skibotn.

Corner, G. D., 1980, Preboreal deglaciation chronology and marine limits of the Lyngen-Storfjord area, Troms, North Norway: Boreas, v. 9, no. 4, p. 239-249.

-, 2005a, Atlantic coast and fjords, Oxford, Oxford University Press, The Oxford regional environments series.

-, 2005b, Scandes Mountains, Oxford, Oxford University Press, The Oxford regional environments.

Corner, G. D., (in prep.), STORFJORD 1633 IV. Kvartærgeologisk kart 1:50 000. Norges geologiske undersøkelse.

Dahl, R., and Sveian, H., 2004, Ka dokker mein førr stein! : geologi, landskab og ressurser i Troms, Trondheim, Norges geologiske undersøkelse, 154 p.:

Dehls, J. F., Lauknes, T. R., Blikra, L. H., Kristensen, L., Christiansen, H., Eriksen, H. Ø., and Grydeland, T., 2012, Extensive Insar Observations of the Jettan Rockslide in

Northern Norway, Using Radarsat-2, Terrasar-X, and Corner Reflectors: Poster at AGU conference 2012.

Dehls, J. F., Olesen, O., Olsen, L., Blikra, L.H., 2000, Neotectonic faulting in northern Norway; the Stuoragurra and Nordmannvikdalen postglacial faults: Quaternary Science Reviews, v. 19, no. 14, p. 1447-1460.

Frauenfelder, R., Tolgensbakk, J., Farbrot, H., and Lauknes, T. M., 2008, Rockglaciers in the Kåfjord Area, Troms, Northern Norway: In Kane, D.L., Hinkel, K.M. (eds.), 9th International Conference on Permafrost, Extended Abstracts, Alaska, Fairbanks. Institute of Northern Engineering, University of Alaska Fairbanks, p. 77–78.

Gabrielsen, R. H., Braathen, A., Dehls, J., and Roberts, D., 2002, Tectonic lineaments of Norway: Norsk Geologisk Tidsskrift, v. 82, p. 153-174.

Goldstein, R. M., Engelhardt, H., Kamb, B., and Frolich, R. M., 1993, Satellite Radar Interferometry for Monitoring Ice Sheet Motion: Application to an Antarctic Ice Stream: Science, v. 262, p. 1525-1530.

Hannus, M., 2012, Structural geometry and controlling factors for a rock slope failure area at Hompen/Váráš, Signaldalen, Troms, North Norway.

Hansen, J.-A., Bergh, S. G., Henningsen, T., and Davis, C., 2011, Brittle fault zones in North-Norway: Onshore-offshore link and regional implications. Abstracts and Proceedings of the Geological society of Norway. NGF.

Hansen, J. A., 2009, Onshore-offshore tectonic relations on the Lofoten and Vesterålen Margin : Mesozoic to early Cenozoic structural evolution and morphological implications, University of Tromsø, Faculty of Science, Department of Geology, 229 p.:

Hanssen, R. F., 2001, Radar Interferometry: Data Interpretation and Error Analysis (Remote Sensing and Digital Image Processing): Springer, p. 326.

Harris, C., Kern-Luetschg, M., Smith, F., and Isaksen, K., 2008, Solifluction processes in an area of seasonal ground freezing, Dovrefjell, Norway: Permafrost and Periglacial Processes, v. 19, no. 1, p. 31-47.

Henderson, I. H. C., Lauknes, T. R., Osmundsen, P. T., Dehls, J., Larsen, Y., and Redfield, T. F., 2011, A structural, geomorphological and InSAR study of an active rock slope failure development: Geological Society Special Publications, London, v. 351.

Henderson, I. H. C., Osmundsen, P. T., and Redfield, T., 2008, ROS Fjellskred i Troms: Statusrapport 2007: Norges geologiske undersøkelse, v. NGU Rapport 2008.025.

-, 2009, ROS Fjellskred i Troms: status og planer: Norges geologiske undersøkelse, v. NGU Rapport 2009.023.

-, 2010, ROS Fjellskred i Troms: status og planer 2010: NGU Rapport 2010.021.

Henderson, I. H. C., Saintot, A., Venvik-Ganerød, G., and Blikra, L. H., 2007, Fjellskredkartlegging i Troms: NGU Rapport 2007.041 p. 107.

Hilley, G. E., Bürgmann, R., Ferretti, A., Novali, F., and Rocca, F., 2004, Dynamics of slow-moving landslides from permanent scatterer analysis: Science, v. 304, no. 5679, p. 1952-1955.

Husby, E. H., 2011, Fjellskred i Nomedalstinden: En strukturstyrt masseutglidning på et underliggende storskala glideplan, p. 142.

Joughin, I. R., Kwok, R., and Fahnestock, M. A., 1998, Interferometric estimation of three-dimensional ice-flow using ascending and descending passes: Geoscience and Remote Sensing, IEEE Transactions on, v. 36, no. 1, p. 25-37.

Kääb, A., Kaufmann, V., Ladstädter, R., and Eiken, T., 2003, Rock glacier dynamics: implications from high-resolution measurements of

surface velocity fields, Swets & Zeitlinger, Permafrost: Proceedings of the 8th International Conference on Permafrost.

Landmark, K., and Møller, J., 1979, Tromsøya : berggrunn, løsmasser og strandlinjer, Tromsø, Universitet i Tromsø, Tromsø museum, 1 fold. bl. p.:

Larsen, Y., SAR processing geometry (unpublished): Technical document.

Larsen, Y., Engen, G., Lauknes, T. R., Malnes, E., and Høgda, K. A., A generic differential interferometric SAR processing system, with applications to land subsidence and snow-water equivalent retrieval (unpublished): Technical document.

Lauknes, T. R., 2010, Rockslide Mapping in Norway by Means of Interferometric SAR Time Series Analysis: PhD dissertation, University of Tromsø, p. 124 pages.

Lauknes, T. R., Zebker, H. A., Larsen, Y., 2011, InSAR Deformation Time Series Using an L_1-Norm Small-Baseline Approach: Geoscience and Remote Sensing, IEEE Transactions on, v. 49, no. 1, p. 536-546.

Lister, G. S., Etheridge, M. A., and Seymonds, P. A., 1986, Detachment faulting and evolution of passive continental margins: Geology, v. 14, p. 246-250.

Lister, G. S., Etheridge, M. A., and Symonds, P. A., 1991, Detachment models for the formation of passive continental margins: Tectonics, v. 10, no. 5, p. 1038-1064.

Massonnet, D., Briole, P., and Arnaud, A., 1995, Deflation of Mount Etna monitored by spaceborne radar: Nature, v. 375, p. 567-570.

Massonnet, D., and Feigl, K. L., 1998, Radar interferometry and its application to changes in the Earth's surface: Reviews of Geophysics, v. 36, no. 4, p. 441-500.

NNFO, 2012, GPS data from Nordnes Rockslide.

Pollard, D. D., and Fletcher, R. C., 2005, Fundamentals of Structural Geology, Cambridge University Press.

Quenardel, J. M., and Zwaan, K. B., 2008, Manndalen. Geological map; Manndalen; 16331; 1:50 000; Preliminary version.

Rasmussen, E., 2011, Fjellskred i Laksvatnfjellet, Balsfjord, Troms: indre struktur, morfologi og skredmekanismer.

Rosen, P. A., Hensley, S., Joughin, I. R., Li, F. K., Madsen, S. N., Rodriguez, E., and Goldstein, R. M., 2000, Synthetic aperture radar interferometry: Proceedings of the IEEE, v. 88, p. 333-382

Singh, V. P., Haritashya, U. K., and Shroder, J. F., 2011, Encyclopedia of Snow, Ice and Glaciers, Springer.

Strozzi, T., Farina, P., Corsini, A., Ambrosi, C., Thüring, M., Zilger, J., Wiesmann, A., Wegmüller, U., and Werner, C., 2005, Survey and monitoring of landslide displacements by means of L-band satellite SAR interferometry: Landslides, v. 2, no. 3, p. 193-201.

Thomas, D. S. G., and Goudie, A., 2000, The Dictionary of Physical Geography, Oxford: Blackwell.

Tolgensbakk, J., Sollid, J. L., 1988, Kåfjord, kvartærgeologi og geomorfologi 1 : 50 000, 1634 II: Geografisk Institutt, Universitetet i Oslo.

Vorren, T. O., and Mangerud, J., 2007, Chapter. 15. "Istider kommer og går" in: Ramberg, Ivar B. Bryhni, Inge Nøttvedt, Arvid (red.), Landet blir til Trondheim, Norsk geologisk forening, 478-531 p.:

Vorren, T. O., Mangerud, J., Blikra, L. H., and Torsvik, T. H., 2007, Chapter. 16. "Norge trer fram" in: Ramberg, Ivar B. Bryhni, Inge Nøttvedt, Arvid (red.), Landet blir til Trondheim, Norsk geologisk forening, 532-555 p.:

Wright, T. J., Parsons, B. E., and Lu, Z., 2004, Toward mapping surface deformation in three dimensions using InSAR: Geophysical Research Letters, v. 31, no. 1, p. L01607.

Zebker, H. A., and Villasenor, J., 1992, Decorrelation in interferometric radar echoes: Geoscience and Remote Sensing, IEEE Transactions on, v. 30, no. 5, p. 950-959.

Zwaan, K. B., 1988, Geologisk kart over Norge. Berggrunnskart NORDREISA - M 1:250 000: Norges geologiske undersøkelse.


UNIVERSITY OF TROMSØ